Report No. FAA-RD-73-198 ,IV

ADA038116

COMPARATIVE PERFORMANCE OF STRUCTURAL LAYERS IN PAVEMENT SYSTEMS

VOLUME IV

Analysis Of Insulating Layers In Pavement Test Sections

Walter R. Barker and Frazier Parker, Jr.

U. S. Army Engineer Waterways Experiment Station
Soils and Pavements Laboratory
P. O. Box 631, Vicksburg, Miss. 39180

JANUARY 1977
FINAL REPORT

Document is available to the public through the
National Technical Information Service,
Springfield, Va. 22151

Prepared for

DEPARTMENT OF DEFENSE
DEPARTMENT OF THE ARMY
Office, Chief of Engineers
Washington D. C. 20314

U. S. DEPARTMENT OF TRANSPORTATION
FEDERAL AVIATION ADMINISTRATION
Systems Research & Development Service
Washington, D. C. 20591

DDC
APR 5
C

NOTICES

1. Report No.	2. Government Accession No.	3. Recipient's Catalog No.
FAA-RD-73-198 Vol IV		

4. Title and Subtitle	5. Report Date
COMPARATIVE PERFORMANCE OF STRUCTURAL LAYERS IN PAVEMENT SYSTEMS. VOLUME IV. ANALYSIS OF INSULATING LAYERS IN PAVEMENT TEST SECTIONS.	January 1977
	6. Performing Organization Code

7. Author(s)	8. Performing Organization Report No.
Walter R. Barker and Frazier Parker, Jr.	Technical Report S-74-8 Volume IV

9. Performing Organization Name and Address	10. Work Unit No. (TRAIS)
U. S. Army Engineer Waterways Experiment Station Soils and Pavements Laboratory P. O. Box 631, Vicksburg, Miss. 39180	
	11. Contract or Grant No.
	DOT-FA71WAI-218
	13. Type of Report and Period Covered

12. Sponsoring Agency Name and Address	
Office, Chief of Engineers, U. S. Army Washington, D. C. 20314 and Federal Aviation Administration Washington, D. C. 20591	Final report.
	14. Sponsoring Agency Code

15. Supplementary Notes
WES-TR-S-74-8-Vol-4

16. Abstract

This report describes an analysis of results from tests of pavements containing insulating layers to determine the structural adequacy of pavements containing the various types of insulating materials and to determine the location of the insulating layers to ensure adequate structural performance of the pavements. Volume I of this report describes the design, construction, and behavior under traffic of both flexible and rigid prototype airfield pavements containing expanded polystyrene panels and lightweight concrete containing expanded polystyrene beads as the coarse aggregate. The results from the traffic tests are analyzed herein to determine why the pavements containing layers of the insulating materials performed as they did and the proper location within the pavement structure for the insulating layers to ensure adequate structural performance. Conclusions from the study indicate that the insulating materials behave differently than conventional paving materials. For flexible pavement design, the vertical compressive stresses and horizontal tensile stresses in the insulating materials should be kept below measured strength values. For rigid pavement design, granular or chemically stabilized base or subbase material should be provided between the concrete slab and the insulating material, and a base or subbase course should be placed between the polystyrene panels and subgrade materials susceptible to pumping.

17. Key Words	18. Distribution Statement
Flexible pavement Rigid pavement Insulating materials Frost design Pavement performance	Document is available to the public through the National Technical Information Service, Springfield, Va. 22151

19. Security Classif. (of this report)	20. Security Classif. (of this page)	21. No. of Pages	22. Price
Unclassified	Unclassified	145	

Form DOT F 1700.7 (8-72)   Reproduction of completed page authorized

PREFACE

The investigation reported herein was jointly sponsored by the Office, Chief of Engineers, U. S. Army (OCE), as a part of the Military Construction Short-Range Airfield Pavement Research Program and by the Federal Aviation Administration (FAA) as a part of Inter-Agency Agreement No. DOT FA71WAI-218, "Development of Airport Pavement Criteria." OCE technical monitor for this investigation was Mr. A. F. Muller (DAEN-MCE-D), and the FAA technical representative was Mr. Fred Horn (ARD-430).

The investigation was conducted during the period March 1972-August 1973 at the U. S. Army Engineer Waterways Experiment Station (WES) by personnel of the Soils and Pavements Laboratory (S&PL), under the general supervision of Messrs. James P. Sale and Richard G. Ahlvin, Chief and Assistant Chief, respectively, of S&PL. This report was prepared by Dr. Walter R. Barker and Dr. Frazier Parker, Jr.

Directors of WES during the conduct of the investigation and the preparation of this report were BG E. D. Peixotto, CE, COL G. H. Hilt, CE, and COL J. L. Cannon, CE. Technical Director was Mr. F. R. Brown.

1

TABLE OF CONTENTS

METRIC CONVERSION FACTORS

Approximate Conversions to Metric Measures

Symbol	When You Know	Multiply by	To Find	Symbol
		LENGTH		
	inches	2.5	centimeters	cm
	feet	30	centimeters	cm
	yards	0.9	meters	m
	miles	1.6	kilometers	km
		AREA		
	square inches	6.5	square centimeters	
	square feet	0.09	square meters	
	square yards	0.8	square meters	
	square miles	2.6	square kilometers	
	acres	0.4	hectares	
		MASS (weight)		
	ounces	28	grams	g
	pounds	0.45	kilograms	kg
	short tons (2000 lb)	0.9	tonnes	t
		VOLUME		
	teaspoons	5	milliliters	ml
	tablespoons	15	milliliters	ml
	fluid ounces	30	milliliters	ml
	cups	0.24	liters	l
	pints	0.47	liters	l
	quarts	0.95	liters	l
	gallons	3.8	liters	l
	cubic feet	0.03	cubic meters	
	cubic yards	0.76	cubic meters	
		TEMPERATURE (exact)		
	Fahrenheit temperature	5/9 (after subtracting 32)	Celsius temperature	°C

Approximate Conversions from Metric Measures

Symbol	When You Know	Multiply by	To Find	Symbol
		LENGTH		
	millimeters	0.04	inches	
	centimeters	0.4	inches	
	meters	3.3	feet	
	meters	1.1	yards	
	kilometers	0.6	miles	
		AREA		
	square centimeters	0.16	square inches	
	square meters	1.2	square yards	
	square kilometers	0.4	square miles	
	hectares (10,000 m²)	2.5	acres	
		MASS (weight)		
	grams	0.035	ounces	
	kilograms	2.2	pounds	
	tonnes (1000 kg)	1.1	short tons	
		VOLUME		
	milliliters	0.03	fluid ounces	
	liters	2.1	pints	
	liters	1.06	quarts	
	liters	0.26	gallons	
	cubic meters	35	cubic feet	
	cubic meters	1.3	cubic yards	
		TEMPERATURE (exact)		
	Celsius temperature	9/5 (then add 32)	Fahrenheit temperature	
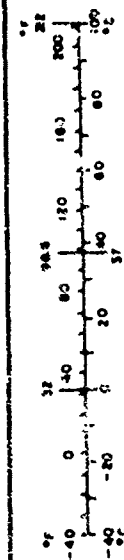
INTRODUCTION

BACKGROUND

One pavement design concept used in regions where frost action is a problem is to place insulating layers in the pavement structure to prevent the penetration of freezing temperatures into frost-susceptible materials. Innovations in material utilization have included the use of prefabricated polystyrene panels and polystyrene bead concrete as insulating layers.

A significant factor in the design of pavements containing insulating layers is the depth at which the insulating layer should be placed. To be most effective, the insulating material should be located as near the surface as possible. The exact location should be controlled by the strength of the material and the structural adequacy of the resulting pavement system.

Volume I of this report[1] describes the design, construction, and behavior under traffic of prototype rigid and flexible airfield pavement test sections. Included in these test sections were test items containing insulating layers. The insulating layers were placed at various locations within rigid and flexible pavement structures to evaluate the structural performance of the insulating materials and to study the effects of the location of the insulating layers within the pavement structures.

OBJECTIVES

The objectives of this report are to analyze the results from tests of the pavements containing insulating layers, to determine the structural adequacy of pavements containing various types of insulating layers, and to determine the location of the insulating layers to ensure adequate structural performance of the pavements.

PROPERTIES OF INSULATING MATERIALS

Two types of materials were used as insulating layers. The first type was an expanded polystyrene panel manufactured by Dow Chemical Corporation under the trade name of Styrofoam. Three different strength materials were employed: Styrofoam HD-300, Styrofoam HI, and Styrofoam SM. These have nominal strengths of 120, 60, and 35 psi, respectively. (Note: The strength values are the manufacturer's published minimum compressive strength measured perpendicular to the panel face at 5 percent strain.) The HD-300 material was supplied in 3- by 16- by 108-in. panels, the HI material in 4- by 24- by 96-in. panels, and the SM material in 3- by 24- by 48-in. panels. The second type material was a lightweight concrete manufactured under a patented process held by BASF Wyandotte Corporation. The coarse aggregate was an expanded polystyrene bead. The trade name of the lightweight concrete is Styropor concrete. The strength can be increased by decreasing the polystyrene bead content, but the resulting Styropor concrete will be denser and have poorer insulating qualities. The opposite effect is achieved by increasing the polystyrene bead content. A discussion of the production of Styropor concrete along with various properties of the material can be found in Hohwiller and Köhling.[2]

Of importance in the structural behavior of the lightweight concrete are its strength and load-deformation characteristics. Figure 1 presents the 28-day compressive cube strength as a function of the unit weight, and Figure 2 presents dynamic modulus (28 day) as a function unit weight.[2]

In the test section, lightweight concrete mixes having unit weights of 44 and 52 pcf were used. The material generally followed the trends illustrated in Figures 1 and 2; i.e., the 52-pcf material was stiffer and has a higher strength than the 44-pcf material. Table 1 summarizes the results of compression and flexural tests performed on 6- by 12-in. cylinders and 6- by 6- by 36-in. beams, respectively. The beams and cylinders were cast during construction according to American Society for Testing and Materials (ASTM) Designation: C 192-69,[7] which

6

is equivalent to Method CRD-C 10.[4] The data shown in Table 1 indicate
that the strength and modulus of the lighweight concrete are rather
insensitive to age but highly dependent on density. This is caused by
the overshadowing effects of the polystyrene beads. Eliminating the
tests at ages of 7 and 66 days and averaging those remaining yields, re-
spectively, average compressive strengths of 446 and 770 psi, flexural
strengths of 161 and 163 psi, compressive moduli of 0.215×10^6 and
0.301×10^6 psi, and flexural moduli of 0.452×10^6 and 0.646×10^6 psi
for the concrete mixes with unit weights of 44 and 52 pcf. The strengths
indicated in Figure 1 for the two different lightweight concrete mixes
are greater than their respective measured strengths, and the dynamic
moduli indicated in Figure 2 are greater than the measured compressive
moduli but less than the measured flexural moduli. The 52-pcf material
was used in the flexible pavement test section and the 44-pcf material
in the rigid pavement.

A limited number of tests were conducted on the insulating mate-
rials to define their load-deformation and strength characteristics.
For the 120- and 60-psi polystyrene panels, unconfined compression and
cyclic unconfined compression (resilient modulus) tests were conducted.
Results of unconfined compression tests are shown in Figure 3. For com-
parison, the results of an unconfined compression test on the 4-CBR clay
(CH) subgrade material are also presented. As can be seen in the fig-
ure, both the 120- and the 60-psi panels met the manufacturer's speci-
fied compressive strength. Although no tests were run, the stress-
strain and strength characteristics of the 35-psi panels were assumed to
be similar to those of the 120- and 60-psi materials. Results from the
cyclic tests are presented in Figure 4. The results from cyclic tests
on the clay are also presented for comparison. It can be seen in Fig-
ure 4 that the resilient modulus of the panels decreases only slightly
with increases in deviator stress. The slight decrease in resilient
moduli of the two panels is in marked contrast to the decrease in
resilient modulus of the clay with increases in deviator stress. At
very low values of deviator stress, the modulus of the clay is higher
than that of either of the panels, but at values of subgrade stress

7

which would normally be expected in airport pavement structures (5 to
7 psi), the resilient modulus is about equal to or slightly less than
the modulus for the 60-psi panel. The static moduli computed (at a
strain level of 2 percent) from the data presented in Figure 3 are close
to but below the resilient moduli (for 6-psi deviator stress) for the
120- and 60-psi panels. The static modulus of the clay is much lower
than its resilient modulus. The moduli are 3000 and 4500 psi for the
60-psi panel, 6000 and 6900 psi for the 120-psi panel, and 1200 and
4100 psi for the clay.

Tests similar to laboratory CBR tests were conducted on all three
polystyrene panels located on a firm surface. The load penetration
curves for these tests are shown in Figure 5. For comparison, a range
of load penetration curves for the subgrade soil is presented. Although
only one curve is presented in Figure 5 for each panel, three tests were
conducted for each; however, little variation was noted. The computed
CBR's for the 120-, 60-, and 35-psi panels were 10, 6, and 3.8,
respectively.

FLEXIBLE PAVEMENT TEST SECTION

The layout of the flexible pavement section, including the sub-items containing the insulating layers, is shown in Figure 6. The vertical locations of the insulating layers within the pavements are shown in Figure 7.

The locations of the polystyrene panel insulating layers were selected by considering the expected vertical stress distribution, as obtained from a linear or nonlinear finite element analysis, through the sections without the insulating layers. The selection process for the vertical locations for the 60-psi panels placed in item 4 is illustrated in Figure 8. The expected vertical stresses at the top of the insulating layers were calculated as 15 and 45 psi for the deep and shallow locations, respectively. The linear elastic analysis was used for item 4 because it was felt that, for the materials in this pavement, a linear elastic approximation of the load-deformation response was sufficiently accurate. The selection process for the 120-psi panels placed in item 5 is illustrated in Figure 9. The expected stresses at the top of the insulating layers were calculated as 36 and 80 psi for the deep and shallow locations, respectively. A nonlinear analysis was performed for item 5 because of the stress-dependent nature of the response of the granular materials (crushed limestone and sandy gravel). The moduli of elasticity of the crushed limestone and sandy gravel were assumed to be functions of the horizontal stress.

The locations for the lightweight concrete were checked based on the tensile stress at the bottom of the layer as computed by layered elastic theory. For the shallow and the deep locations in items 4 and 5, the tensile stresses at the bottom of the layers were less than 100 psi. They were considerably less than the tensile strength of the lightweight concrete as measured with beam tests. The results from the beam tests are summarized in Table 1.

CONSTRUCTION

The construction of the test section is described in detail in

9

Volume I of this report,[1] but will be summarized here for easy refer-
ence. An existing pavement was removed and 6 to 12 in. of the in-place
clay subgrade was reprocessed with material added or removed where nec-
essary to obtain the desired grades; the water content was adjusted as
required; and the material was compacted with a 30-ton pneumatic-tired
roller.

The polystyrene layers were constructed by placing the panels by
hand in a staggered pattern as illustrated in Figure 10. The light-
weight concrete was mixed in 1/2-cu-yd batches, placed in forms, the
surface screeded to grade, and cured with wet burlap for 40 hr.

The soil and cement for subitems 4a-4d were premixed in a windrow
adjacent to the test section, placed with a front-end loader, and spread
loosely in layers about 6 in. thick. The gravelly sand subbase and
crushed limestone base in subitems 5a-5d were placed in the same manner.
Each layer was compacted by 8 coverages of the 30-ton roller with tire
pressures of about 70 psi, and for those lifts not over the insulating
materials, an additional 8 coverages of a 50-ton roller were applied.
The 50-ton roller was not used over the insulating layers for fear of
damaging the materials.

The asphaltic concrete surfacing was laid down with a finisher in
10-ft-wide lanes. Compaction was accomplished with a 10-ton tandem
steel-wheeled roller and the 30-ton pneumatic-tired roller.

PROPERTIES OF AS-CONSTRUCTED PAVEMENTS

The material properties for the material in items 4 and 5 mea-
sured prior to traffic are contained in Table 2. Since the material
above the insulating layers was compacted only with the 30-ton roller,
it was expected that the density of the material above the insulating
layers in the subitems would be less than it was in the main items.
However, from the data in Table 2 this is not evident. It was also
expected that the density of the lift above the polystyrene panels would
be less than that of lifts nearer the surface, because of the effects of
of the low panel stiffness. This effect was generally observed for all
the other items (including 1, 2, and 3) where the density of the lift

10

above the subgrade was less than that of lifts nearer the surface. However, this effect is not apparent from the data in Table 2, and in fact, the measured densities of the material above the stiff lightweight concrete layer were less than they were above the polystyrene panels.

TRAFFIC

Traffic was applied to the flexible pavements containing insulating layers with a 50-kip single-wheel assembly having a tire inflation pressure of 190 psi. A detailed description of the application of traffic and subsequent pavement performance is contained in Volume I.[1] Table 3 summarizes the traffic data. The rating given a subitem was based on permanent deformation of the pavement and cracking of the asphaltic concrete layer. A pavement was considered failed when either of the following occurred:

 a. Surface upheaval of the pavement adjacent to the traffic lane reached 1 in. or more.

 b. Cracking extended through the asphaltic concrete layer.

Subitems 4a-4d developed extensive cracking under the 50-kip single-wheel assembly and were considered failed when the cracks penetrated the full depth of the asphaltic concrete. Subitems 4a and 4b were considered failed at 170 coverages and subitems 4c and 4d at 240 coverages. Subitems 5a, 5c, and 5d sustained severe cracking and subitem 5b slight cracking under the 50-kip single-wheel assembly. All subitems were considered failed at 240 coverages when the cracks extended through the asphaltic concrete.

AFTER-TRAFFIC INVESTIGATIONS

After termination of traffic, test pits were excavated in each subitem for visual inspection of the insulating materials. In-place CBR tests were conducted, and water content and density determinations were made at various locations inside and outside the traffic lane in subitems 4a, 4c, 5a, and 5c. Moisture content determinations were made near the surface of the stabilized base course in subitem 4b. Profiles of the layers are shown in Figures 11-14. The CBR test results, moisture contents, and densities are shown in Table 4. Load penetration

curves for the CBR tests conducted on the polystyrene panels are shown in Figure 15, and curves for tests on the lightweight concrete are shown in Figures 16 and 17.

SUBITEM 4a

The results of the CBR tests on the stabilized clayey sand were erratic, ranging from a high of 114 to a low of 22. The CBR values measured outside the traffic lane were 114, 33, and 22 for depths of 3, 15, and 22 in., respectively, and inside the traffic lane were 67, 27, and 56 for depths of 3, 15, and 22 in., respectively. In the main portion of the test section, the CBR of the stabilized clayey sand varied from 93 to 150+ for all tests conducted prior to traffic and all tests conducted after traffic but outside the traffic lane. The CBR values for the main test section inside the traffic lane measured after traffic were 150+ and 70 for a depth of 3 in., 50 for a depth of 12 in., and 26 for a depth of 15 in.[1]

A comparison of the CBR's measured in the main test section with the CBR's measured in subitem 4a indicates that the stabilized material in the subitem was weaker than the stabilized material in the main test section.

The average of the CBR's measured after traffic in the subgrade of the main test section was 6.2 as compared to an average of 3.3 for subitem 4a. It can also be noted that the subgrade CBR's of subitem 4a measured inside the traffic lane were less than the CBR's measured outside the traffic lane. The tests conducted outside the traffic lane were on the south side of the subitem. The lower values inside the traffic lane and higher values outside the traffic lane were consistent with the observation that the most severe rutting due to traffic occurred to the north of the center line of the traffic lane.

The stiffness of the polystyrene, as measured by the load penetration curves in Figure 15, was unaffected by the traffic. With the exception of flexural cracking, the condition of the polystyrene (Figure 18) was excellent; i.e., there appeared to be no crushing of the insulating material. The cause of the flexural cracking of the

12

polystyrene panels which were placed transverse to the traffic lane appeared to be permanent deformation of the material beneath the panels. Such deformations are indicated by the layer profiles in Figure 11.

SUBITEM 4b

The only tests run in subitem 4b were moisture content determinations near the surface of the stabilized base course. However, the performance of the pavement and the lack of crushing in the polystyrene substantiate the conclusion that the polystyrene was not directly the cause of failure. The condition of the panels after 240 coverages, which was long after failure, is illustrated in Figure 19.

SUBITEM 4c

The CBR's measured for the stabilized clayey sand in subitem 4c, particularly beneath the lightweight concrete, indicated poor stabilization. While the subgrade CBR's were not as low as those for the subgrade of subitem 4a, the CBR's measured inside the traffic lane were less than those measured outside the traffic lane. The load penetration curves shown in Figure 16 indicate that at two locations inside the traffic lane the stiffness of the lightweight concrete had been reduced and that at one location the stiffness was unchanged. This indicates that, in some areas, crushing of the surface of the lightweight concrete had occurred.

Cracks had developed parallel to traffic in the lightweight concrete at the edge of the traffic lane and near the center of the traffic lane. The profiles shown in Figure 12 indicate rutting occurred in the stabilized clayey sand beneath the insulating material which probably caused the cracking.

The results of the after-traffic testing indicated that failure was caused by the lack of stabilization of the clayey sand beneath the lightweight concrete.

SUBITEM 4d

A test pit was opened at the east end of subitem 4d and the west end of subitem 5a at 170 coverages to observe the condition of the

13

lightweight concrete. The cracking that had developed in subitem 4d is shown in the right side of Figure 20. The cracking of the lightweight concrete in this subitem indicated failure of this materiel, particularly in the area of the transition between subitem 4d and subitem 5a.

SUBITEM 5a

On the crushed stone base in subitem 5a, in-place CBR values inside and outside the traffic lane were 63 and 53, respectively. In the main test section, the CBR values measured at the top of the base both inside and outside the traffic lane were 150+ for traffic lane 1 and 133 for traffic lane 2. Thus, the CBR tests indicate a weaker base material existed in subitem 5a than existed in the main test section. Likewise, the subbase and subgrade CBR's were lower in subitem 5a than in the main test section.

The condition of the lightweight concrete at 170 coverages is indicated in the left-hand portion of Figure 20. Although not visible in the photograph, hairline cracks parallel to traffic were noted in the surface of the lightweight concrete. The load penetration curves of the CBR tests conducted on the surface of the lightweight concrete, shown in Figure 17, indicated a weakening of this materiel due to traffic. Such weakening would be the result of crushing of the concrete matrix in the lightweight concrete.

SUBITEM 5b

An examination of the surface of the lightweight concrete in subitem 5b showed one small longitudinal hairline crack near the center of the traffic lane. A test pit was located at the center of the subitem, and it was determined that only about 0.4 in. of permanent deformation had occurred at the top of the lightweight concrete. This roughly corresponds to the deformation observed at the surface.

SUBITEM 5c

The CBR's measured at the surface of the crushed stone base were lower than those for the base of the main test section, but the CBR values measured on the gravelly sand roughly corresponded to those

14

measured in the gravelly sand of the main test section. The CBR's measured in the subgrade of this subitem were higher than the CBR's measured for the subgrade of the other subitems and were approximately the same as those measured in the subgrade of item 5 in the main test section. The load penetration curves (Figure 15) showed no difference in stiffness of the polystyrene inside the traffic lane from that outside the traffic lane.

The polystyrene in subitem 5c was placed with the long dimension of the panels parallel to the direction of traffic as shown in Figure 21. Placement in this manner permitted the insulation to deform with the rutting, and thus no flexural cracking of the polystyrene occurred. No crushing of the surface of the polystyrene could be detected.

SUBITEM 5d

Figure 22 shows the surface of the polystyrene in subitem 5d. The polystyrene of this subitem appeared, as was the case in subitem 5c, to be in excellent condition.

ANALYSIS OF TEST RESULTS

REVIEW OF PERFORMANCE

In reviewing the results of the traffic tests the following general observations were made:

a. Failures began at the transitions between items. This is illustrated in Figure 23, which shows the initial distress for subitem 4a. For this particular distress, the point of maximum deformation was directly over the transition between subitems 4a and 4b. Figure 24 shows the failure of subitem 4d, which began at the transition between subitem 4d and subitem 5a.

b. The center of the permanent deflection basin of permanent deformation was not in the center of the traffic lane but was offset to the north side of the traffic lane. This effect is illustrated in Figures 25 and 26. This offset was toward the outside edge of the test section.

c. For subitems 5c and 5d, in which the polystyrene panels were placed parallel to traffic, distinct cracks developed in the asphaltic concrete directly above the joints between panels. This is illustrated in Figure 27 which shows the longitudinal cracking in subitem 5c.

15

The above observations led to the conclusion that the failures in the insulated test items were initiated by discontinuities such as transitions, panel cracks, and the edges of the lightweight concrete. This conclusion has been substantiated by the performanc of other full-sized test sections in which premature failures have often occurred at transitions. The cause of these failures has been attributed directly to the lack of compaction. With the exception of subitem 4d, which failed because of crushing of the lightweight concrete, this concept seems applicable to the failures of the subitems containing the insulated layers. It should be noted that the performance of subitems 5a and 5b was considered superior to the performance of the other items, although failure was assigned at 240 coverages. As can be seen in Figures 28 and 29, only a few cracks had occurred in these items at 240 coverages. Considering the discontinuities, subitem 5b performed remarkably well. For subitem 5b, Figure 29 shows there was very little cracking and the cross section in Figure 26 shows very little permanent deformation. The superior performance of subitems 5a and 5b can be attributed to the fact that the lightweight concrete provided a rigid base to support the granular materials during traffic.

The failure of subitem 4d cannot be blamed on poor performance of othe pavement materials. In this case, the lightweight concrete was placed directly under the asphaltic concrete and failure occurred due to crushing of the polystyrene beads within the lightweight concrete. In this case, the compressive strength of the lightweight concrete was not sufficient to withstand stress concentrations at its surface.

The failure of subitems 4a, 4b, 5c, and 5d indicated a lack of stabilization and/or the influence of discontinuities. In these items, the lack of compaction at the discontinuities resulted in reduced load-distributing characteristics and shear strength of the granular and stabilized materials. This resulted in large deformations, both above and below the insulating layers. In subitems 4a and 4b, the panels were placed transverse to the traffic. The large permanent deformation, as shown in Figures 11 and 25, caused flexural cracking of the panels parallel to the direction of traffic, as shown in Figures 18 and 19. In

16

subitems 5c and 5d, the longitudinal placement of the panels permitted
deformation without cracking of the panels. This resulted in severe
rutting, as illustrated in Figures 12 and 26, and longitudinal cracking,
as shown in Figure 27.

THEORETICAL ANALYSIS

A theoretical analysis was conducted for subitems 5c and 5d to
determine the influence of placing the insulating layers within the
granular material. The analysis consisted of estimating the resilient
modulus of the pavement components, computing the resilient response
utilizing a linear elastic layered response model (Chevron computer pro-
gram[9]), and relating the computed response to allowable response. Al-
though a nonlinear response model had been used in placement of the poly-
styrene panels, a linear elastic layered response model was used in the
analysis to conform to the design scheme presented by Barker and
Brabston.[10] In addition, the resilient response was related to the per-
manent deformation of the pavement system.

The first step in the analysis was to estimate the resilient
modulus and Poisson's ratio of the pavement components. The results of
resilient modulus tests conducted on samples taken from the main part of
the test section and on laboratory prepared samples of the clay (CH)
subgrade are shown in Figure 30. The field samples were taken at vari-
ous depths. It should be noted that the resilient moduli of the field
samples were considerably higher than the resilient moduli of laboratory
samples of comparable moisture contents. The subgrade had been in place
for several years, and the effects of thixotropic stiffening and compac-
tion by traffic in past tests probably caused the differences in stiff-
ness. In addition, the CBR tests indicated that the subgrade in the
subitems was less stiff than it was in the main items. It should be
noted that the top 6 to 12 in. of the subgrade was reprocessed and there-
fore characterization with the laboratory data, at least for the upper
part of the subgrade, would appear to be justified. For these reasons,
a resilient modulus of 3,000 psi was selected for characterizing the
subgrade. This is based on the laboratory curves and an estimated

17

deviator stress of 5 to 6 psi. The measured Poisson's ratio for the clay
was relatively insensitive to the state of stress, and was approximately
equal to 0.4. The results from resilient modulus tests of the polysty-
rene panels have been presented earlier. These tests were conducted
perpendicular to the panel face and represented the direction of maximum
stiffness. In the test section, the panels appeared to be subjected to
bending, and thus the modulus in the direction parallel to the panel
faces would significantly influence the layer behavior. Also, there were
weak planes along the joint between panels. To account for these two
factors, the resilient modulus of the polystyrene was reduced to one
half, giving a resilient modulus of 3,500 psi. By comparing measured
load penetration curves computed with elastic theory, it was determined
that Poisson's ratio for the polystyrene was close to zero, and thus
zero was used for this material. To characterize the granular materials,
the granular layers were subdivided into sublayers of 6 to 8 in. in
thickness. The modulus of each sublayer depended on the modulus of the
layer beneath, according to a characterization scheme presented in
Barker and Brabston.[10] Poisson's ratio for the gravelly sand and
crushed limestone was estimated at 0.2 and 0.35, respectively. In the
analysis, two modulus values were estimated for the asphaltic concrete:
500,000 psi for a winter day and 30,000 psi for a hot summer day. The
value 0.45 was used for Poisson's ratio for both the winter day and
summer day. The schemes described resulted in characterization of the
pavements as shown schematically in Figures 31 and 32.

The pavement response was computed utilizing the Chevron computer
program.[9] One pavement response of particular interest was the vertical
deflection at the surface, which could be compared with the measured
deflections. The comparisons of the computed deflections and measured
deflections are illustrated in Figure 33. The agreement of the measured
deflections with computed deflections was obtained with the computed
deflections adjusted to account for the assumption in the layered
elastic theory of an indefinite depth of subgrade. This assumption re-
sults in computed deflections at very large distances from the tire,
which have not been observed in actual tests. The adjustment in this

case is made by moving the computed deflection upward such that the indicated deflection at 80 in. from the center line of load would be zero. The agreement between this adjusted curve and the measured deflection is considered excellent, especially considering the scatter in the measured data.

Computed vertical stress distributions, with depth, are given in Figures 34 and 35 for summer and winter conditions, respectively. In each figure, the distribution is given for subitems 5c and 5d. In comparing the distributions, it can be seen that there is little difference in the stress for a given depth between subitems 5c and 5d. There is a substantial difference, near the surface, in stress between a summer day and a winter day. Also, there are differences in the vertical stress at the top of the polystyrene in subitem 5c (15 psi for a winter day and 18 psi for a summer day) and in subitem 5d (38 psi for a winter day and 51 psi for a summer day).

The distribution of vertical strain with depth for summer conditions is given in Figure 36 for subitems 5c and 5d. The vertical lines in the figure represent the strain at the middle of a layer (except for the subgrade, in which the distribution within the layer is represented). In the upper granular layers the strain is greater in subitem 5d than in 5c by approximately 35 percent, whereas below the polystyrene the strain in both items is almost the same. Within the polystyrene, the strain in subitem 5d is over twice that in subitem 5c. Thus, from the standpoint of stress and strain, it would appear that subitem 5c should perform better than subitem 5d. This is contrary to the assigned behavior where both were assumed to have failed at the same time. The problem is therefore one of degree of distress under what are considered failure conditions.

In the design procedure for flexible pavement proposed in Barker and Brabston,[10] the vertical strain is used as the criterion for predicting the performance of a pavement. For the subgrade conditions and applied traffic, the allowable strain is about 0.001 in./in. From the plot in Figure 36, it can be seen that for both items the computed subgrade strain is almost twice the allowable. The purpose of limiting the

19

subgrade strain is to prevent rutting of the subgrade. In addition to
resilient modulus tests as discussed earlier, rutting tests on the sub-
grade soil were conducted using laboratory prepared samples. Two rela-
tionships were developed from these tests. The first is the relation-
ship between permanent strain and resilient strain presented in Fig-
ure 37, and the second is the relationship between the ratio of permanent
strain to resilient strain and resilient modulus of the subgrade mate-
rial presented in Figure 38. The relationships were developed for
1000 stress repetitions, but the applied traffic is given in terms of
coverages. Traffic producing 1 coverage was considered to produce
3 repetitions of the maximum strain at the subgrade surface; i.e. each
pass within 3 tire widths of a point would be considered as a strain
repetition. Since the relationship for 1000 stress repetitions was
available, it was used as an approximation for 720 strain repetitions
which resulted from the applied traffic. The permanent strain at a
point in the subgrade can be determined from the relationships shown in
Figures 37 and 38. For example, at the top of the subgrade, a resilient
strain of 0.0018 in./in. is obtained from Figure 36. With this value of
resilient strain, a permanent strain of approximately 0.003 is obtained
from Figure 37 for a 3-CBR material. By using the distribution of re-
silient strain as shown in Figure 36 for subitem 5d and the relationship
between resilient strain and permanent strain in Figure 37, the distri-
bution of permanent strain in the subgrade can be determined. The com-
parison between resilient strain and permanent strain to a depth of
70 in. is given in Figure 39.

If it is assumed that the permanent strain goes to zero at some
depth (say, 170 in.), then an approximation of the permanent deformation
in the subgrade can be made by computing the area under the permanent
strain distribution curve. From Figure 39, the area from 70 in. to
170 in. is approximated as a triangle with an area representing
0.0385 in. of deflection. The remaining curve is broken into three
trapezoids from depths of 42 to 50 in., 50 to 60 in., and 60 to 70 in.
The trapezoids have areas of 0.0172, 0.0130, and 0.0090 sq in., respec-
tively. Summing these values gives a permanent deformation at the top

20

of the subgrade of 0.08 in. The distribution of permanent deformation with depth is given in Figure 40.

The permanent deformation at the top of the subgrade can also be estimated using the relationship presented in Figure 38 and the computed resilient deformation. In this case, if it is assumed that the ratio remains constant with depth and that the subgrade is infinite, then the permanent deformation is equal to the computed resilient deformation times the strain ratio. Interacting (graphically) the resilient strain with depth curve to a depth such that the strain is essentially zero yields a resilient deformation at the top of the subgrade of 0.115 in. From . ≥ 38, a strain ratio of 1.6 was obtained for a subgrade soil of 3000 psi. With a resilient strain of 0.115 in. and a strain ratio of 1.6, the permanent deformation of the surface of the subgrade in sub-item 5d was estimated as 0.184 in. This estimated deformation is greater than the value previously estimated but was expected since the subgrade stiffness probably increases with depth and the strain ratio decreases with depth.

For either case, the estimated permanent deformation at the top of the subgrade is insignificant when compared to the measured (somewhat greater than 1 in.) permanent deformation at the surface of the pavement. This is not inconsistent with observed behavior of the test item in which no detectable permanent deformation was measured at the top of the subgrade. The theoretical analysis of the permanent deformation in the subgrade and the observed condition of the polystyrene panels lead to the conclusion that nearly all of the observed permanent deformation occurred in the granular materials.

The conclusions reached as a result of an analysis utilizing layered elastic theory must be considered in the light of the probability that the vertical stresses are underpredicted. Morgan and Scala,[11] in a review of flexible pavement behavior and application of elastic theory to pavement analysis, came to the following conclusion: "The general failure of two and three layer systems to satisfy the Burmister prediction appears to be due to lower than expected modulus for the stiffer layers resulting from their inability to withstand

21

tension, or their dependence on confining stress which may not be suffi-
cient." The selection of values of moduli in this analysis was made
with the knowledge that materials not capable of sustaining tension
exhibit poorer load-distributing quality than a material of the same
modulus but having the capability of sustaining tension. The design
procedure presented in Barker and Brabston[10] provides for use of elastic
theory by direct correlation of computed strain values with pavement
performance. The real danger is when an attempt is made to predict per-
formance by directly comparing computed values of pavement response with
laboratory determined material properties. In the design of pavements
containing insulating layers, stresses computed by elastic layered
theory should be used with caution. In Figure 36, which shows the re-
silient deformation in the granular material, it can be seen that above
the polystyrene panels resilient strains on the order of 0.004 in./in.
are computed, which is about four times the strain allowed for the sub-
grade. Although no information is available on the resilient strain and
permanent strain for the granular material, it must be assumed that, at
such large resilient strains, large permanent strains would occur. If
the relationship between resilient strain and permanent strain for the
granular material is similar to the relationship developed for the sub-
grade, then the analysis would indicate that the major portion of per-
manent deformation occurred in the granular material between the as-
phaltic concrete surface and the insulating layer. Such a conclusion is
in agreement with the observed behavior of the test items.

No theoretical analysis was conducted for the other items, but
from the analysis of subitems 5c and 5d, some general deductions can be
made. In item 4, where there was less structure above the subgrade, it
would be expected that the permanent deformation in the subgrade would
contribute more to the total deformation than was the case in item 5.
The total result would be poorer performance of these items. If the
same characterization were used for the granular materials in sub-
items 5a and 5b as was used for subitems 5c and 5d, it would be found
that the modulus of the granular material above the lightweight concrete
would be much higher than that above the polystyrene panels. The

increased modulus values would result in lower computed strains within
these materials and a better load-distributing capability for these mate-
rials. The results of placing the stiffer material would be to improve
the load-carrying and distributing characteristics of the granular mate-
rials, thus improving the performance of the items. The improved stiff-
ness of these items is indicated by the measured deflections which were
less than 0.1 in.

The layout of the rigid pavement test section, including the sub-
items containing insulating layers, is shown in Figure 41. Item 5,
which contained the insulating layers, was divided into subitems 5a-5d
each composed of four 12-1/2- by 12-1/2-ft slabs. Subitem 5a contained
a 3-in.-thick layer of 35-psi polystyrene placed on the clay subgrade
over which was placed 6 in. of cement-stabilized lean clay. Subitem 5b
contained 9 in. of lightweight concrete directly on the subgrade. Sub-
item 5c contained 3 in. of 120-psi polystyrene placed directly on the
subgrade, and subitem 5d contained 3 in. of 35-psi polystyrene placed
directly on the clay subgrade. Fifteen-inch portland cement concrete
(PCC) slabs were placed on the above-described foundations.

CONSTRUCTION

The construction of the test section is described in detail in
Volume I of this report,[1] but will be summarized here for easy reference.
The subgrade was prepared by removing an existing rigid pavement test
section and reprocessing, compacting, and grading as necessary to obtain
the desired strength and elevation. The subgrade for subitems 5a and 5b
was excavated 6 in, deeper than that for subitems 5c and 5d to accom-
modate the 9-in. thickness of lightweight concrete in subitem 5b and the
6-in.-thick layer of cement-stabilized lean clay over the 3-in.-thick
layer of 35-psi polystyrene in subitem 5a.

After the subgrade was graded, the cement-stabilized lean clay
base for item 4 and the transition slab between items 4 and 5 were
placed. The reinforced concrete transition slab between items 4 and 5
was then placed. Next the lightweight concrete was placed, as described
for the flexible pavement section. The polystyrene panels in sub-
items 5a, 5c, and 5d were then placed, by hand, directly on the sub-
grade. The panels were staggered in a pattern as illustrated in Fig-
ure 42. The cement-stabilized lean clay for subitem 5a was premixed,
placed on the panels, spread, and compacted with a 30-ton pneumatic-
tired roller which had a tire pressure of about 60 psi. The

cement-stabilized lean clay had to be placed in the space between the lightweight concrete and the transition slab between items 4 and 5. As can be seen in Figure 42, the construction sequence restricted the space available for operating construction equipment.

The 15-in.-thick PCC surfacing was placed in two 25- by 50-ft lanes; the north lane being placed first. Concrete was mixed in ready-mix trucks, placed between forms with a crane and bucket, and consolidated with internal hand vibrators. The surface was screeded with a straightedge and hand finished with bull floats and trowels. Construction techniques are illustrated in Figure 43. The concrete was wet-cured with burlap and plastic sheeting for 7 days.

The north and south lanes were separated by a keyed-and-tied longitudinal construction joint as shown in Figure 44. The keyway was formed in the north slabs by wooden strips fastened to the forms. Thin metal strips were attached to the base to provide weakened planes at 12-1/2-ft spacings both transversely and longitudinally. In addition, saw cuts were made in the tops of the slabs to further weaken the section, and to form a straight groove for ease in sealing. A crack developed between subitems 5b and 5c in the north lane prior to sawing, resulting in an irregular joint. Grooves for joint seal installation were sawed in the construction and contraction joints and filled with hot-poured joint sealing compound meeting Federal Specification SS-S-164(4).[12] The crack between subitems 5b and 5c was not sealed.

PROPERTIES OF AS-CONSTRUCTED PAVEMENTS

No field tests were conducted in item 5 as construction was progressing. However, plate bearing tests, conducted according to Military Standard MIL-STD-621A, Method 104,[13] on items 1-4, yielded modulus of soil reaction values for the subgrade of from 40 to 85 pci with an average of 65 pci. The subgrade in item 5 was similar.

· Flexural tests on 6- by 6- by 36-in. beams,[5] compression tests,[3] and split ng tensile tests[14] on 6-in.-diam by 12-in.-long cylinders yielded average flexural and compressive tensile strengths of 542 and 5150 psi, respectively, at 28 days age. Properties of the lightweight

25

concrete and polystyrene panels have been enumerated previously.

TRAFFIC

Traffic was applied to the rigid pavements containing insulating layers with 200- and 240-kip twin-tandem assemblies having 190- and 250-psi tire inflation pressures, respectively. The layout of the traffic lanes is shown in Figure 41. Traffic with the 200-kip assembly was applied along the longitudinal construction joint in lane 1, and traffic with the 240-kip assembly was applied in lane 2. A detailed description of the application of traffic and subsequent performance of the pavement is contained in Volume I.[1]

Table 5 summarizes the traffic data for the rigid pavements containing insulating layers. Three failure conditions are listed: initial crack, shattered slab, and complete failure. The pavement conditions considered to constitute failure for unreinforced PCC pavements are as follows:

a. Initial crack failure. A crack that is visible at the surface of the pavement, extends through the depth of the slab, and is caused by traffic loading constitutes the initial crack failure condition. This should not be confused with surface cracking resulting from such minor defects as spalls, popouts, shrinkage, etc. It must also be recognized that concrete may crack during its early life due to causes other than traffic loadings, and any such cracks should not be construed as denoting the initial crack failure condition.

b. Shattered slab failure. Cracking that is visible on the pavement surface or subdivides a pavement slab into six pieces or more constitutes the shattered slab failure condition. The cracking must be associated with traffic loading rather than resulting from some minor defect or early life cracking prior to application of traffic.

c. Complete failure. Cracking that is visible on the pavement surface and subdivides the pavement slab into individual pieces having an area of less than about 15 to 20 sq ft each and that is characterized by relatively large permanent deformations and faulted cracks or joints constitutes complete failure.

Failure for subitems 5a-5d was difficult to assign because the behavior was somewhat different from that normally observed. Cracking did not develop in the usual manner; i.e., dividing the slabs into large pieces.

26

Cracking usually developed along joints (at times being short discontinuous cracks). As cracking progressed, spalling and eventually total disintegration occurred along joints. Faulting along joints and pumping were also observed. Another anomaly in the performance of several subitems was that cracking developed outside the traffic lane, but not within the traffic lane. The exceptions were subitem 5c with the 200-kip loading and subitem 5d with the 240-kip loading. In these two subitems, cracking developed and progressed as expected.

Pumping occurred in all subitems and was considered a significant factor in performance of all subitems. The pumping was normally associated with rainfall and would continue after rainfall had ceased. The duration and severity of pumping increased as the level of applied traffic increased.

Because of the unusual performance of the pavement containing insulating layers and the uncertainties involved in assigning failure as listed in Table 5, the detailed descriptions of the behavior of the pavements contained in Volume I[1] will be repeated herein. This is provided so that the reader can develop an accurate picture of the pavement condition and draw his own conclusions regarding the serviceability of the pavements at the various levels of applied traffic.

Traffic was applied in lane 1 with the 200-kip load and then in lane 2 with the 240-kip load. The development of cracking is shown in Figure 45. The development of permanent deformation in each subitem with traffic is shown in Figures 46-49.

SUBITEM 5a, LANE 1

The first cracks developed parallel to and about 1 ft south of the longitudinal construction joint (Figure 50) at about 1770 coverages. As traffic progressed the cracking and spalling along the joint continued until traffic was discontinued after 3000 coverages (Figure 51). As can be seen in Figures 45, 50, and 51, no structural cracking, as normally observed in PCC pavements, was evident; thus the indication of joint failure in Table 5. Pumping of the cement-stabilized material at the transverse joints was first observed at 750 coverages. The pumping

27

began after a rainfall of 0.25 in. The severity of pumping increased as traffic was applied. The measured permanent deformation at 3000 coverages averaged about 1.1 in. with a maximum of 1.4 in. A maximum differential movement of about 0.6 in. occurred along the longitudinal construction joint at 3000 coverages. It can be seen in Figure 46 that the permanent deformation and differential movement were more severe at the ends of the subitem than they were in the interior.

SUBITEM 5a, LANE 2

Some cracking developed in the slabs north of the longitudinal construction joint prior to application of the 240-kip traffic in lane 2. Some spalling had also occurred along the transverse joints north of the longitudinal construction joint prior to traffic in lane 2. This cracking and spalling, portions of which are visible in Figure 52, developed during traffic in lane 1, during turnaround operations while traffic (beyond 3000 coverages) was applied to items 1-4, and during collection of static instrumentation data in lane 2. The location of the cracks is shown in Figure 45b. This cracking was outside the traffic lane and was not considered in assigning failure during application of traffic in lane 2. No major structural cracks developed during traffic but cracking and spalling occurred along the longitudinal contraction joint and the transverse joint between subitems 5a and 5b. The condition of the pavement at 200 coverages is shown in Figure 53. At 500 coverages spalling was noted at the west end of the longitudinal joint and progressed with continued application of traffic. The cracking and spalling were severe at 750 coverages and the longitudinal joint and the transverse contraction joint between subitems 5a and 5b were considered as failed. Traffic was continued to 950 coverages at which time the condition of the pavement was as shown in Figure 54. Pumping of the cement-stabilized material was initially noted at 350 coverages and became progressively more severe as traffic progressed. Evidence of pumping can be seen in Figure 54. The pumping followed a period of rainfall in which 2.05, 0.15, and 0.16 in. of rain occurred on 3 successive days. The measured pavement deformation at 950 coverages averaged about 0.6 in. with a maximum

28

of about 0.7 in. As can be seen in Figures 48 and 54, the differential movement, even at 950 coverages, along the longitudinal joint was small. However, in Figure 54, there appears to be considerable differential movement between subitems 5a and 5b.

SUBITEM 5b, LANE 1

The deterioration of this subitem was limited to a strip along the south side of the longitudinal construction joint. The first spalling and cracking was noted at 1770 coverages (Figure 55). Cracking and spalling progressed with the application of traffic and were severe at 3000 coverages as indicated in Figure 56. No structural cracking, as normally observed in PCC pavements, was evident; thus the indication of joint failure in Table 5. Pumping was first observed at the transverse joint separating subitems 5b and 5c at about 340 coverages (following a 0.49-in. rainfall) and at the joint separating subitems 5a and 5b at 740 coverages (following a 0.25-in. rainfall). The pumped material was apparently from beneath subitems 5a and 5c, rather than 5b. The measured permanent deformation, at 3000 coverages, averaged about 0.65 in. with a maximum of 0.9 in. A maximum differential movement of 0.3 in. had developed along the longitudinal construction joint at 3000 coverages. In Figure 46 it can be seen that the permanent deformation and differential movement were greater at the west end of the subitem than they were in the interior.

SUBITEM 5b, LANE 2

The performance of subitem 5b was similar to 5a. The only structural cracking occurred outside the traffic lane prior to traffic and consisted of one crack as shown in Figure 45. Spalling along the transverse joint between subitems 5b and 5c began soon after traffic was started. This was the joint which formed before the top groove could be sawed. Spalling began along the longitudinal joint at 540 coverages and at 740 coverages extended for the full length of the subitem. The spalling along both the east transverse joint and the longitudinal joint is shown in Figure 57. Pumping along the longitudinal joint and the

29

transverse joint between subitems 5b and 5c began at about 320 coverages (following 2.05-in. rainfall). The severity of pumping increased as the applied traffic increased. Evidence of pumping can be seen in Figure 57. The measured permanent deformation averaged about 1.3 in. with a maximum of about 1.9 in. at 950 coverages. There was a differential movement of about 1 in. along the longitudinal joint. This is shown in Figures 48 and 57.

SUBITEM 5c, LANE 1

The initial crack failure condition was assigned at 1000 coverages. The condition of the pavement is illustrated in Figure 58. Additional cracking occurred until the shattered slab failure condition was reached at 1230 coverages as illustrated in Figure 59. There was rather severe cracking and spalling along the longitudinal construction joint and the transverse contraction joint between subitems 5b and 5c just north of the longitudinal construction joint (Figures 58 and 59). The transverse joint was the one where cracking occurred before the groove in the top could be sawed and this accentuated the spalling. Landing mat was placed over subitem 5c after 1230 coverages. Pumping of the clay subgrade was observed at the east end at about 200 coverages (following a 1.08-in. rainfall) and at the west end at 340 coverages (following a 0.49-in. rainfall). The pumping became extremely severe as traffic was continued. The cross sections in Figure 47 indicate that the maximum permanent deformation at 1000 coverages was about 0.3 in. with very little differential movement between the north and south slabs. This seemed inconsistent with the amount of pumping. However, at 1230 coverages a differential movement of 0.6 in. was measured.

SUBITEM 5c, LANE 2

The failure of this subitem was much like that in subitems 5a and 5b in that the primary distress was the spalling and faulting along the longitudinal contraction joint. The only cracking occurred prior to traffic outside the traffic lane and consisted of a longitudinal crack north of the longitudinal construction joint and cracking along the

transverse contraction joint between subitems 5c and 5d. Spalling and
cracking along the longitudinal joint began at about 160 coverages and
extended along the entire length of the joint at 430 coverages. The
spalling was severe and the joint was considered as failed at 740 cover-
ages although traffic was continued to 840 coverages, at which time the
pavement had reached the condition shown in Figure 60. Pumping was ini-
tially noted at the transverse joint between subitems 5c and 5d at
320 coverages (following a 2.05-in. rainfall). The measured permanent
deformation at 840 coverages averaged about 1 in. with a maximum of
1.1 in. The cross sections in Figure 49 show a maximum differential
movement of about 0.6 in. along the longitudinal joint near the west end
of the subitem at 840 coverages.

SUBITEM 5d, LANE 1

The first crack observed in this subitem was a longitudinal crack
located about 2 ft south of the south edge of the traffic lane. This
crack did not extend from a free edge to a free edge but extended from
the east edge to the center of the slab. The crack did not propagate
to a second free edge, open up, or spall with additional traffic up
to 3000 coverages. The history of this crack is illustrated in Fig-
ures 45, 61, and 62. Because the crack occurred outside the traffic
lane and because it did not deteriorate with traffic, it probably did
not extend for the full depth of the slab and was not considered repre-
sentative of a failure condition. Therefore, in Table 5 the failure of
the item is denoted by a joint failure. At 2220 coverages cracking and
spalling developed along the longitudinal construction joint and at
3000 coverages extended for the full slab length as shown in Figure 62.
The deterioration was not, however, as severe as it was in sub-
items 5a-5c. Pumping was observed initially along the transverse joint
between subitems 5c and 5d at 220 coverages (following a 1.08-in. rain-
fall), but was not observed along the east edge until 750 coverages
(following a 0.25-in. rainfall). The cross sections shown in Figure 47
indicate a maximum permanent deformation of about 0.3 in. at the west
end and very little differential movement between the north and south

31

slabs. The cross sections also show that the permanent deformation and differential movement were largest at the west end which is consistent with observations of pumping.

SUBITEM 5d, LANE 2

At 20 coverages, cracks developed within the traffic lane as shown in Figure 45. Cracking continued and spalling began along the cracks until the shattered slab failure condition was reached at 200 coverages (Figures 45 and 63). Cracking along the longitudinal joint at the west end was evident at 200 coverages. Traffic was continued to 350 coverages. No additional major structural cracks occurred, but spalling along the cracks and along the entire length of the longitudinal joint was quite severe as shown in Figure 64. No pumping of any consesequence occurred prior to termination of traffic at 350 coverages. At 350 coverages a maximum permanent deformation of about 0.6 in. was measured. As shown in Figure 49, the maximum permanent deformation did not occur along the longitudinal joint, but occurred north of the joint near the center of the traffic lane. This coincided with the intersection of the major structural cracks. The differential movement along the longitudinal joint was small as shown by the cross sections in Figure 49.

AFTER-TRAFFIC INVESTIGATIONS

The after-traffic testing program consisted of the excavation of test pits for observation of the condition of the insulating layers, performing plate bearing tests to evaluate the modulus of soil reaction of the foundation material, and sampling and testing the portland cement and lightweight concrete to assess their strength and modulus. The measured properties are summarized in Table 6. Beams and cores of the lightweight concrete tested in compression and flexure yielded a flexural strength of 127 psi, a flexural modulus of 0.373×10^6 psi, a compressive strength of 271 psi, and a compressive modulus of 0.134×10^6 psi. Load-deflection curves for the plate bearing tests are contained in Figures 65 and 66.

Upon examination of the results from the plate bearing tests, the following observations were made:

32

<u>a</u>. The average soil reaction modulus was 132 pci This is con-
    sistent with values measured in items 1-4 (aft.. traffic)
    where the average was 146 pci. Because of the similarities
    in the after-traffic soil reaction modulus, it was assumed
    that the as-constructed subgrade in item 5 was similar to
    that in items 1-4. Items 1-4 had an average modulus of soil
    reaction, measured prior to traffic, of 64 pci.

<u>b</u>. The polystyrene layers reduced the modulus of soil reaction.
    In Figure 67, it can be seen that the 3-in. layer of 120-psi
    polystyrene in subitem 5c reduced the modulus from 120 to
    63 pci and that the 3-in. layer of 35-psi polystyrene in sub-
    item 5d reduced the modulus from 143 to 103 pci. In sub-
    item 5a the modulus of soil reaction on top of the 35-psi
    polystyrene was 78 pci. Assuming that the effect of the
    35-psi polystyrene layer would be similar to that in sub-
    item 5d, the modulus of soil reaction on top of the subgrade
    in subitem 5a was probably greater than 78 pci.

<u>c</u>. The modulus of soil reaction values on top of the ,5-psi poly-
    styrene were higher than the value for the 12ᴄ-psi polysty-
    rene. This ᵢs inconsistent with the strength and stiffness
    properties of the material. However, because only a small
    number of tests were run, no definite conclusions can be drawn
    concerning this apparent anomaly. Possible causes for the in-
    consistencies are differences in the subgrade stiffness (as
    indicated betwee:. subitems 5c and 5d), the inherent variabil-
    ity in the test procedures, and poor seating of the panels.

<u>d</u>. The measured modulus on top of the cement-stabilized lean
    clay in subitem 5a was 188 pci as compared to 328 pci in
    item 4. The difference was probably caused by the effects of
    the polystyrene in the structure and/or lack of compaction in
    the 6-in. cement-stabilized layer. The lack of compaction
    was thought to be caused by the presence of the polystyrene
    and the confined working space (see Figure 42).

<u>e</u>. The stiffening effect of the 9-in. lightweight concrete in
    subitem 5b is evident from the measured modulus of soil
    reaction of 420 pci.

    The cracking along the longitudinal construction joint in sub-
items 5a, 5b, and 5d, and to some extent in 5c, developed about 1 ft
south of the joint. This is about at the end of the tie bars, and the
spalling and breakout of material along the joint appeared to progress
at about a 45-deg angle to the joint. However, during removal of the
slabs from the test pits, the tie bars and joint were disturbed so that
the actual condition of the joints could not be verified.

    The test pit in subitem 5c, lane 1, revealed that the panels were

33

cracked along the longitudinal construction joint. The cracks were located about 1 ft south of the joint. In addition, there were several cracks in the center of the slab about 6 ft south of the longitudinal construction joint. The condition of the 120-psi polystyrene panels is illustrated in Figure 68.

The test pit in subitem 5b, lane 2, revealed that a crack had developed in the lightweight concrete along the longitudinal joint. As can be seen in Figure 69, the surface of the lightweight concrete on the north side of the joint was about 1 to 2 in. lower than on the south side. Evidence of differential movement in the pavement can also be seen in the cross sections shown in Figure 48. During removal of the slab in the test pit, it was observed that the slab was bonded to the lightweight concrete. When the lightweight concrete was removed, evidence that the subgrade material had pumped up through the crack in the material was noted. Evidence of this is shown in Figure 70 which shows a seam of clay material through the crack in the lightweight concrete.

The test pit in subitem 5c, lane 2, revealed that the 120-psi polystyrene panels were cracked along the longitudinal contraction joint at a distance of from 6 to 12 in. north of the joint. The condition of the panels is illustrated in Figure 71.

ANALYSIS OF TEST RESULTS

The analysis of the results of the tests will consist of a comparison of the actual performance of the pavements with expected performance based on current design criteria (Corps of Engineers (CE) and Federal Aviation Administration (FAA) criteria). The behavior will then be analyzed to determine why the pavements performed as they did. This will basically involve a study of the support provided by the foundations containing insulating layers and the effects of a number of factors on the stresses and deflections in the pavement system which influenced the performance of the pavements.

COMPARISON OF OBSERVED AND PREDICTED PERFORMANCE

The performance data for the pavements containing insulating

layers are contained in Table 5. The performance of the pavements was
characterized by failure along the longitudinal construction and contrac-
tion joints in all but three situations. These being subitem 5c, lane 1,
and subitem 5d, lane 2, where failure due to cracking occurred, and suo-
item 5d, lane 1, where some distress along the longitudinal joint had
occurred when traffic was stopped (3000 coverages) but the joint was not
considered failed.

FAA and CE first crack failure (initial failure) design criteria
are based on cracking of the slabs. Using these criteria and the prop-
erties of the pavements listed below, the expected performance of the
pavements was computed:

> Slab thickness = 15 in.
>
> Concrete modulus of elasticity = 6×10^6 psi
>
> Concrete Poisson's ratio = 0.2
>
> Concrete flexural strength
>
> > Lane 1 = 833 psi
> >
> > Lane 2 = 863 psi
>
> Modulus of soil reaction
>
> > Subitem 5a = 190 pci
> >
> > Subitem 5b = 420 pci
> >
> > Subitem 5c = 60 pci
> >
> > Subitem 5d = 100 pci

The predicted performance is summarized in Table 7 along with the
actual performance. It can be seen that joint failures generally oc-
curred at coverage levels much lower than those predicted. The excep-
tions being subitem 5c, lane 1, where the predicted and observed perfor-
mances were close, and subitem 5c, lane 2, where the observed performance
was somewhat better than predicted.

A comparison of the observed and predicted performances may also
be made by computing the ratio of the concrete flexural strength to the
computed stress, referred to as the design factor, and plotting this
r   versus the log of the observed coverage level, as shown in Fig-
ure 72. . . · shown in the figure is the CE and FAA relationship for
first cra.: fai ·ꞏꞏe (design or performance) criteria. With the

35

exception of two situations mentioned previously, the points all plot
above the performance relationship indicating that the pavement perfor-
mance was not as good as expected.

When comparing the observed performance with the established per-
formance criteria, several factors should be considered. The scatter in
the data points (Figure 72) appears quite large, but historically pave-
ment performance data has exhibited large variability. Some of the
possible reasons for the large variability will be considered subse-
quently. The mode of failure observed (joint failure rather than crack-
ing of the slabs) is a factor in assessing not only the scatter but also
the relative performance of the pavements. The data points exhibit con-
siderable scatter and indicate poorer performance than the established
criteria, but it should be noted that the points, for the two cases
where the failure was due to cracking, are reasonably close to the es-
tablished performance relationship.

In assessing pavement performance, there is the ever-present
problem of assigning representative flexural strength values. The as-
signment of foundation support values is also a problem. In particular,
the modulus of soil reaction used was the value measured after comple-
tion of traffic, which should have been larger than it was the
beginning of traffic. Although no tests were run in item 5 prior to
traffic, before and after tests in items 1-4 indicated that the stiff-
ness of the subgrade increased with traffic. Tests on the base in all
but item 3 also showed an increase in modulus of soil reaction with
traffic. Therefore, the support values used in the analysis were prob-
ably larger than those which were effective during traffic; thus, the
predicted performance should have been better than that observed. How-
ever, the differences indicated for subitems 5a and 5b are too large to
be attributed to the foundation support.

There was some evidence to indicate that the difference between
the before- and after-traffic soil modulus values on the polystyrene in
subitems 5c and 5d should have been larger than could be attributed to
an increase in the subgrade stiffness. Poor seating between the poly-
styrene panels and the subgrade could have produced unusually low

support values until traffic produced sufficient plastic deformation to provide uniform contact between the panels and the subgrade. As a result, the initial support values could have been much lower than indicated by after-traffic tests.

The poor seating of the panels and the confined working space could have affected the compaction of the cement-stabilized layer in subitem 5a. However, the lack of compaction should have been most pronounced at the ends of the slabs which would have been manifest by deterioration of the transverse joints. However, as noted previously, the longitudinal joints deteriorated rather than the transverse joints. The performance of the transverse joints also discredits the theory that the discontinuity (nonuniformity) of the foundation was a primary factor in the unusual performance. While it is true that deterioration usually starts near transitions (of which there were five), this did not appear to be an important factor, since all transverse joints remained relatively free from cracking and spalling.

The primary difficulty in assessing the performance of the pavements, however, revolved around the mode of distress in the pavements; i.e., cracking and spalling along the joints. There were apparently some rather significant differences between the responses to imposed loads of the slabs on the insulating layers and those on normal foundations. This difference was manifested in the joint distress rather than cracking.

The relatively small slab size (12-1/2 by 12-1/2 ft), large thickness (15 in.), and large load (magnitude and 44 by 58 in. spacing of four wheels) could have created unusual stress and deflection patterns within the pavement. This may have resulted in rocking or rotation, rather than bending, of the short, stiff slabs. This would have produced tensile stresses in the slabs which were within tolerable limits but deflections at joints which could have caused unusually large localized stresses along the joints. Once again, the fact that the transverse joints did not deteriorate reduces the credibility of this argument.

However, the concept appears much more attractive when the manner in which loads were applied and the unusual properties of the insulating

37

materials are considered. The loads were applied primarily along one side of the longitudinal construction joint in lane 1 and along the longitudinal contraction joint in lane 2. This resulted in permanent deformation along one side of the joint which accentuated the rocking of the slab and deflection along the joint.

It is tempting to attribute the unusual pavement response to the unusual properties of the insulating materials (these properties being a Poisson's ratio of approximately zero and a crushing mode of failure). For the polystyrene panels, there is the additional factor of anisotropic load deformation and strength characteristics; i.e., the material is stronger and stiffer when loaded perpendicular to the faces of the panels. These properties combined with the application of loads over a limited pavement width would have led to pavement response which was different than that for conventional paving materials. In particular, a zero Poisson's ratio and a crushing failure mode would not have resulted in a tendency for the material to expand horizontally upon loading. Therefore, there would have been no buildup of residual horizontal stresses and no resulting increase in stiffness with traffic. The crushing mode of failure would also have prevented any remolding of the material with the application of loads along adjacent paths. Because of the anisotropic material response, the stiffness of the polystyrene layers may have been less than predicted with the material properties, as measured from compression tests with the load applied perpendicular to the direction of the panel face. However, the response and condition of the pavements did not indicate that the properties of the insulating layer were a significant factor in the performance of the pavements.

The permanent deformations in subitems 5c and 5d appeared to occur primarily in the subgrade and were apparently caused by densification and shear. In subitem 5a, the permanent deformation appeared to be primarily caused by pumping of the cement-treated lean clay. There was also evidence of pumping of the subgrade material (especially in lane 2) in subitems 5c and 5d. The response of the pavement in subitem 5b, lane 2, was unique. A differential movement along the longitudinal contraction joint of about 1 in. was observed on the surface

38

and on top of the lightweight concrete in the test pits. A crack had developed in the lightweight concrete along the joint. It is not known what caused this crack, but it may have been a shear failure caused by the loading along the joint. Another possibility is that, due to the bond between the PCC slab and the lightweight concrete, the crack could have been caused by bending or a combination of bending and tensile stresses, the bending being caused by loading and the tensile stresses by shrinkage of the PCC surfacing. The effect of the crack was to increase the stresses on the subgrade and to cause pumping of the subgrade material through the crack.

The combined effects of slab size, magnitude of load, application of load on one side of the joints, and large permanent deformations may have caused unusually large stresses near the joints. As the slabs rotated and deflected downward, large horizontal compressive forces would have resulted in the top of the slabs, as illustrated in Figure 73. This force combined with the shearing forces transferred across the joint would have resulted in large shear stresses in the material, and would account for the cracking and spalling along the edge of the joint nearest to the center of the traffic lane. The deterioration is illustrated in Figures 51, 54, 56, 57, 59, 60, 62, and 64, and it can be seen that the cracking and spalling occurred primarily along only one side of the joint.

An additional factor which may possibly have affected the performance of the pavements containing polystyrene panels was the fact that the layers were discontinuous; i.e., made up of separate panels. As will be discussed in more detail in the following section, the presence of the polystyrene layers decreased the supporting capacity of the foundation, rather than increasing it as it should have, based on the properties of the material. It is possible that the reduction in the supporting capacity, as measured with a 30-in.-diam plate, would be smaller than that experienced by the slabs; i.e., the effective supporting capacity experienced by the slab was less than that measured by the plate bearing test. This may have accentuated the deflections along the joints.

39

The discontinuities in the layer and rigidity of the individual panels probably also accentuated the pumping of the subgrade. The panels probably had sufficient stiffness to rebound after the load had passed, whereas the subgrade would have been permanently displaced, creating a small void beneath the panels which would have acted as a reservoir for water. With additional applications of load, the panels would have again deflected, ejecting the water and suspended subgrade material. This would have continued until the panels cracked, as they apparently did in some cases. An unexplainable anomaly to this argument was the transverse joints where the pumping was more noticeable than along the longitudinal joints, but which performed satisfactorily.

ANALYSIS OF SUPPORTING CHARAC-
TERISTICS OF INSULATING LAYERS

Measured load deformation curves from plate bearing tests on the subgrade and the insulating layers are shown in Figures 65 and 66. The values of modulus of soil reaction and the locations where they were measured are illustrated in Figure 67. Some of the apparent anomalies in the measured supporting characteristics of the insulating layers were pointed out previously and will be considered in detail in this section.

In order to study the nature of the supporting characteristics of the insulating layers, the plate bearing tests were simulated with an axisymmetric linear finite element program. The mesh used for the simulation is shown in Figure 74.

A modulus of 1950 psi was selected for the subgrade from a trial-and-error procedure. The subgrade was assumed to have a modulus of soil reaction of 132 pci (average of values measured in subitems 5c and 5d). With a plate pressure of 10 psi, the modulus was varied until a plate deflection of 10/132 in. was obtained. A Poisson's ratio of 0.4 was assigned for the subgrade material.

The 35-psi polystyrene was assigned a modulus of 1950 psi. This is based on the assumption that this material would behave similar to the 120- and 60-psi polystyrene as shown in Figure 3; i.e., the ultimate compressive strength (35 psi) is developed at 2 percent strain, and up

40

to this level of strain the stress-strain curve is approximately linear. A Poisson's ratio of zero was assigned based on observations of the response of the material in unconfined compression tests and in previously described CBR tests. Similarly, a modulus of 6000 psi was assigned for the 120-psi material; i.e., the stress-strain relationship from the unconfined compression tests in Figure 3. The resilient modulus for the material is similar, as shown in Figure 4. A Poisson's ratio of zero was also assigned to this material.

The lightweight concrete was assigned a modulus of 250,000 psi. This is based on unconfined compression tests of cylinders conducted according to ASTM 469-65.[6] Modulus values computed from flexural tests on beams were somewhat larger. However, it was felt that the results from the compressive tests were more representative of the response of the material. A Poisson's ratio of zero was assigned to the lightweight concrete. This results because the polystyrene beads control the response of the material and are crushed, with little lateral volume change, as load is applied.

A modulus value of 50,000 psi was assigned the cement-stabilized lean clay. This was based on the results of unconfined compression tests on cylinders of the material mixed in the field and compacted in the laboratory. Modulus values from flexural tests on beams, indirect tensile tests on cylinders, and repetitive load tests on cylinders. yielded larger values. However, it was felt that the static unconfined compression tests were the most representative for the static plate loading tests. A Poisson's ratio of 0.15 was assigned.

The plate bearing tests were simulated by applying a plate pressure of 10 psi to the layered systems described by combinations of the elastic constants. The resulting load-deformation relationships for subitems 5a-5d are plotted with the measured relationships in Figures 75-78. For all four subitems, the computed stiffness of the system is greater than the measured stiffness.

In Figure 75, the measured and computed cruves for subitem 5a are shown. The difference in the slopes of the early portions of the curves is 124 pci or about 66 percent of the measured value. There are three

41

possible causes for the differences in the measured and computed stiffness. The compaction of the 6-in. layer in the field may not have been as good as that obtained in the laboratory because of the flexibility of the underlying polystyrene panels on the clay subgrade. Secondly, the 35-psi polystyrene was in panels and may have been more flexible than if it were continuous as modeled. This would mean that the effective modulus of the layer was less than 1,750 psi. This factor will be considered in subitems 5c and 5d. Finally, traffic may have caused cracking or localized failures in the stabilized layer reducing the effective modulus of the material to some value lower than 50,000 psi.

The load-deformation curves for subitem 5b shown in Figure 76 show that the measured stiffness of the system is approximately one half the computed stiffness (difference of 415 pci). No verified explanation can be offered for this difference. The modulus of the lightweight concrete might be suspect, but the results from compression tests, which were considerably less than the results from flexure tests, were used. The most likely possibility seems to be that traffic caused some reduction in the stiffness of the lightweight concrete and thus a reduction in the stiffness of the system. A reduction in the stiffness of the subgrade is excluded since all evidence in other items points toward an increase with traffic. The plate bearing test was conducted in lane 2 where the 240-kip assembly load was applied. Cracking of the lightweight concrete along the joint was observed in the test pit, and the slab was bonded to the lightweight concrete and had to be broken loose during construction of the test pit. There may have been additional cracking in the lightweight concrete which was not noted which could have affected the plate bearing results. The removal of the slab may also have adversely affected the stiffness of the materiel. The repeated application of pressures of between 10 and 20 psi may also have resulted in some crushing of the polystyrene beads in the concrete matrix. Once the structure within the beads had been destroyed, they could have become very weak, resulting in a weakening of the total matrix. This is a possible cause of the differences in the stiffness,

42

although unsubstantiated since no repeated load tests were run on the lightweight concrete.

Curves for subitems 5c and 5d are shown in Figures 77 and 78, respectively. As noted previously the lower strength (more flexible) 35-psi panels had a higher stiffness than did the 120-psi panels. This has been discussed previously and may be attributable to local differences in the subgrade stiffness and test variation. However, it is also interesting to note that the computed stiffness for both cases is less than the measured stiffness. This is probably caused by the fact that the material was in discontinuous panels rather than in a continuous layer as modeled. The 30-in. diameter would have had to span at least one joint since the panels were 16 and 24 in. wide, respectively, for 120- and 35-psi panels. As a result the effective modulus of the layer was probably lower than 6000 psi for the 120-psi polystyrene and 1750 psi for the 35-psi polystyrene. The combined effects of differences in subgrade stiffness (different than the average modulus of soil reaction of 132 pci) may explain the differences between the measured and computed stiffness and the variation in the magnitude of the difference between the two items. There is also the possibility that poor seating of the panels on the subgrade could have caused a reduced stiffness of the system, although the application of traffic should have minimized these effects.

In summary, it can be concluded that the measured stiffness was always less than the computed stiffness. The modulus values used in the simulation of the plate bearing tests were conservative estimates usually based on the test procedure giving the smallest values. Therefore, it is concluded that the insulating layers have different supporting characteristics than normal paving material and that the polystyrene layers reduced the supporting capacity of the subgrade. The primary reasons for this are thought to be the flexibility of the polystyrene layers caused by the discontinuities in the layer, the compressibility of the polystyrene beads in the lightweight concrete, and the low or nearly zero Poisson's ratio of the insulating materials. The low Poisson's ratio permits vertical compression without any lateral expansion.

43

Therefore, there is no buildup of horizontal confining stresses and the resulting stiffening of the material.

ANALYSIS OF PAVEMENT
STRESSES AND DEFLECTIONS

In this section, the stresses in the PCC slabs and the deflections experienced by the pavements will be examined. Measured deflections, computed deflections, and computed stresses will be examined to determine the causes for the unusual performance of the pavements containing the insulating layers; i.e., why localized cracking and spalling occurred along the longitudinal joint rather than cracking of the slab.

The measured deflections were obtained with a rod and level. The initial readings were taken with the dual-tandem gear in place (centered longitudinally in the slabs with two of the wheels tangent to either the longitudinal const uction joint in lane 1 or the longitudinal contraction joint in lane 2) and final readings taken after the load was removed. The deflection was obtained by subtracting the initial reading from the final reading. This rebound deflection is representative of the elastic deflection experienced by the pavement.

Stresses and deflections were computed for edge and interior load positions on dense liquid foundation conditions with equations as developed by Westergaard.[15-19] The actual computations were accomplished using influence charts developed by Pickett, et al.[20] and Pickett and Ray.[21] Stresses and deflections were also computed using the discrete element method as developed by Hudson and Matlock.[22] Actual computations were accomplished using a computer code developed by Panak and Matlock.[23] The discrete element method is based on the same basic model as the Westergaard method (i.e., a thin slab on a dense liquid foundation), but uses finite difference approximations for solving the equations of bending rather than a closed form solution. With the discrete element method, discrete slabs may be considered, whereas, the equations developed by Westergaard and graphically displayed in the influence charts are based on the assumption of semi-infinite slabs.

Table 8 contains a summary of maximum measured and computed

44

deflections. Properties of the slabs and foundation support values used
in the computations were as previously described. Maximum computed
stresses are summarized in Table 9. Deflections and stresses at the
pavement edge (with the load at the edge) and deflections and stresses
within the interior of a slab (with the load located within the slab
interior) were computed using the influence charts. These are contained
in Columns 4 and 5 of Table 8 and Columns 2 and 3 of Table 9. The
values in parentheses in Column 2 of Table 9 are computed values of edge
stress multiplied by 0.75. This procedure is followed in design to
represent the stress conditions at a joint where the actual stresses
would be less than the computed free-edge stresses because of the upward
force on the loaded slab produced by the adjacent slab.

For the discrete element method, deflections and stresses are
shown for 12-1/2- by 12-1/2-ft slabs and for 25- by 25-ft slabs. The
actual slab size was 12-1/2 by 12-1/2 ft, and the pavement as modeled
with the finite element method is shown in Figure 79. The increment
length used was 1-1/2 ft. The bending stiffness along the contraction
joints and along the doweled construction joint between the transition
slab and subitem 5a was reduced by 100 percent; i.e., the joints func-
tioned as hinges with no moment capacity but with full shear transfer.
The bending stiffness along the keyed-and-tied longitudinal construction
joint was reduced by 94 percent. The shear transfer capability along
the joints was 100 percent. The load was applied along the longitudinal
construction joint as illustrated for subitem 5a in Figure 79, and along
the longitudinal contraction joint as illustrated for subitem 5c in
Figure 79.

In order to study the effects of slab size, stresses and deflec-
tions were computed assuming that the slabs were 25 by 25 ft. For
15-in.-thick slabs, a 25-ft joint spacing is more realistic than a
12-1/2-ft spacing. An illustration of the discrete element model for
this condition is shown in Figure 80. Subitems 5b-5d are modeled as if
the slabs were 25 by 25 ft. This model was used for loading in sub-
items 5c and 5d, lane 1. For loading in lane 2, the longitudinal joint
was changed to a contraction joint. For loading in subitem 5b,

45

subitem 5a was added and subitem 5d was eliminated from the model. It was necessary to restrict the extent of the pavement modeled because of computational requirements; i.e., with a 1-1/2-ft increment length it would have been excessively costly and time-consuming to model the entire item as was done for the 12-1/2- by 12-1/2-ft slabs.

Measured and computed deflection basins are shown in Figures 81-92. In these figures, measured deflection basins for transverse lines through two of the wheels of the dual-tandem assembly and for longitudinal lines through the centroid of the dual-tandem assembly are plotted. In addition, deflection basins computed with the discrete element method are shown for transverse lines through two of the wheels and for lines along the longitudinal construction joint in lane 1 and along the longitudinal contraction joint in lane 2. For the transverse lines the measured and computed positions were the same. However, for the longitudinal lines, the measured values were taken along the longitudinal axes of the gear but the computed values were force lines along the longitudinal joints. Basins are shown for the computations with 12-1/2- by 12-1/2-ft slabs and in selected cases for the computations with 25- by 25-ft slabs assumed. For lane 1 the loading on four wheels was 200 kips, and for lane 2 the loading on four wheels was 240 kips.

Deflections. From the analysis of the measured and computed deflections, the following was observed:

   a. The measured deflections were generally larger than the computed deflections. This is apparent from comparison of the measured values in Columns 2 and 3, Table 8, with the computed deflections and from comparisons of the computed and measured deflection basins in Figures 81-92. There was considerable scatter in the measured data as evidenced by the measured curves in Figures 81-92. The accuracy of the measuring devices for deflections of the magnitude in question is somewhat suspect, and therefore the comparisons between the measured and computed deflections should be considered cautiously. In regard tc the comparison of the measured and computed deflections, it should also be noted that the measurements were made prior to traffic and that the computed values were based on modulus of soil reaction values from plate tests run after traffic was completed.

   b. The general trend (disregarding the scatter) is that the slope of the measured deflection basins is steeper than that

46

of the computed basins (Figures 81-92). The slopes both measured and computed appear to be steeper in the transverse than in the longitudinal directions. This is an indication of more rotation of the slabs, without bending, which is consistent with the distress along the longitudinal joints. The apparent rotation is more pronounced in lane 2 than in lane 1 and more pronounced in subitems 5c and 5d than in 5a and 5b. These observations are consistent with the proximity of lane 2 to the pavement edge and the weaker foundation support in subitems 5c and 5d.

<u>c</u>. The deflections computed with the discrete element model along the joints (Columns 6 and 8 of Table 8) are approximately equal to, but always slightly larger than, the deflections computed with the influence charts for the slab interior conditions (Column 5), and always smaller than the edge deflections (Column 4). This is consistent with the discrete element model for the joints which assumes full shear transfer or equal deflection on either side of the joint.

<u>d</u>. Slab size does affect deflections as evidenced by the difference between the value computed with semi-infinite slabs, 25- by 25-ft slabs, and 12-1/2- by 12-1/2-ft slabs. Generally, the computations with the larger slabs resulted in smaller deflections (Columns 5, 6, and 8, Table 8, and Figures 81-90). The one exception is subitem 5c (Figures 87-89); but it is felt that, for the 12-1/2- by 12-1/2-ft slab model, the deflections were influenced by the proximity of the loading to the high-strength foundations in subitem 5b, whereas, for the model with the 25- by 25-ft slabs, the influence of the higher strength foundation in subitem 5b was diminished.

<u>e</u>. The effect of slab size on deflection is more noticeable in lane 2 where the loads are near the edge of the pavement (Figures 83, 85, 87, and 89). The effect is also more pronounced in subitem 5d than in the other subitems due to the proximity of the load to the end of the item (Figures 90 and 92). The foundation strength diminishes the effect of slab size and loading near an edge. This can be observed by comparing the deflection basins in Figures 85 and 89. The deflection at the slab edge for subitem 5b is practically zero whereas the deflection at the slab edge for subitem 5c is 0.0036 in. For both items, the deflection at the slab edge for 25- by 25-ft slabs was practically zero. The measured, and to a certain extent the computed, deflection basins indicate more rotation of the outer slab in lane 2 than the slabs in lane 1.

<u>f</u>. There is no apparent relationship between the measured deflections and the pavement performance nor is there any apparent relationship between the computed deflections and the pavement

47

performance. In Figure 93, the measured (maximum at the joints) and computed (discrete element theory with 12-1/2- by 12-1/2-ft slabs) deflections are plotted as a function of the traffic applied to the pavements in terms of coverages, and in Figure 94 the measured and computed deflections are plotted as a function of the log of the coverages. No well-defined relationship is apparent from either of these plots, although the general trends seem to be that the performance is independent of computed deflection and that the performance improves as the deflections decrease for the measured deflections.

Stresses. From the analysis of the computed stresses, the following was observed:

a. The bending stresses computed with the discrete element theory with 25- by 25-ft slabs (Column 5, Table 9) were approximately equal to the interior stresses (Column 3, Table 9) computed with influence charts, but both were smaller than the edge stresses (Column 2, Table 9) computed with influence charts. This is as expected since the 25 percent reduction in edge stress is a conservative estimate for design, plus the fact that the assumption in the discrete element model of full shear transfer at the joints (equal deflections on either side of the joints) would not really represent the behavior of joints since some differential movement does occur. As it affects the stress in the slab, the condition modeled at the joints is not significantly different from interior conditions.

b. The bending stresses computed with 12-1/2- by 12-1/2-ft slabs (Column 4, Table 9) were smaller than those computed with Westergaard theory (Columns 2 and 3, Table 9) or those with 25- by 25-ft slabs (Column 5, Table 9). This indicates that slab size did influence the state of stress in the pavement slabs and therefore may have significantly influenced the performance of the pavements. This factor is consistent with the slab rotation that was discussed previously in conjunction with the deflections.

48

CONCLUSIONS AND RECOMMENDATIONS

The conclusions and recommendations contained herein are based on the tests conducted on the flexible and rigid test pavements containing insulating layers, the tests on the materials contained in these pavements, and the analyses of the data obtained from these tests.

FLEXIBLE PAVEMENTS; CONCLUSIONS

Based on the field observations and the theoretical study, the following conclusions are drawn:

a. The principal cause of the failure in subitems 4a, 4b, 5c, and 5d was a lack of shear strength of the materials above the insulating layer. The lack of strength was due to the more flexible insulating layer within the material to be compacted, the reduction in compaction effort, the nearness to the edge of the section, and discontinuities between test items.

b. In subitem 4c the pavement failure was primarily caused by the progressive failure of the stabilized material above the lightweight concrete which finally resulted in failure of the lightweight concrete itself.

c. The failure of the pavement in 4d was due to a failure of the lightweight concrete. The cover above the lightweight concrete was not sufficient to prevent stress concentrations, particularly at the edge of the section. Failure started at the edge and progressed inward until complete failure of lightweight concrete had occurred.

d. The lightweight concrete subitems in item 5 performed remarkably well, considering their size and the discontinuities present at the transitions between them. The lightweight concrete increased the stiffness of the subitems as indicated by the deflection measurements which did not increase when measured at 170 coverages.

e. Although the computed compressive stress on the insulating material was, in all cases, much less than the compressive strength of the insulating material, damage to the materials did occur. The indication is that the actual stresses were greater than the computed stresses.

FLEXIBLE PAVEMENTS; RECOMMENDATIONS

The recommendations are as follows:

<u>a</u>. Caution must be used in placing of insulating materials within a pavement section. When using the ratio of the laboratory measured compressive strength and computed stress, it should be kept in mind that most analytical procedures for computing stress will underpredict.

<u>b</u>. Although consideration must be given to the compressive strength of insulating materials, consideration must also be given to the magnitude of the resilient strains in the insulating materials and in the pavement material above and below the insulating layer. In the absence of other supporting data, all resilient strains should be kept below those recommended for allowable subgrade strains in Barker and Brabston.[10]

RIGID PAVEMENTS; CONCLUSIONS

The conclusions are as follows:

<u>a</u>. The rigid pavements containing insulating layers did not perform as expected. The behavior of the PCC slabs was characterized by spalling and cracking along longitudinal joints rather than cracking of the slabs. There were two exceptions to the above; i.e., subitem 5c, lane 1, and subitem 5d, lane 2. Generally the observed performance was less than predicted with conventional rigid pavement evaluation procedures.

<u>b</u>. The cause of the unusual performance of the pavements is not known. It is theorized that it could have been partly caused by the slab size; i.e., thick (15-in.), small (12-1/2- by 12-1/2-ft) slabs that rotated and did not bend. It was impossible to assess the effect of slab size to ascertain if it actually affected the performance of the pavements.

<u>c</u>. All of the pavements pumped. It is theorized that the presence of the insulating layers accentuated pumping (pumping may also have been influenced by slab size). The rigidity of the polystyrene panels and the discontinuities in the layer were conducive to the development of voids and subsequent entrapment of water beneath the panels. Ejection of the water and suspended materials resulted with traffic.

<u>d</u>. In addition to the increased pumping potential, the insulating layers do not behave as conventional paving materials. The supporting characteristics of the layers are less than would be indicated by the elastic properties of the material. Several reasons for this were postulated including discontinuities in the layers, poor seating of the panels, and localized crushing of the material. In addition, the zero Poisson's ratio of the material would mean that the material in the layers would not have a tendency to expand laterally upon loading. Therefore, there would be no increase in

50

stiffness (providing the shear strength of the material is not exceeded). The crushing mode of failure of the insulating materials would affect the pavement response in the same manner (provided shear failure does occur) since there would be no tendency for the material to move horizontally and upward when shear failure occurs.

e. Due to the number of extraneous influences, the tests did not provide sufficient evidence to adequately evaluate the performance of rigid pavements containing insulating layers.

RIGID PAVEMENTS; RECOMMENDATIONS

The following are tentative recommendations for the use of insulating layers beneath rigid pavements:

a. There should be a leveling course of sand placed beneath polystyrene panels. The panels should be placed and firmly seated to ensure full contact of the panel with the leveling course.

b. For subgrades susceptible to pumping (CH, CL, MH, ML, and OL, and SM and SC where the water table is high or drainage poor), a minimum of 4 in. of base course should be placed between the polystyrene panels and the subgrade. In the nomenclature used by the FAA, the layer would be referred to as a subbase layer. The material may be a granular material or a chemically stabilized material meeting appropriate CE or FAA requirements.

c. A minimum of 6 in. of base (subbase) course should be placed between the slab and the insulating layer (polystyrene panels or lightweight concrete). The material may be a granular material or a chemically stabilized material and should meet appropriate CE or FAA material and compaction requirements.

d. Although the analyses produced no clear evidence to indicate that the plate bearing test adequately evaluated the supporting characteristics of foundations containing insulating layers, it appears to be as applicable as any other available method. Therefore, it is recommended that slab thickness be based on a measured modulus of soil reaction. The measurement should be made on top of the base course.

e. The joint failures indicate that keyed-and-tied longitudinal construction joints and untied-undoweled longitudinal contraction joints in pavements containing insulating layers may be inadequate. However, the doweled transverse construction joint between subitem 5a and the transition slab and the untied-undoweled transverse contraction joints performed satisfactorily. It is felt that the unusual slab size and pumping were probably the primary causes of the joint failures, and that, with normal size slabs and the requirements contained in recommendations a-c, conventional joint

51

configurations will be adequate. Therefore, it is recommended that no changes be made to current joint measurements and practices until additional data are obtained.

f. Additional full-scale accelerated traffic tests should be performed with slabs of more realistic dimensions. The pavements should be constructed with and without recommended base courses and with various joint configurations including doweled joints. In conjunction with the traffic tests, the effect of the seating of the polystyrene panels and panel size on the load-supporting characteristics of the layer should be investigated. The effect of bond or lack of bond between lightweight concrete layers and the slab should be studied.

Table 1

Material Properties of Lightweight Concrete Mixes

Specimen No.	Curing Time Days	Unit Weight pcf	Compressive Strength* psi	Flexural Strength** psi	Compressive Modulus† 10^6 psi	Flexural Modulus†† 10^6 psi
2-1	7	44		145		0.364
2-4	7	44		140		0.649
2-7	7	44		125		0.406
2-2	280	44		150		0.425
2-8	280	44		175		0.482
2-9	280	44		175		0.478
1-44-3	66	44		155		0.568
1-44-1	339	44		150		0.394
1-44-2	339	44		160		0.363
2-3	227	44	370		0.178	
2-6	227	44	640		0.256	
2-9	227	44	570		0.265	
1-44-1C	336	44	300		0.171	
1-44-2C	336	44	350		0.207	
1-52-4	66	52		195		0.760
1-52-5	66	52		160		0.543
1-52-1	339	52		160		0.595
1-52-2	339	52		165		0.676
1-52-3	339	52		165		0.659
1-52-1C	336	52	750		0.313	
1-52-2C	336	52	780		0.297	
1-52-3C	336	52	780		0.294	

* Determined according to ASTM C 39-71[3] (CRD-C 14[4]).
** Determined according to ASTM C 78-64[5] (CRD-C 16[4]).
† Determined according to ASTM C 469-65[6] (CRD-C 19[4]).
†† Determined according to CRD-C 21.[4]

53

Table 2

Summary of Laboratory Compaction Data and As-Constructed Plate Bearing,
Field CBR, Water Content, and Dry Density Data
for Items 4 and 5

Test Item	Material	Laboratory Data				As-Constructed Data						
		Water Content		Maximum Dry Density pcf	Compaction Effort	Depth in.	Water Content Untreated Material percent	k_u, psi	CBR	Water Content percent	Dry Density pcf	Percent Laboratory Density
		Untreated percent	Treated percent									
4	Clayey sand with 5 percent portland cement (base)	9.2	8.7	130.5	CE 55	3 7 14 21	9.7 9.8 9.4 9.4	448 — — —	150+ 150+ 93 103	8.9 4.6 6.3 7.8	116.9 121.5 112.8 119.3	89.6 93.1 86.4 91.4
	Heavy clay (subgrade)	25.0	—	94.0	CE 12	28 34 40	— — —	— — —	3.7 4.1 4.0	30.5 29.3 32.0	86.9 88.8 84.2	98.0* 98.5* 97.5*
5	Crushed limestone (base)	6.0	—	140.0	CE 55	3	—	—	104	2.4	145.7	103.8
	Gravelly sand (subbase)	7.3	—	132.4	CE 55	9 15 21	— — —	— — —	96 46 9	5.4 4.6 9.4	136.7 133.2 127.5	103.2 100.6 96.2
	Heavy clay (subgrade)	25.0	—	94.0	CE 12	42 48 54	— — —	55 — —	4.2 3.5 4.6	29.9 31.1 31.5	89.2 86.0 86.5	99.0* 97.2* 98.0*
4a	Clayey sand with 5 percent portland cement over 60-psi polystyrene	—	8.7	130.5	CE 55	14	—	—	—	3.8	123.1	94.5
4b	Clayey sand with 5 percent portland cement over 60-psi polystyrene	—	8.7	130.5	CE 55	10	—	—	—	7.0	119.5	91.5
4c	Clayey sand with 5 percent portland cement over lightweight concrete	—	8.7	130.5	CE 55	3	—	—	—	13.3	112.5	86.5
5b	Gravelly sand over lightweight concrete	7.5	—	132.4	—	9	—	—	—	10.9	123.1	93.3
5c	Gravelly sand over 120-psi polystyrene	7.5	—	132.4	—	15	—	—	—	4.9	132.9	100.3
5d	Gravelly sand over 120-psi polystyrene	7.5	—	132.4	—	9	—	—	—	6.3	132.1	100.0

* Percent of CE 12 (ASTM D 698-70) maximum density corresponding to the field in-place water content.

Table 3

Summary of Traffic Test Data for Flexible Pavement Test

Subitems Containing Insulating Layers

Sub-item No.	Rated Subgrade CBR	No. of Coverages	Maximum Permanent Deformation in.	Maximum Elastic Deflection in.	Maximum Upheaval in.	Degree of Cracking	Rating of Item
4a	4.2	0	0.0	0.16	--	--	--
		170	1.3	0.36	0.3	Severe	Failed
		240	1.5	--	1.1	Severe	
4b	4.2	0	0.0	0.10	--	--	--
		170	1.4	0.28	0.2	Severe	Failed
		240	1.8	--	1.1	Severe	
4c	4.2	0	0.0	0.06	--	--	--
		170	1.0	0.20	0.3	Slight	Satisfactory
		240	2.7	--	1.5	Severe	Failed
4d	4.2	0	0.0	0.06	--	--	--
		170	1.0	0.29	0.3	Slight	Satisfactory
		240	2.7	--	1.4	Severe	Failed
5a	4.1	0	0.0	0.08	--	--	--
		170	0.8	0.08	--	Slight	Satisfactory
		240	1.0	--	--	Severe	Failed
5b	4.1	0	0.0	0.09	--	--	--
		170	0.6	0.08	--	None	Satisfactory
		240	1.0	--	0.3	Slight	Failed
5c	4.1	0	0.0	0.15	--	--	--
		170	1.0	0.12	--	Slight	Satisfactory
		240	1.2	--	0.3	Severe	Failed
5d	4.1	0	0.0	0.14	--	--	--
		170	1.2	0.12	--	Slight	Satisfactory
		240	1.3	--	0.2	Severe	Failed

55

Table 4

After-Traffic Water Content, Density, and CBR Data for Flexible
Pavement Test Subitems Containing Insulating Layers

Sub-item No.	Material	No. of Coverages	Depth Below Pavement Surface in.	Inside Traffic Lane				Outside Traffic Lane			
				CBR	Water Content percent	Dry Density pcf	Percent Lab Density	CBR	Water Content percent	Dry Density pcf	Percent Lab Density
4a	Clayey sand with 5 percent portland cement	240	3	67	14.1	109.3	83.8	114	11.6	115.8	88.7
			15	27	16.4	110.4	84.6	33	10.7	121.6	93.2
	60-psi polystyrene		18	8	--	--	---	7	--	--	--
	Clayey sand with 5 percent portland cement		22	56	17.8	109.5	83.9	22	16.8	116.5	89.3
	Heavy clay subgrade		28	2.8	30.9	83.0	93.3*	4.4	27.2	87.3	93.9*
			34	3.1	32.2	87.3	100.3*	3.8	28.6	86.3	94.8*
			40	2.6	34.5	85.5	100.6*	2.8	33.9	84.7	99.6*
4b	Clayey sand with 5 percent portland cement	240	3	--	13.5	116.8	89.5	--	13.0	117.4	90.0
4c	Clayey sand with 5 percent portland cement	240	3	104	14.5	110.9	85.0	130*	14.2	115.2	88.3
	Lightweight concrete		9	39	--	--	--	66	--	--	--
	Clayey sand with 5 percent portland cement		18	51	12.8	112.5	86.2	18	13.4	118.8	91.0
	Heavy clay subgrade		28	4.8	28.7	89.5	98.4*	6	28.9	88.6	95.2*
			34	6	30.7	88.9	99.9*	8	28.9	89.0	97.8*
			40	4.5	32.5	84.9	99.9*	5	32.0	85.4	98.3*
5a	Crushed limestone	240	3	63	4.3	144.3	100.2	53	2.5	146.5	101.7
	Lightweight concrete		9	45	--	--	--	82	--	--	--
	Gravelly sand		18	20	6.1	137.8	104.1	20	9.3	132.8	100.3
			30	20	8.9	136.4	103.0	16	6.1	134.9	101.9
	Heavy clay subgrade		42	3.6	31.4	87.5	98.3*	3.4	31.7	87.8	100.9*
			48	3.7	31.1	89.6	100.7*	3.9	32.6	86.7	100.8*
			54	3.4	33.4	85.0	100.0*	4.3	32.0	85.3	98.0*
5c	Crushed limestone	240	3	68	3.8	148.2	102.9	85	2.8	146.5	101.7
	Gravelly sand		9	69	4.9	139.2	105.1	49	4.0	142.0	107.3
	120-psi polystyrene		24	14	--	--	--	15	--	--	--
	Gravelly sand		27	31	6.7	137.7	104.0	23	7.5	135.9	102.6
			39	9	6.9	130.4	98.5	9	7.0	137.1	103.5
	Heavy clay subgrade		42	3.6	32.6	85.3	99.2*	4.5	30.0	90.4	98.3*
			48	4.4	33.1	85.2	100.2*	4.3	32.3	86.5	99.4*
			54	5.0	32.9	86.5	100.6*	5.1	31.8	86.9	99.9*

* Percent of CE 12 (ASTM D 698-70[8]) maximum density corresponding to field in-place water content.

Table 5

Summary of Performance Data for Rigid Pavement

Subitems Containing Insulating Layers

Sub-item No.	Traf-fic Lane No.	Assembly Load kip	Total No. of Cover-ages	Maximum Static Deflec-tion in.	Maximum Perma-nent Defor-mation in.	No. Coverages for Failure Condition			Remarks
						Ini-tial Crack	Shat-tered Slab	Com-plete Fail-ure	
5a	1	200	3000	0.38	1.4	—*	—*	—*	Joint failure
	2	240	950	0.40	0.7	—*	—*	—*	Joint failure
5b	1	200	3000	0.28	0.9	—*	—*	—*	Joint failure
	2	240	950	0.42	1.9	—*	—*	—*	Joint failure
5c	1	200	1230	0.15	0.6	1000	1230	—**	
	2	240	740	0.43	1.1	—*	—*	—*	Joint failure
5d	1	200	3000	0.21	0.4	—*	—*	—*	
	2	240	350	0.53	0.7	20	200	—*	

* Traffic was discontinued before subitem reached failure condition.
** Pavement was covered with landing mat after 1230 coverages.

Table 6

Summary of After-Traffic Properties of Rigid Pavement

Subitems Containing Insulating Layers

Sub-item No.	Traffic Lane	Subgrade			Base Course		Pavement	
		Water Content percent	Density pcf	Modulus of Soil Reaction* psi	Modulus of Soil Reaction* pci	Flexural Strength** psi	Compressive Strength† psi	Modulus 10^6 psi
5a	1	--	--	--	188	965	--	7.76[++]
	2	--	--	--	--	--	--	--
5b	1	--	--	--	--	--	7280	6.10‡
	2	--	--	--	420	--	6590	5.71‡
5c	1	--	--	--	--	--	6220	5.07‡
	2	30.0	90.4	120	63	868	--	6.70[++]
5d	1	30.9	89.1	143	103	--	--	--
	2	--	--	--	--	--	5310	5.14‡

* Determined according to MIL-STD-621-A.[13]

** Determined according to ASTM C 78-64[5] (CRD-C 16[4]).

† Determined according to ASTM C 39-71[3] (CRD-C 14[4]).

†† Determined according to CRD-C 21.[4]

‡ Determined according to ASTM C 469-65[6] (CRD-C 19[4]).

Table 7

Comparison of Observed and Predicted

First Crack Performance

	Lane 1		Lane 2	
Subitem	Observed Coverages	Predicted Coverages	Observed Coverages	Predicted Coverages
5a	3000*	30,000	750*	7,000
5b	3000*	400,000	750*	70,000
5c	1000	860	430*	60
5d	**	6,500	20	540

* Joint failure at indicated coverage level.
** No failure at completion of traffic (3000 coverages).

Table 8

Elastic Deflections of Rigid Pavement Subitems Containing Insulating Layers Loaded with Dual-Tandem Gears

Sub-item	Maximum Measured Deflection at Longitudinal Joint, in.	Maximum Measured Deflection Along Longitudinal Axis of Gear, in.	Deflections Computed With Influence Charts (Westergaard Theory; Semi-Infinite Slab)		Deflections Computed with Discrete Element Theory (Finite Slabs)			
			Maximum Along Edge of Slab, in.	Slab Interior* in.	12-1/2 by 12-1/2-ft Slabs		25- by 25-ft Slabs	
					Maximum Along Joint in.	At Gear Centroid in.	Maximum Along Joint in.	At Gear Centroid in.**
				Lane 1, 200-kip Load				
5a	0.10	0.09	0.08	0.03	0.0368	0.0343	--	--
5b	0.12	0.11	0.05	0.02	0.0277	0.0241	0.0238	0.0222
5c	0.10	0.13	0.17	0.06	0.0722	0.0648	0.0818	0.0765
5d	0.17	0.18	0.13	0.05	0.0817	0.0728	0.0622	0.0578
				Lane 2, 240-kip Load				
5a	Not measured	0.15	0.10	0.04	--	--	--	--
5b	Not measured	0.18	0.06	0.03	0.0341	0.0303	0.0308	0.0273
5c	Not measured	0.26	0.20	0.08	0.100	0.0861	0.110	0.0980
5d	Not measured	0.24	0.15	0.06	--	--	0.0843	0.0741

* Gear was located in interior of slab. For all other cases, the longitudinal axis of the gear was located parallel to a joint or slab edge with two of the tires tangent to the joint or edge.

Table 9

Computed Stresses in Rigid Pavement Subitems Containing

Insulating Layers Loaded with Dual-Tandem Gears

| | Pickett and Ray Influence Charts | | Discrete Element Model | |
| | At Edge of Slab | Interior of | | |
Sub-item	Parallel to the Edge, psi	Slab Beneath Wheel, psi*	12-1/2- by 12-1/2-ft Slabs, psi	25- by 25-ft Slabs, psi
		Lane 1, 200-kip Load		
5a	708 (531)**	430	420	--
5b	565 (423)	359	285	315
5c	936 (702)	548	474	562
5d	827 (620)	494	338	463
		Lane 2, 240-kip Load		
5a	850 (637)	516	--	--
5b	679 (509)	431	345	376
5c	1124 (843)	658	570	682
5d	992 (744)	592	--	552

* Gear was located in interior of slab. For all other cases the longi-
tudinal axis of the gear was located parallel to the edge or joint.
** The numbers in parentheses are the computed free-edge stresses multi-
plied by 0.75 to account for reduction in stress provided by support
from adjacent slabs.

61
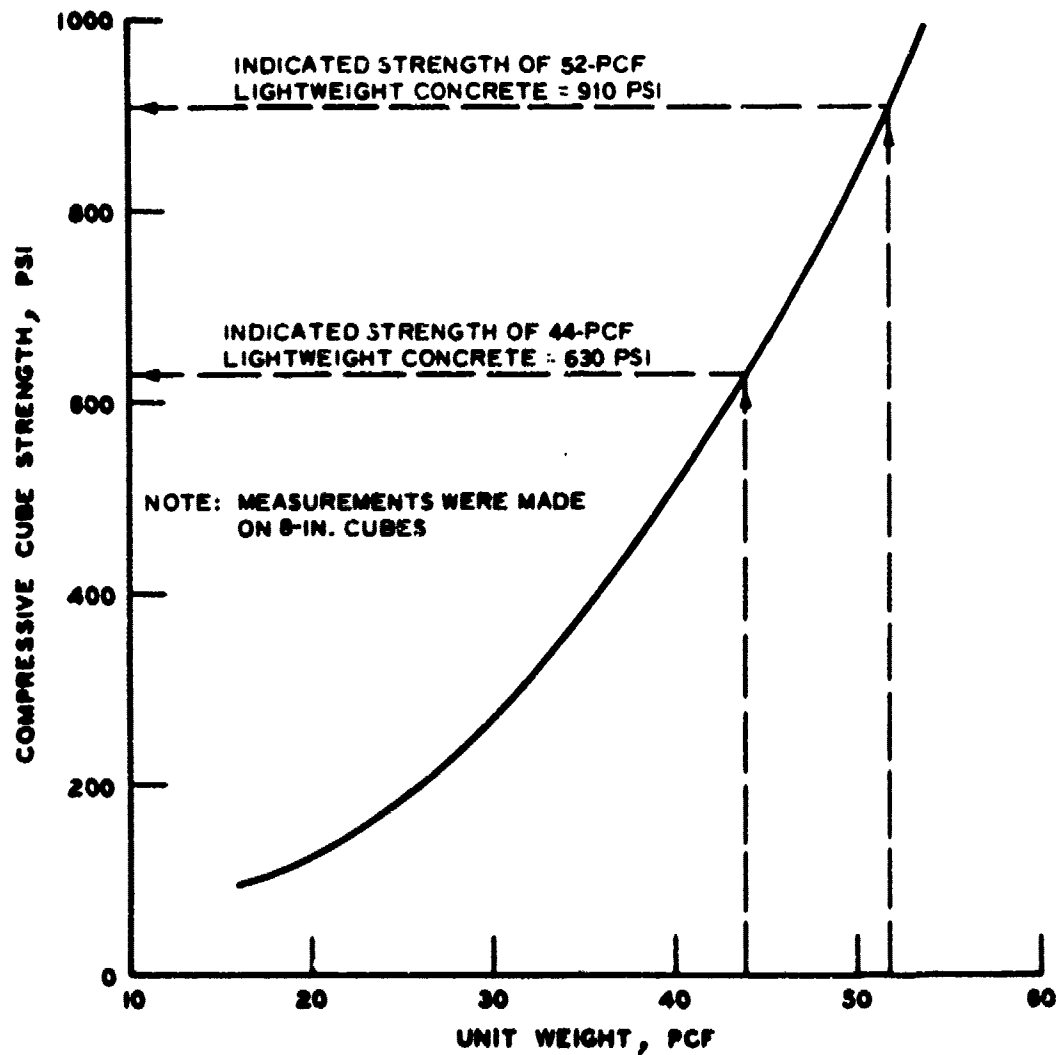
Figure 1. Relationship between 28-day compressive cube strength and unit weight of the lightweight concrete (after Hohwiller and Köhling[2])
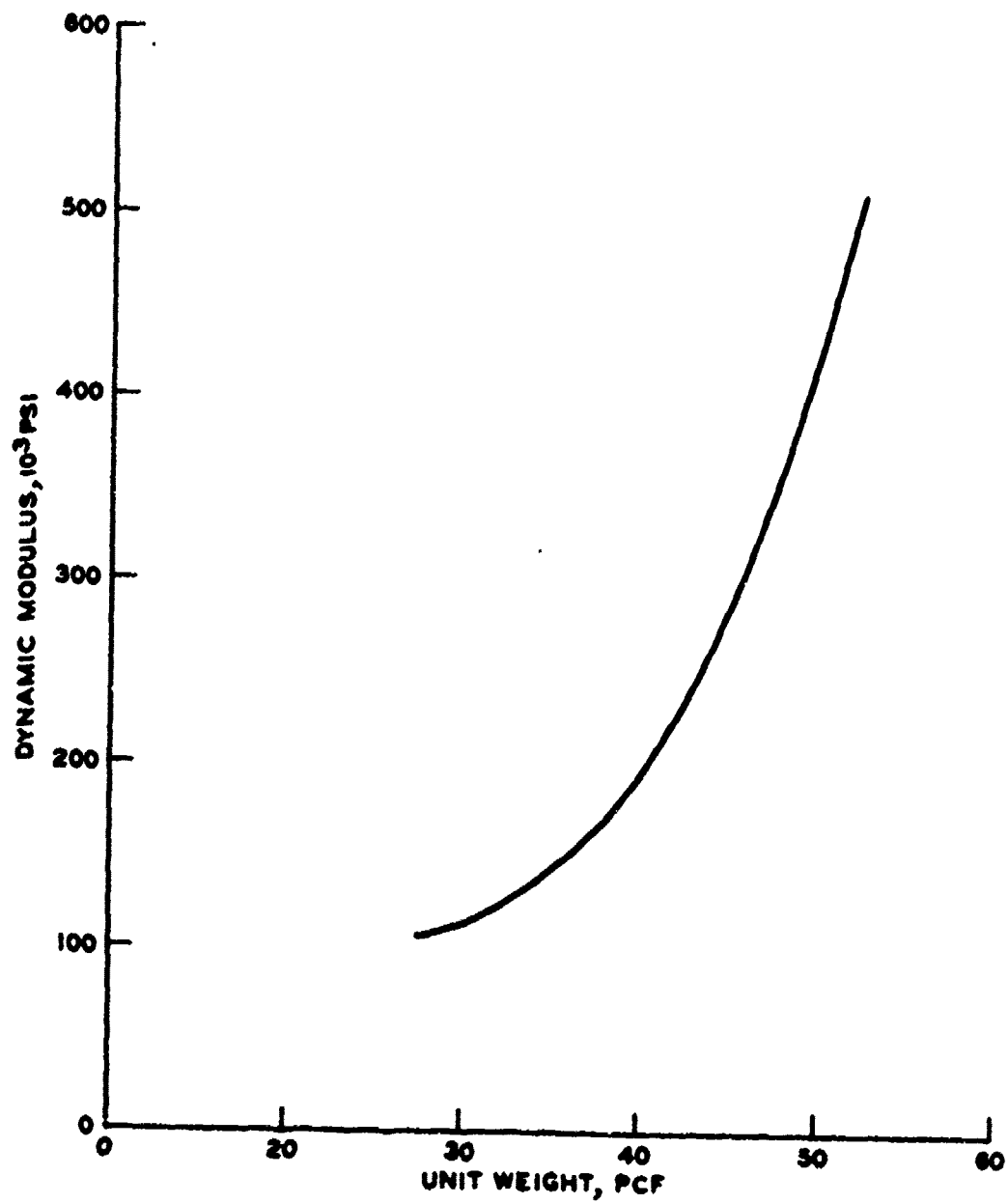
Figure 2. Relationship between dynamic modulus and unit weight of the lightweight concrete (after Hohwiller and Köhling[2])

63
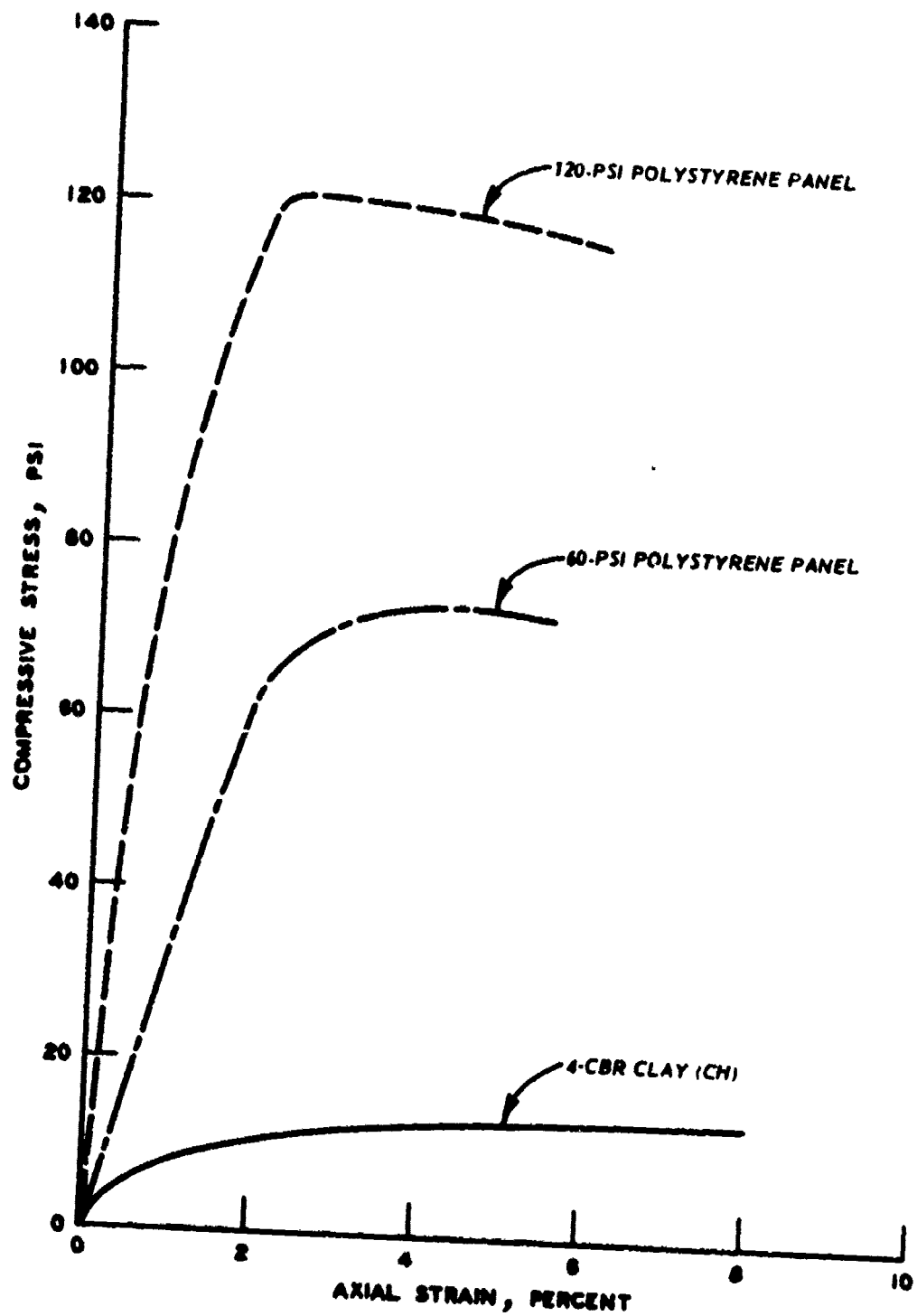
Figure 3. Comparison of stress-strain curves of 120- and
60-psi polystyrene panels and 4-CBR clay (CH)
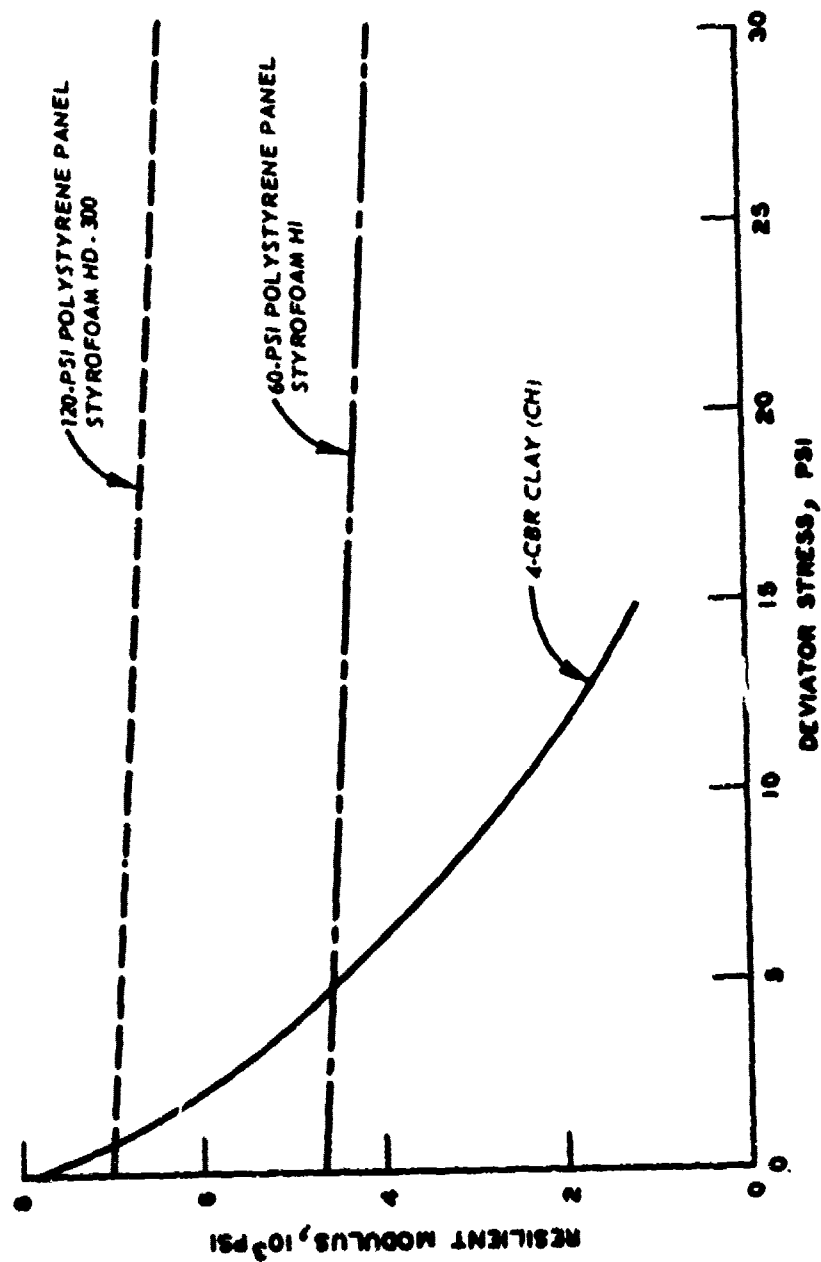
Figure 4. Comparison of resilient moduli of 120- and 60-psi polystyrene panels and 4-CBR clay (CH)
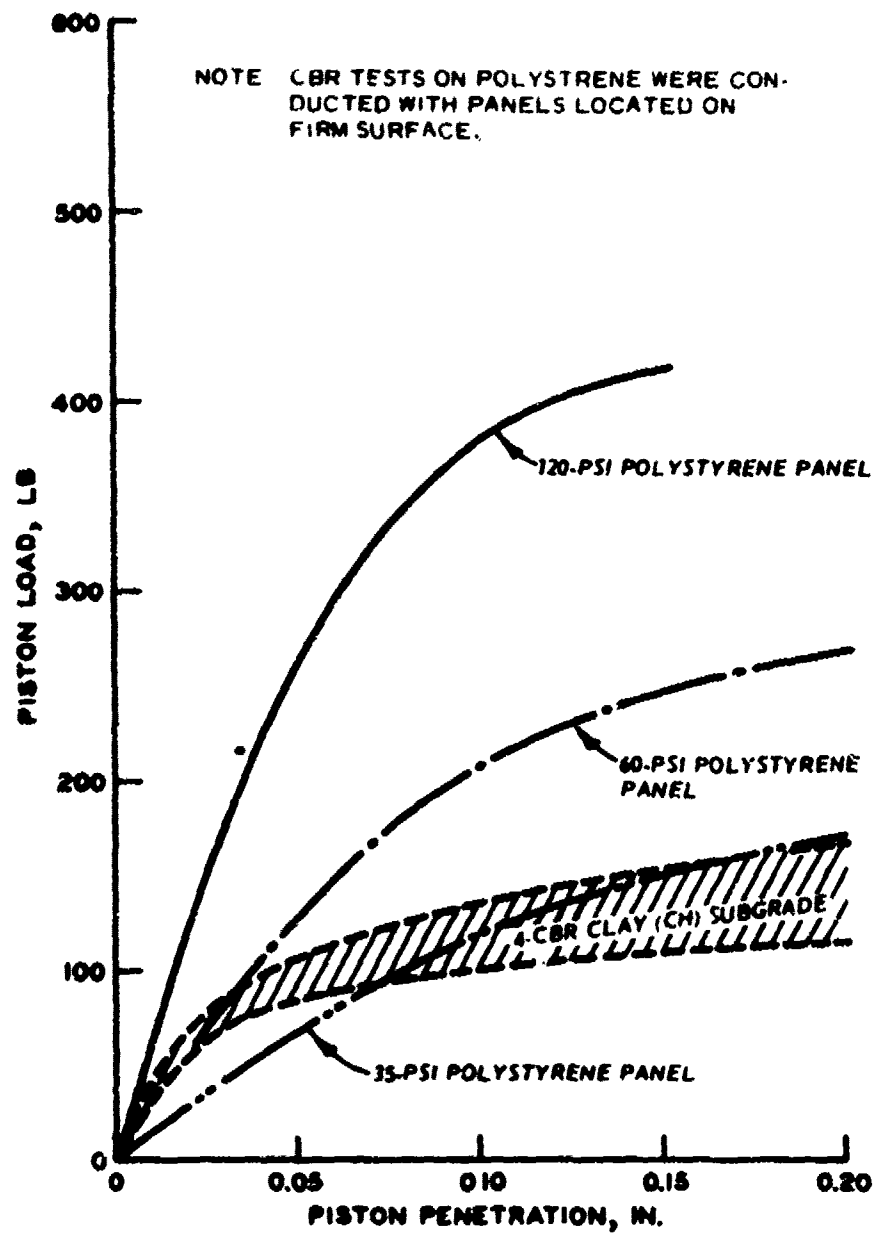
Figure 5. Comparison of CBR curves for 120-, 60-, and 35-psi polystyrene panels and 4-CBR clay (CH)

66

PLAN

ITEM 1 ITEM 2 ITEM 3 ITEM 4 ITEM 5

LANE 1 (200-KIP LOAD)

LANE 2 (240-KIP LOAD)

LANE 3 (90-KIP LOAD)

40' 40' 40' 60' 8 AT 10'

200'

40'

10' 10' 11.3' 10' 5'

10' 70' 35' 25'

SECTION A-A

6" CRUSHED LIMESTONE

24" CLAY (CL) WITH
3% LIME
2% PORTLAND CEMENT
10% FLY ASH

25" CLAY (CL)
WITH 12%
PORTLAND CEMENT

3" ASPHALTIC CONCRETE

25" GRAVELLY SAND (SP)
WITH 5%
PORTLAND CEMENT
(PI=0)

SUBGRADE CLAY (CH)

25" CLAYEY SAND (SC)
WITH 5%
PORTLAND CEMENT

6" CRUSHED LIMESTONE

33" GRAVELLY SAND (SP)
(PI=3)
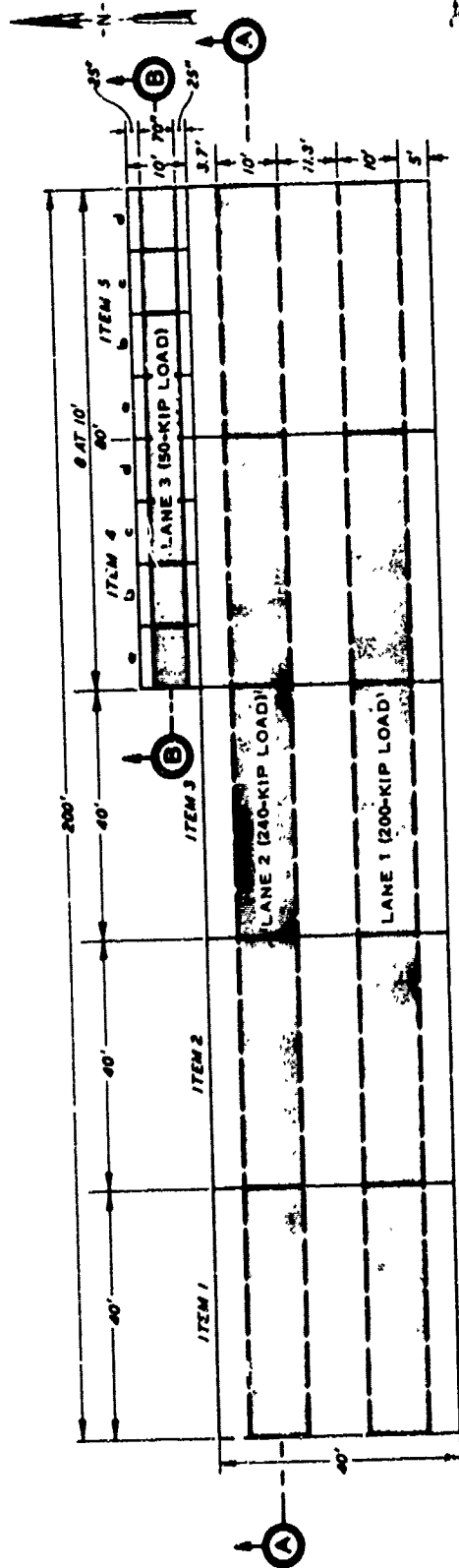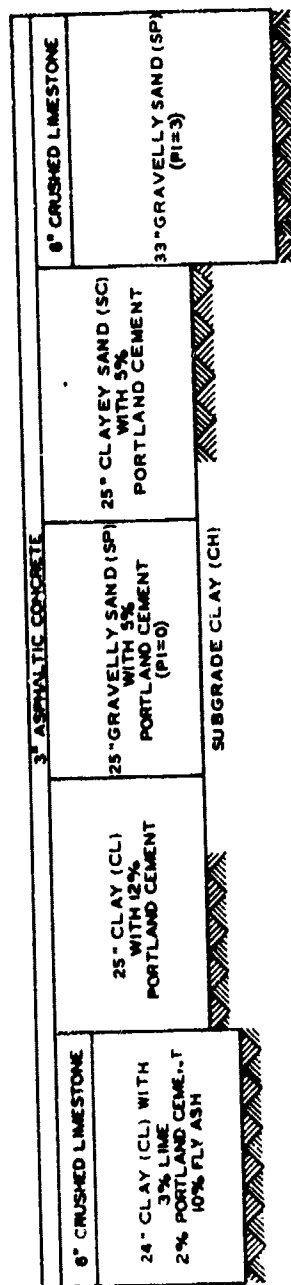
NOTE   SEE FIGURE 7 FOR SECTION B-B

Figure 6.   Layout of the flexible pavement test section

67

Figure 7. Profiles of items in the flexible pavement test section with insulating materials
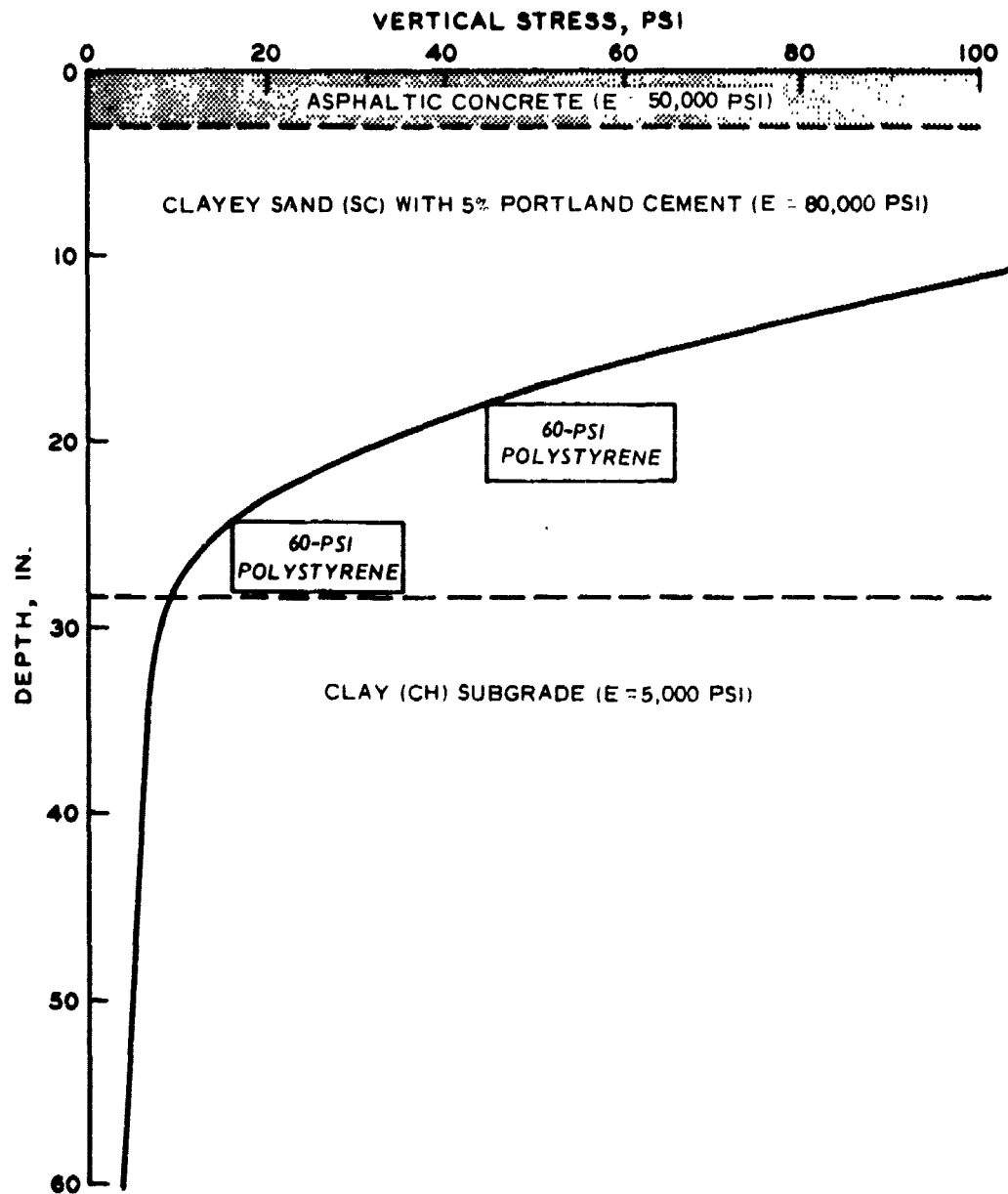
Figure 8. Vertical stress distribution in item 4 without insulating layers computed with linear finite element analysis

69

VERTICAL STRESS, PSI

0   20   40   60   80   100

0

ASPHALTIC CONCRETE (E = 50,000 PSI)

CRUSHED LIMESTONE (SW - SM) $[E = f(\sigma_3)]$

10

GRAVELLY SAND (SP) $[E = f(\sigma_3)]$

120-PSI
POLYSTYRENE

20

120-PSI
POLYSTYRENE

DEPTH, IN.

30

40

CLAY (CH) SUBGRADE (E = 5,000 PSI)

50

60
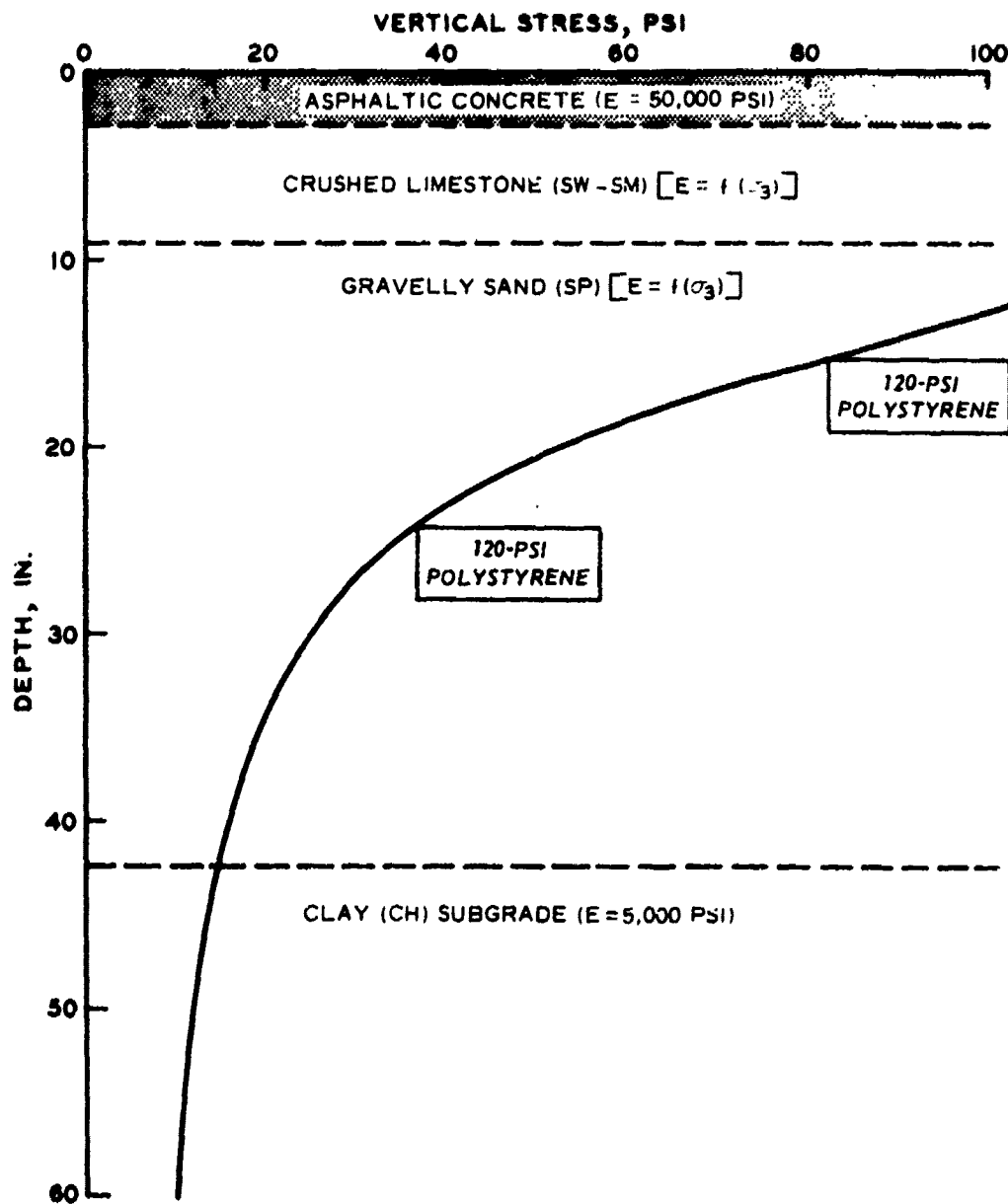
Figure 9. Vertical stress distribution in item 5 without
insulating layers computed with nonlinear finite element
analysis

70
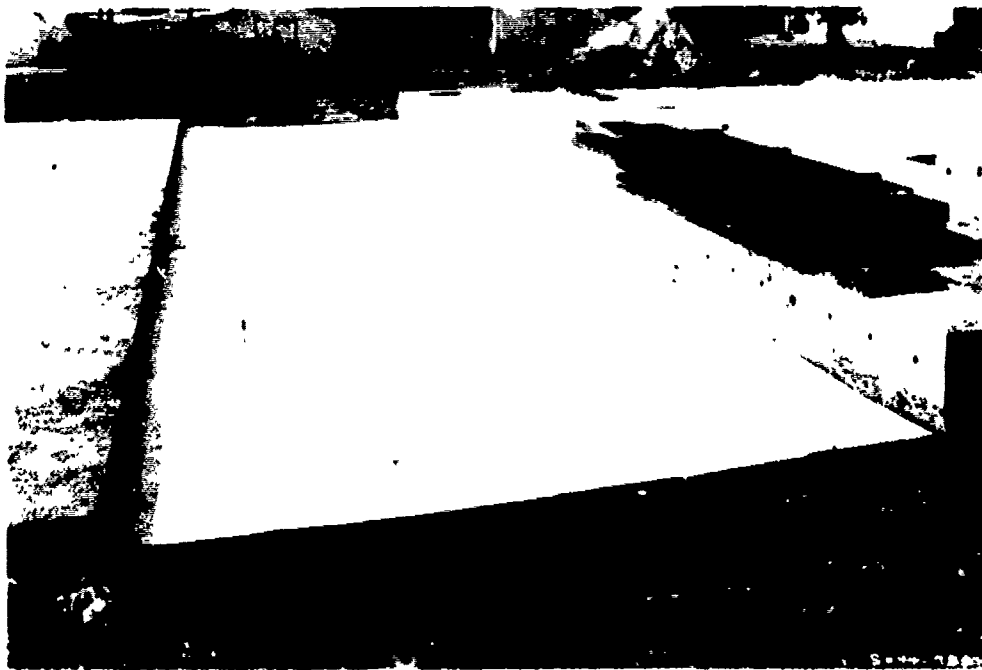
Figure 10. Pattern for placement of polystyrene panels
in insulating layers
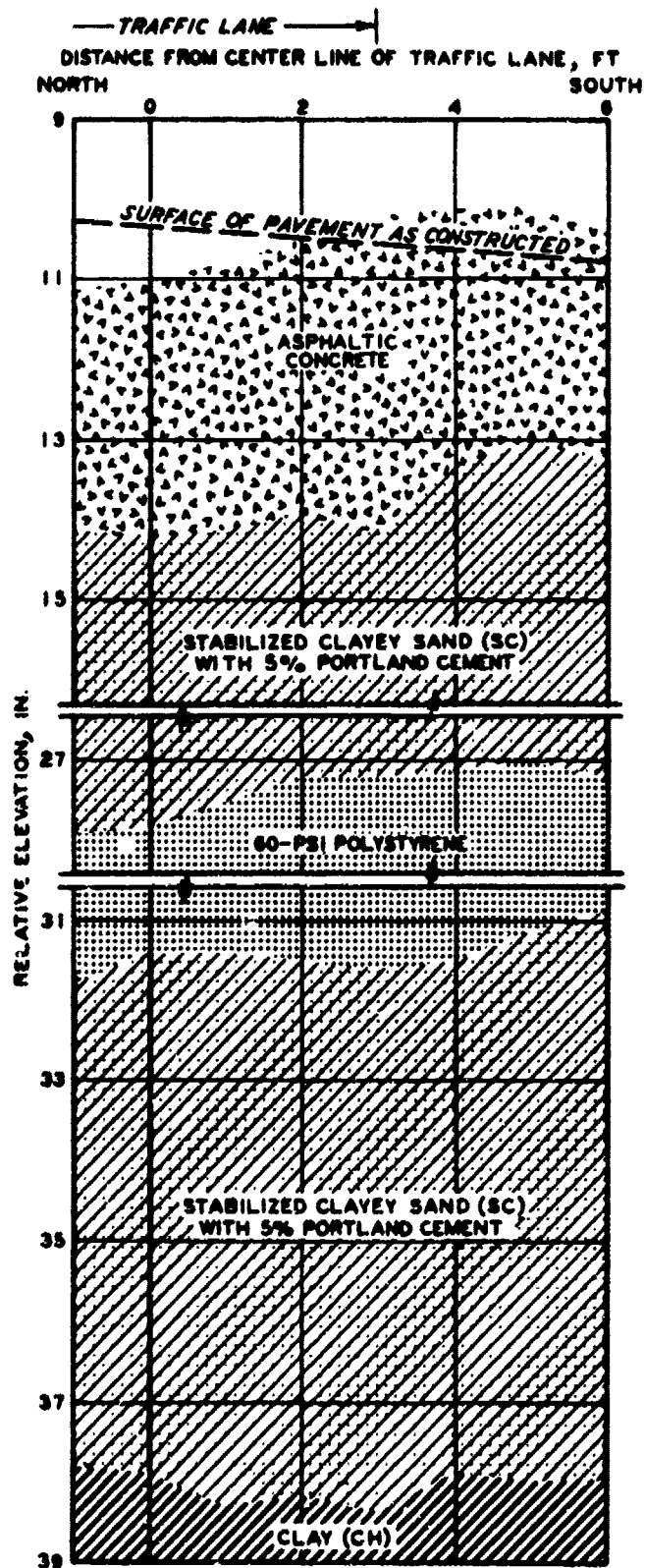
Figure 11. Test pit profile of subitem 4a, flexible pavement test section. Station 1+25 after 240 coverages of 50-kip single-wheel assembly

Figure 12. Test pit profile of subitem 4c,
flexible pavement test section. Station 1+45
after 240 coverages of 50-k, single-wheel
assembly
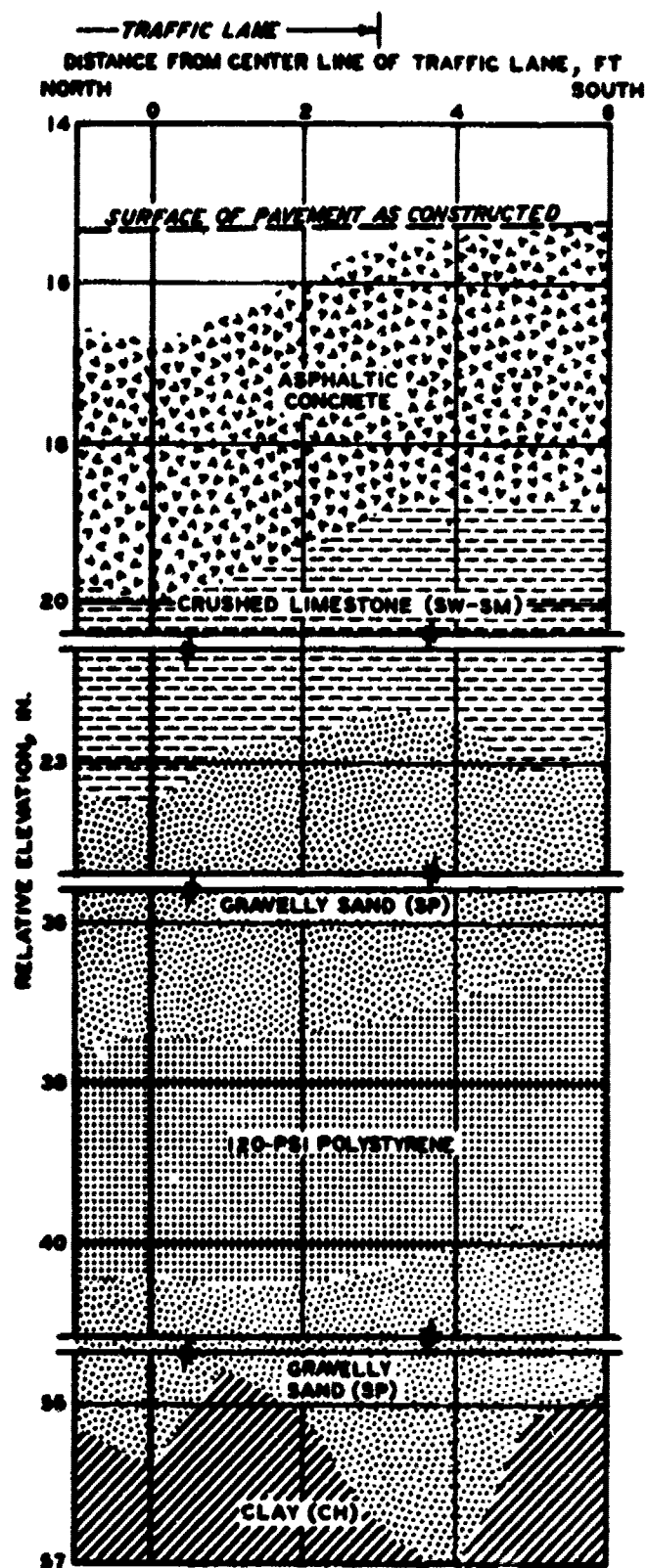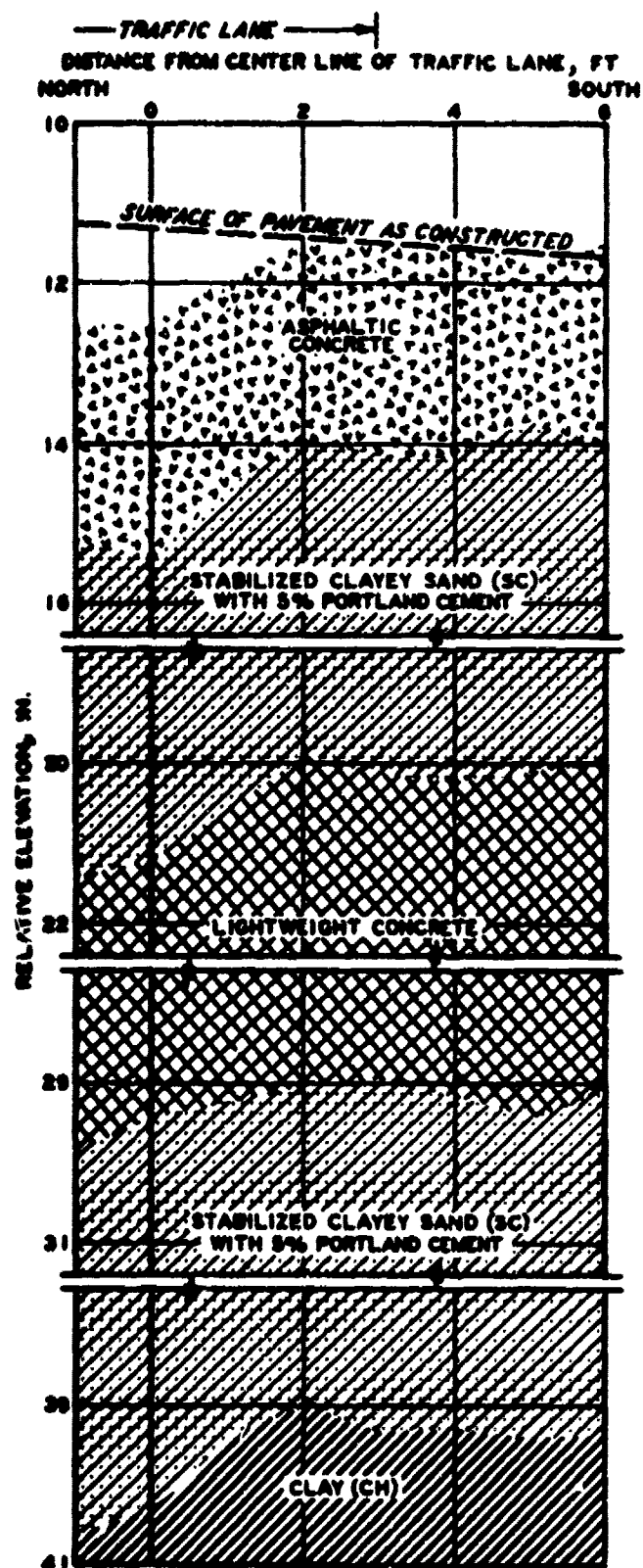
Figure 13. Test pit profile of subitem 5a,
flexible pavement test section. Station 1+65
after 240 coverages of 50-kip single-wheel
assembly
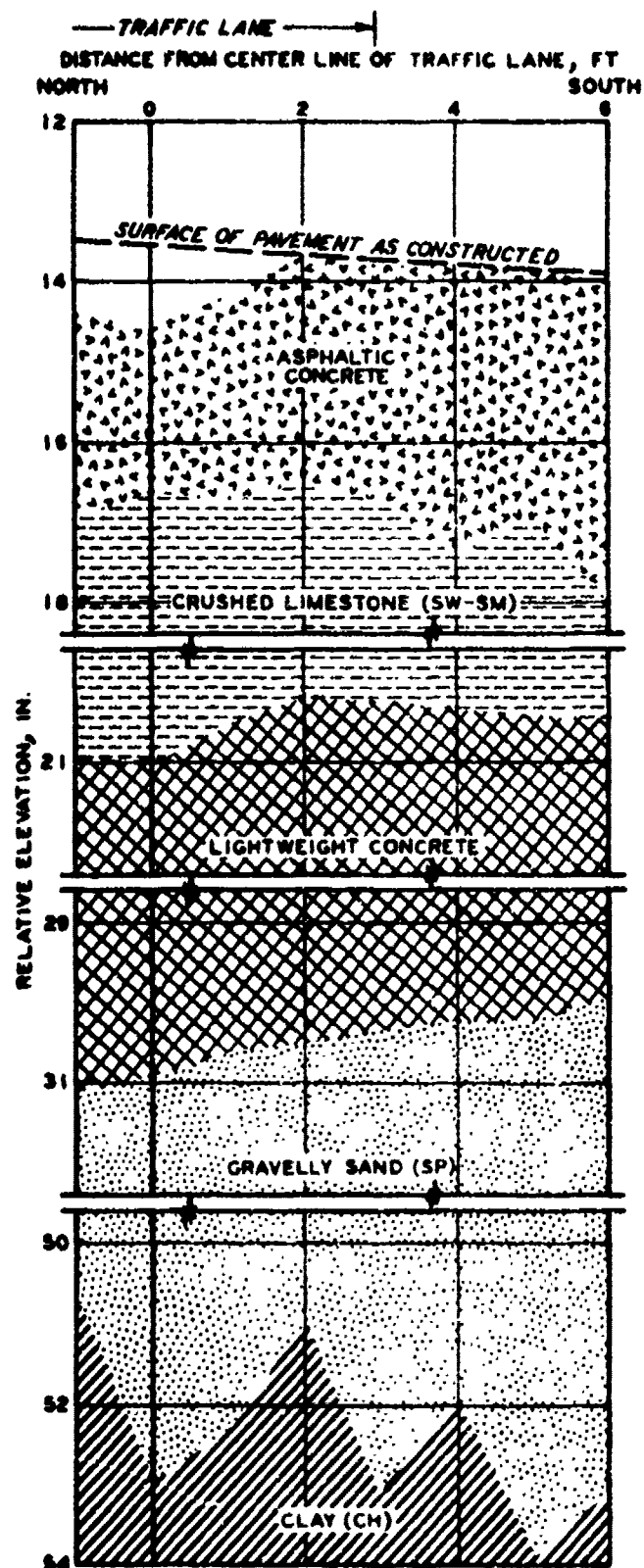
Figure 14. Test pit profile, subitem 5c, flexible pavement test section, Station 1+88 after 240 coverages of 3-dual, ... tricycle-wheel assembly
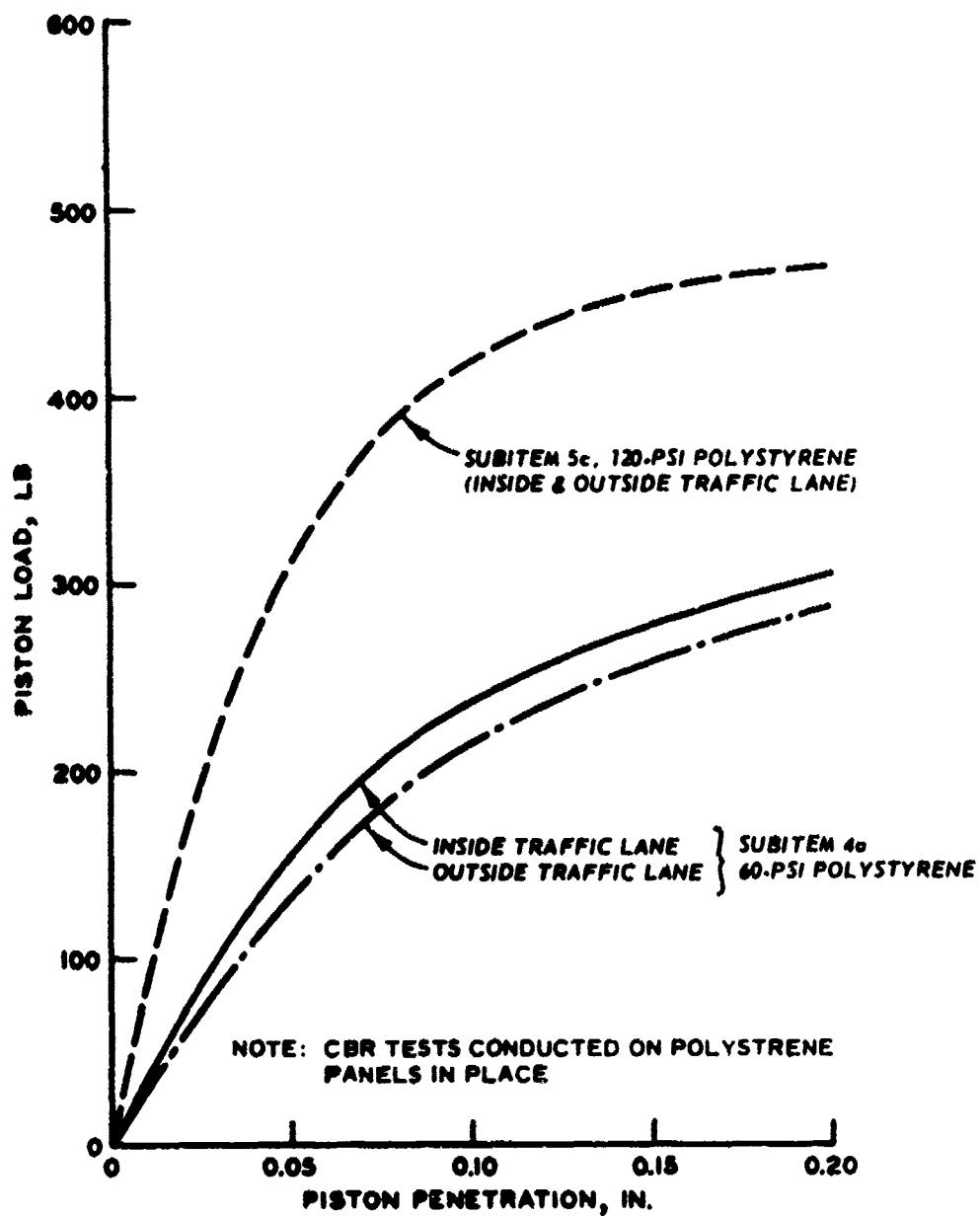
Figure 15. Load penetration curves from CBR tests
conducted on the 120- and 60-psi polystyrene in
subitems 5c and 4a, flexible pavement test section
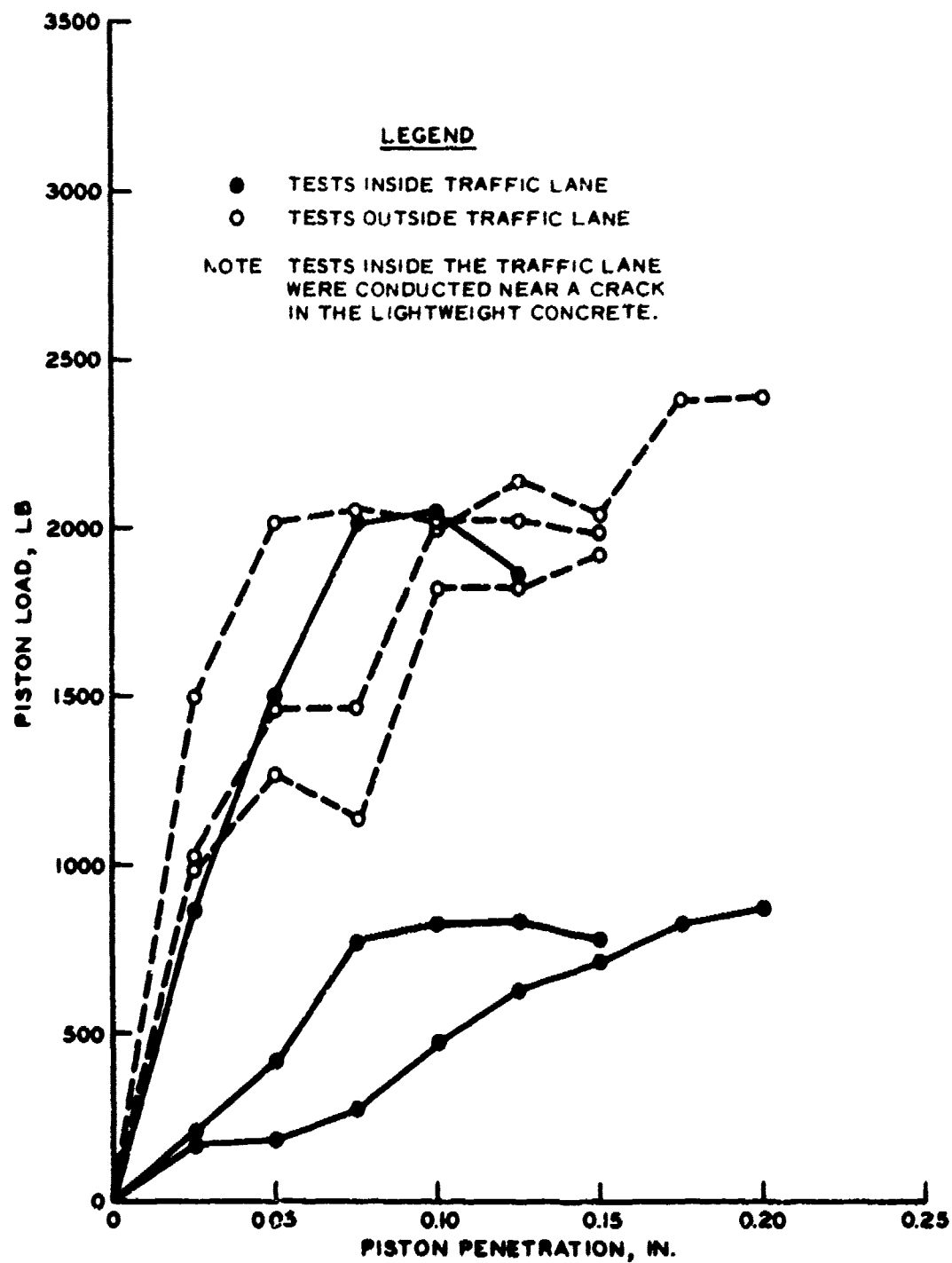
Figure 16. Data points from CBR tests conducted on lightweight
concrete in subitem 4c, flexible pavement test section
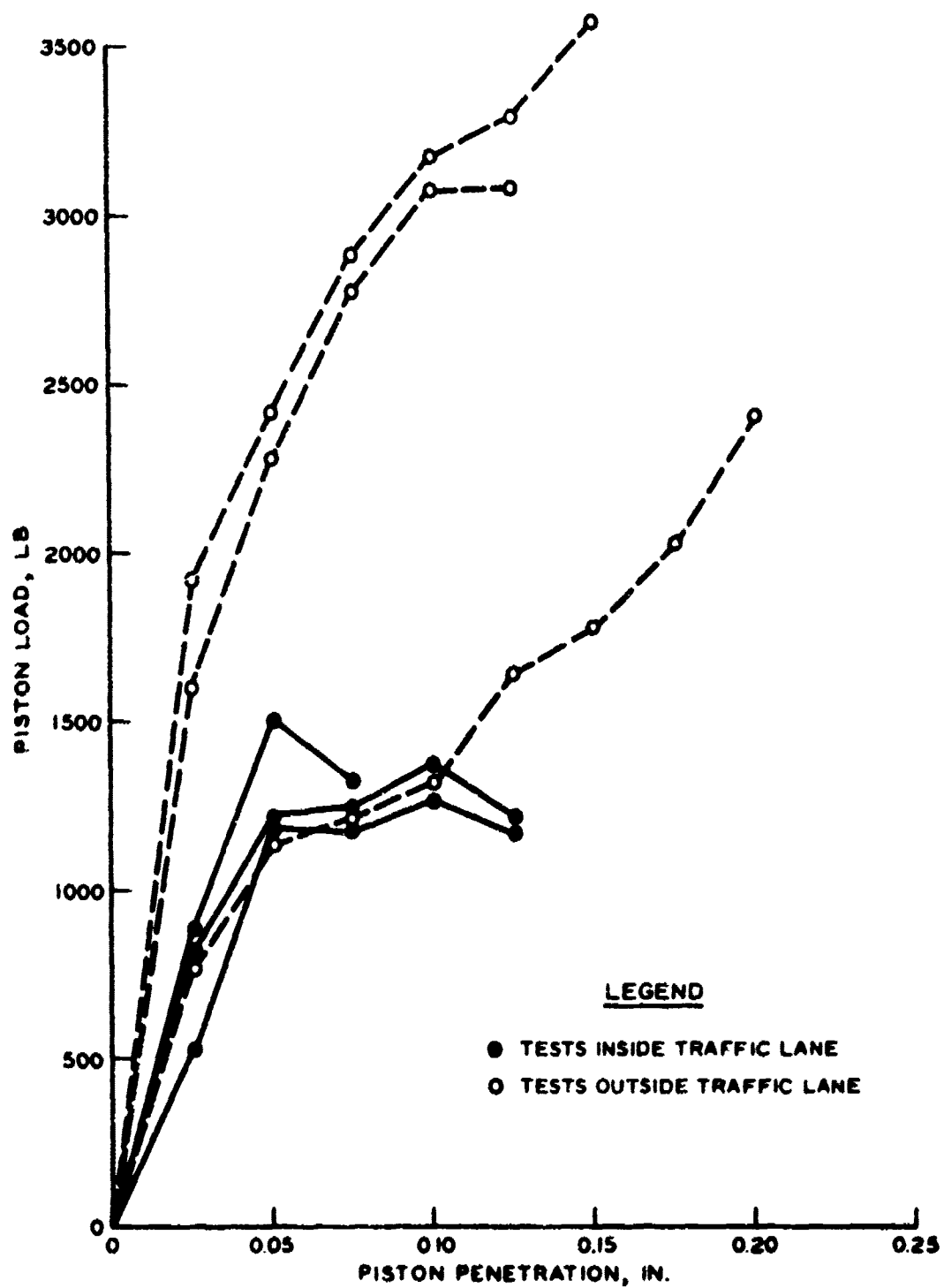
Figure 17. Data points from CBR tests conducted on lightweight concrete in subitem 5a, flexible pavement test section

Figure 18. Cracks in polystyrene panels in subitem 4a, flexible pavement test section
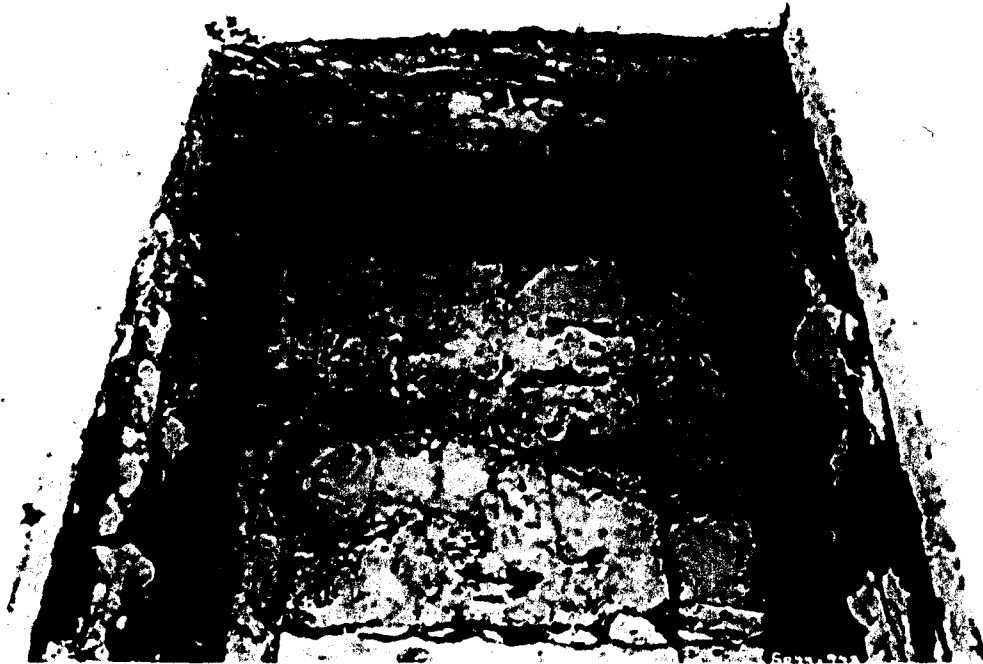
Figure 19. Cracks in polystyrene panels in subitem 4b, flexible pavement test section
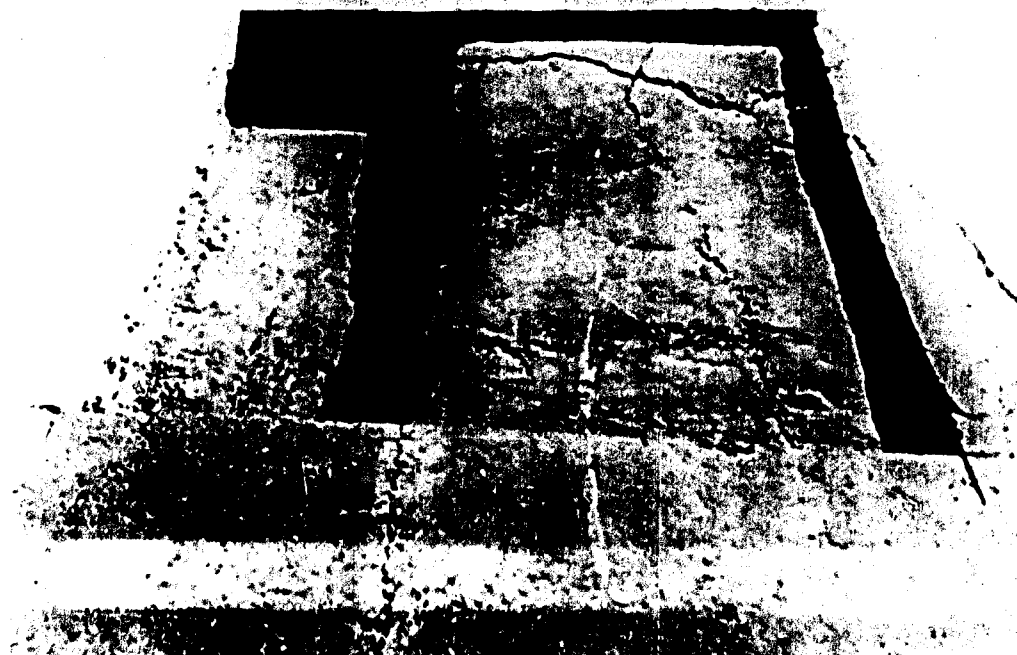
Figure 20. Cracks in lightweight concrete in subitems 4d and 5a, flexible pavement test section
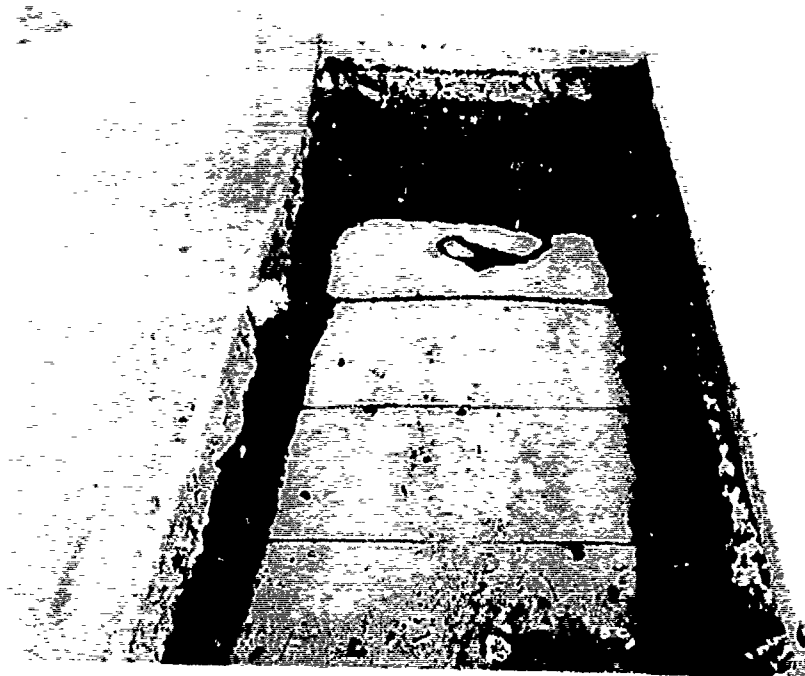
Figure 21. Surface of polystyrene panels in subitem 5c, flexible pavement test section
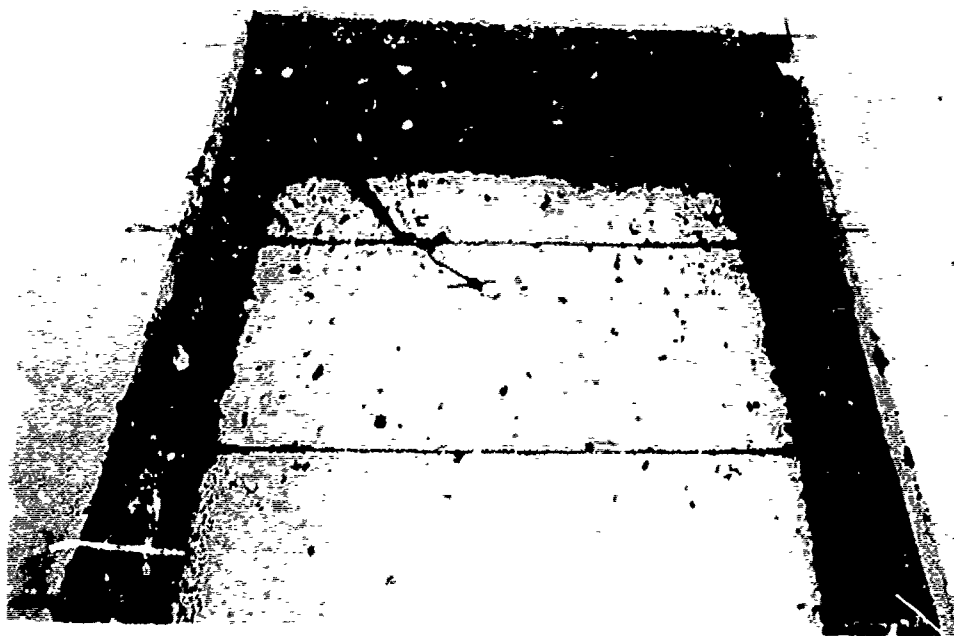
Figure 22. Surface of polystyrene panels in subitem 5d, flexible pavement test section
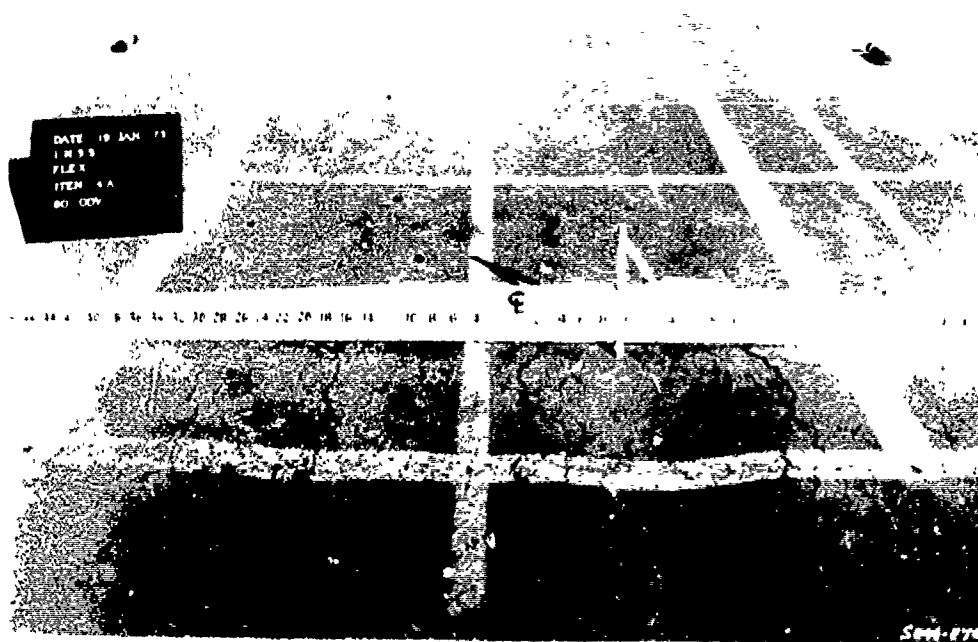
Figure 23. Initial distress at transition between
subitems 4a and 4b, flexible pavement test section
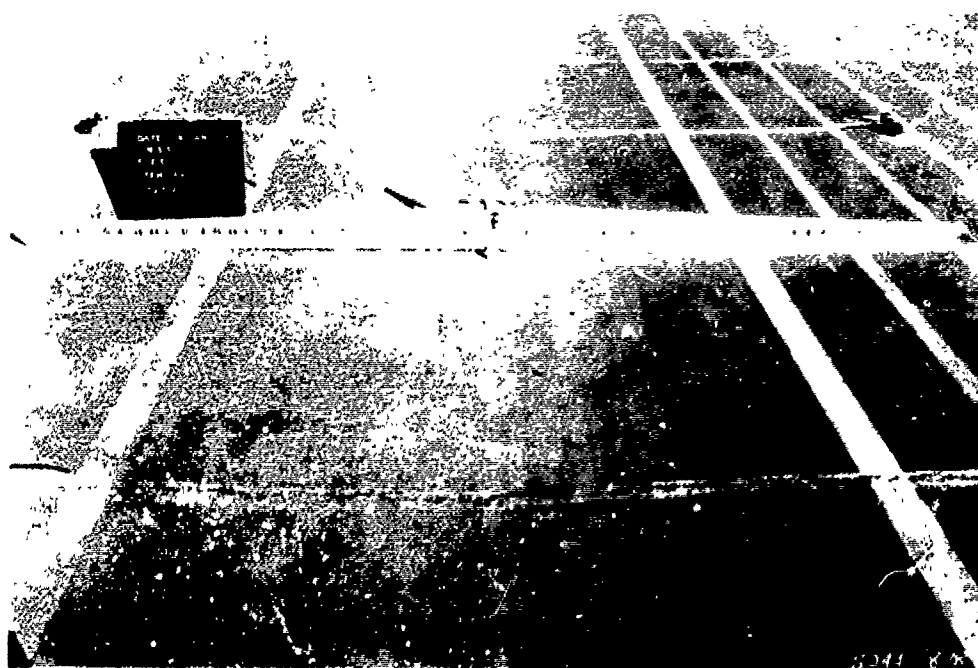
Figure 24. Cracking at transition between subitems 4d
an. 5a, flexible pavement test section
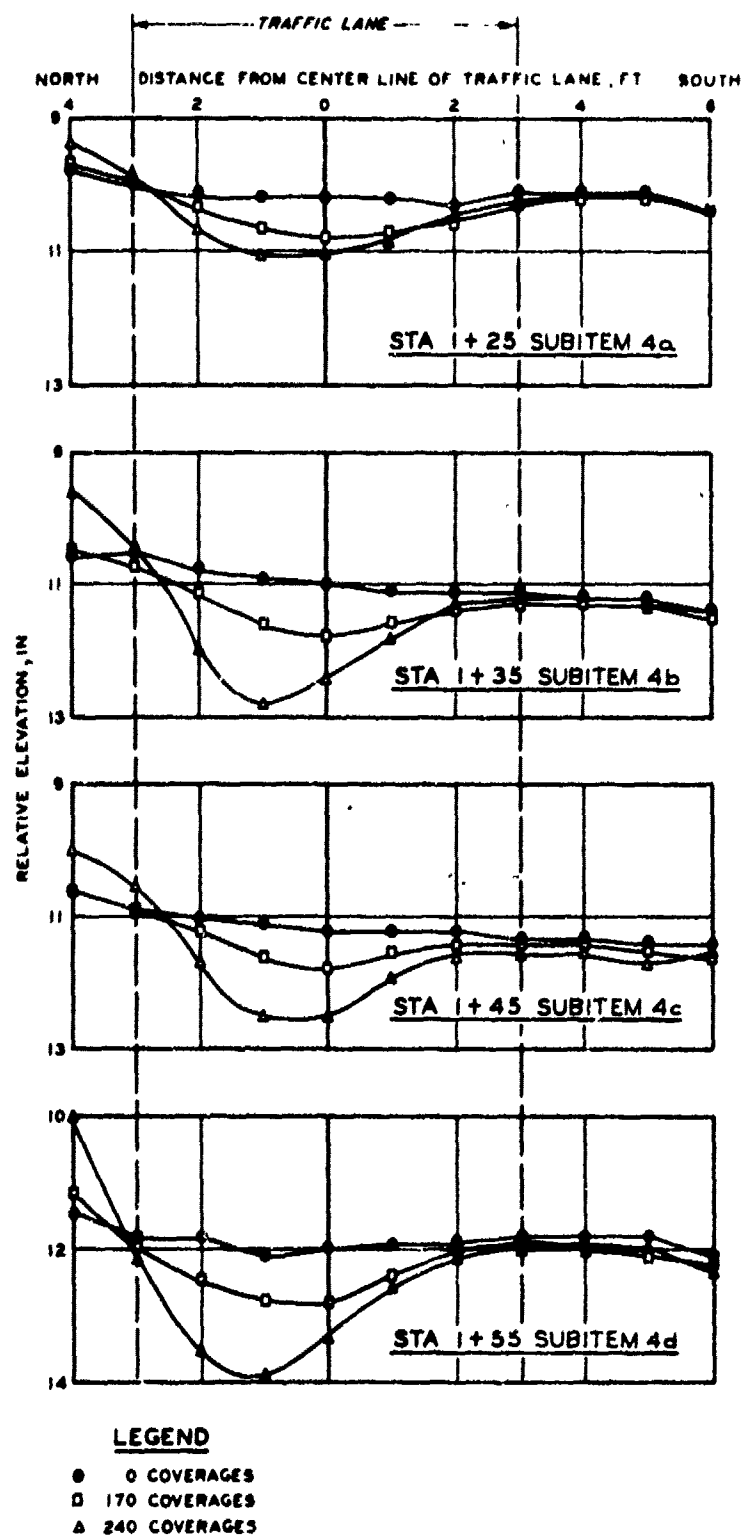
Figure 25. Surface deformation in subitems 4a-4d, flexible pavement test section
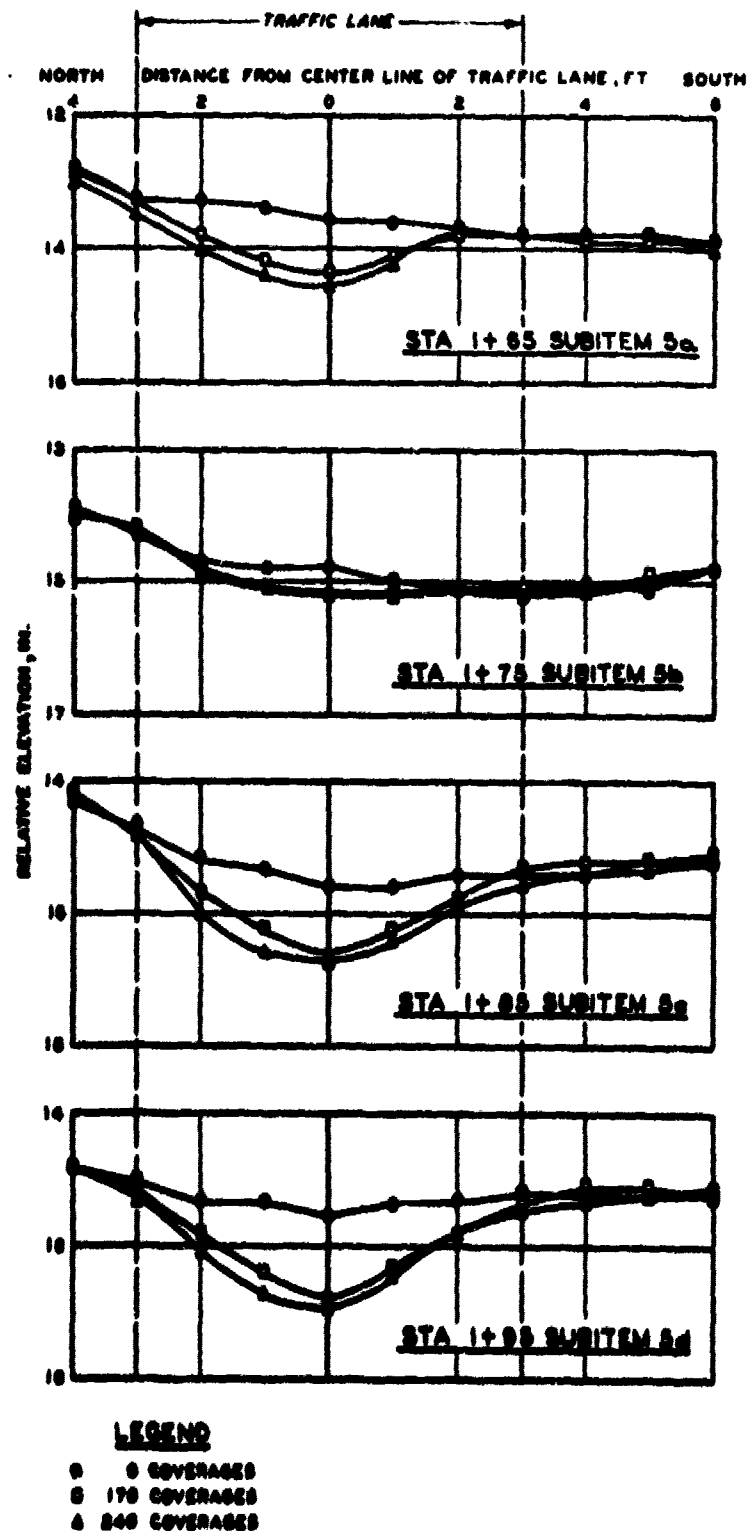
Figure 26. Surface deformation in subitems 5a-5d, flexible pavement test section
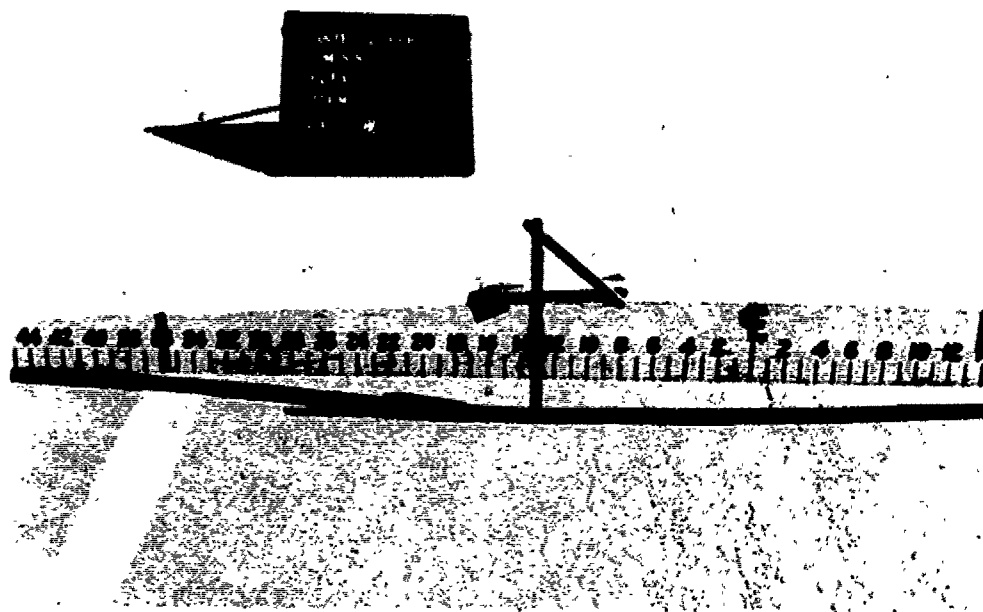
Figure 27. Longitudinal cracking in subitem 5c directly above joints between polystyrene panels, flexible pavement test section
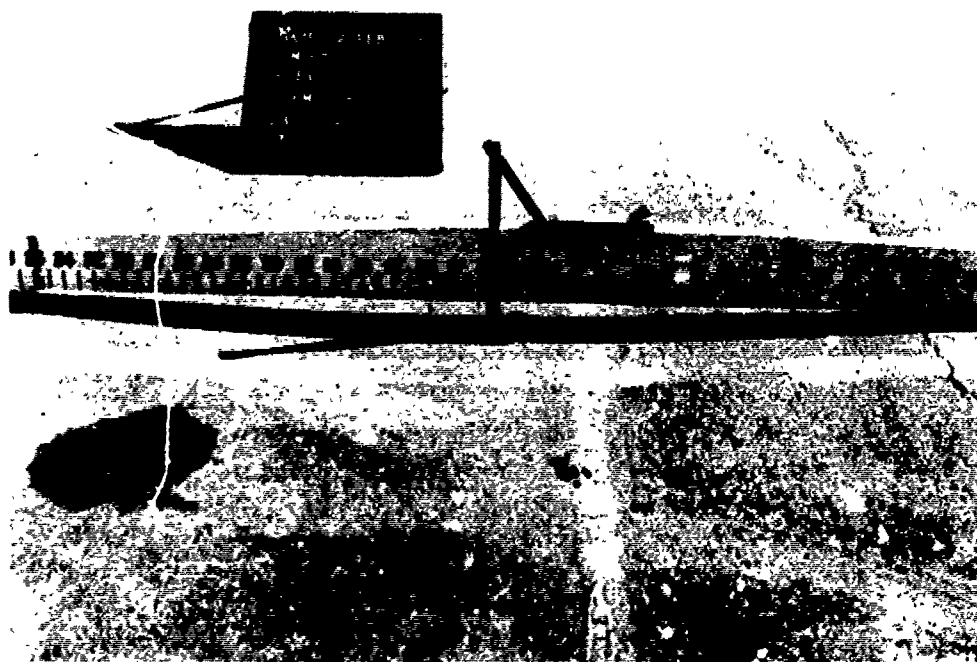
Figure 28. Condition of subitem 5a at assigned failure, flexible pavement test section

Figure 29. Condition of subitem 5b at assigned failure, flexible pavement test section
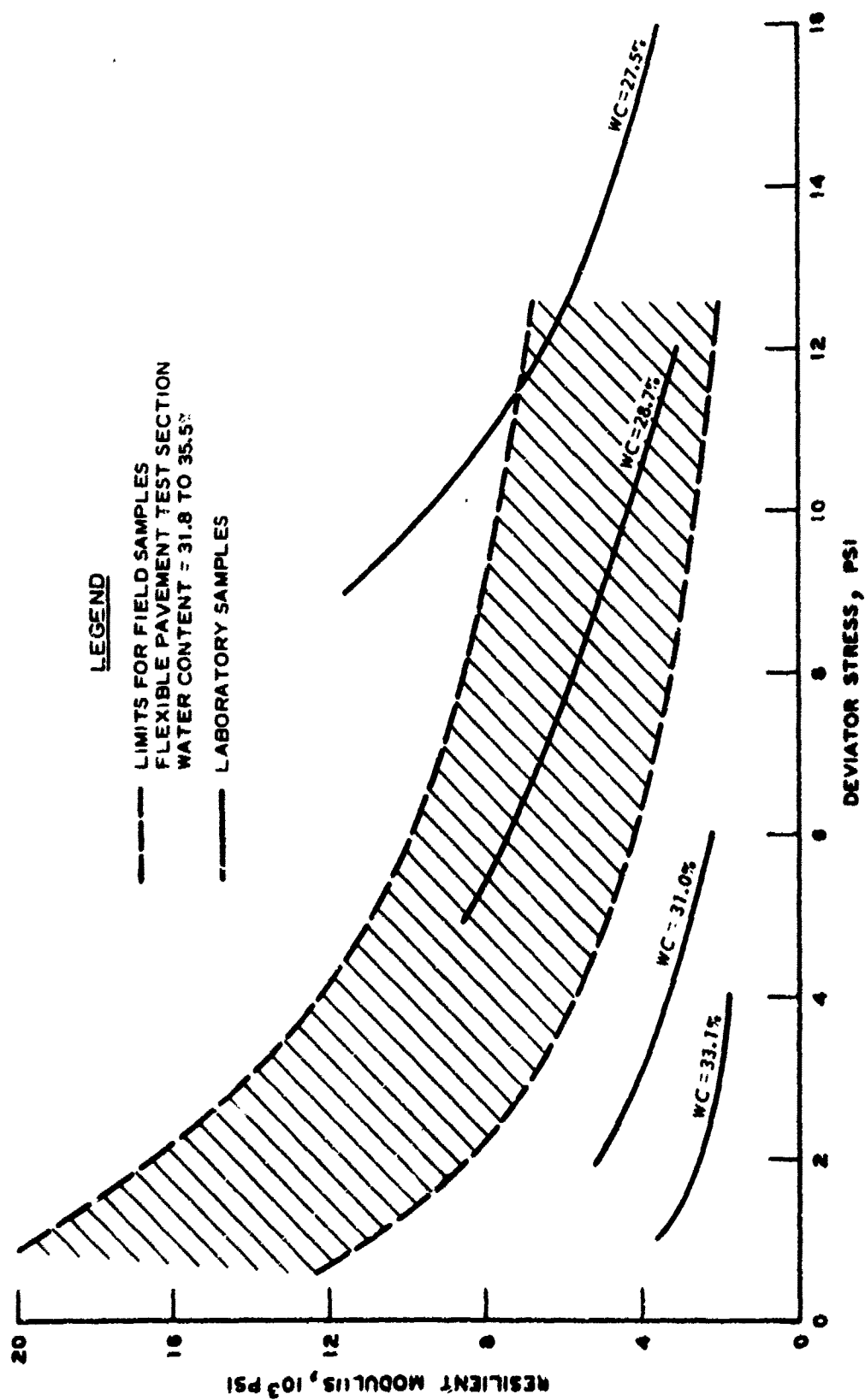
Figure 30. Resilient modulus relationship for field and laboratory samples of clay subgrade

87

LAYER	SECTION	MATERIAL	MODULUS	POISSON'S RATIO
1		ASPHALTIC CONCRETE	30,000 PSI 500,000 PSI	0.45
2		CRUSHED LIMESTONE	37,000 PSI	0.35
3		GRAVELLY SAND	16,400 PSI	0.20
4			8,700 PSI	0.20
5		120-PSI POLYSTYRENE	3,500 PSI	0.00
6		GRAVELLY SAND	15,000 PSI	0.20
7			7,800 PSI	0.20
8		SUBGRADE	3,000 PSI	0.40

DEPTH, IN.
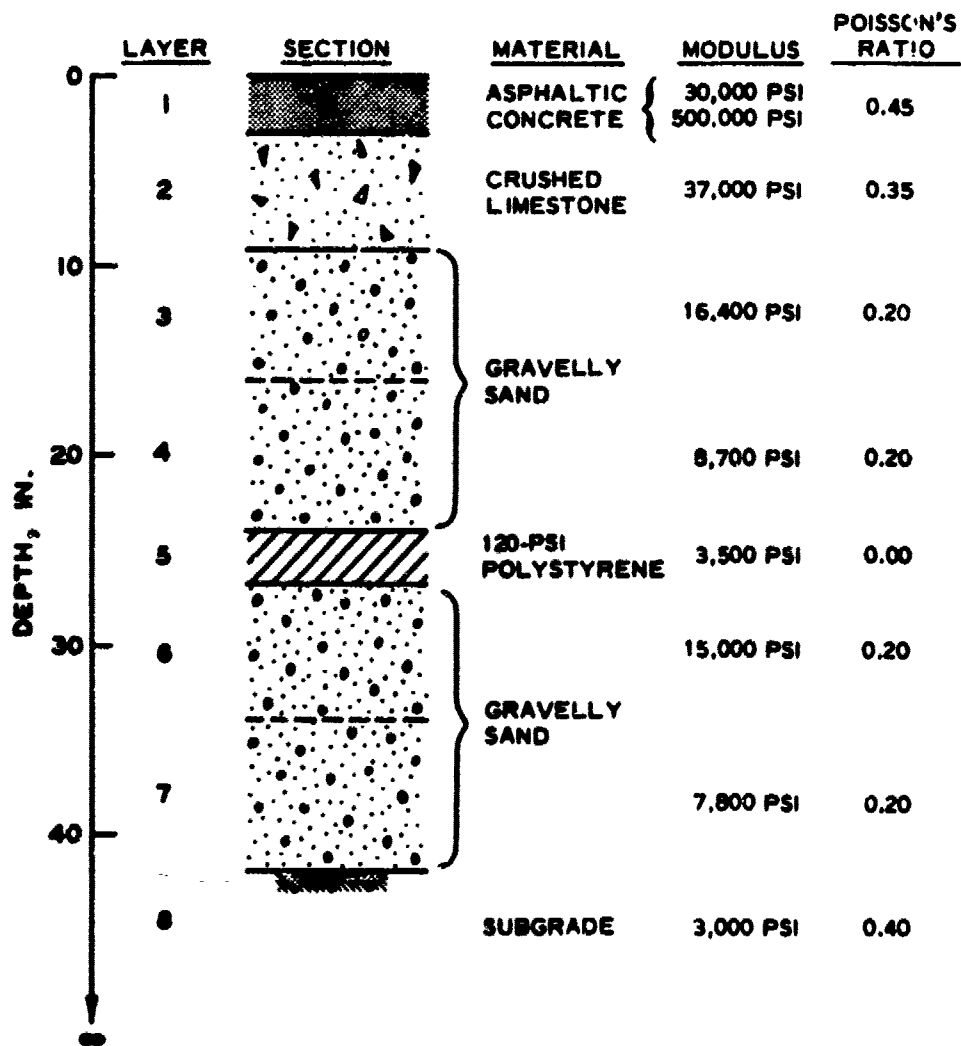
Figure 31. Representation of the material characterization
for subitem 5c, flexible pavement test section

88

LAYER	SECTION	MATERIAL	MODULUS	POISSON'S RATIO
1		ASPHALTIC CONCRETE	30,000 PSI 500,000 PSI	0.45
2		CRUSHED LIMESTONE	22,500 PSI	0.35
3		GRAVELLY SAND	8,000 PSI	0.20
4		120.-PSI STYROFOAM	3,500 PSI	0.00
5		120-PSI POLYSTYRENE	22,000 PSI	0.20
6			19,500 PSI	0.20
7		GRAVELLY SAND	13,500 PSI	0.20
8			7,000 PSI	0.20
9		SUBGRADE	3,000 PSI	0.40

DEPTH, IN.

0, 10, 20, 30, 40, ∞
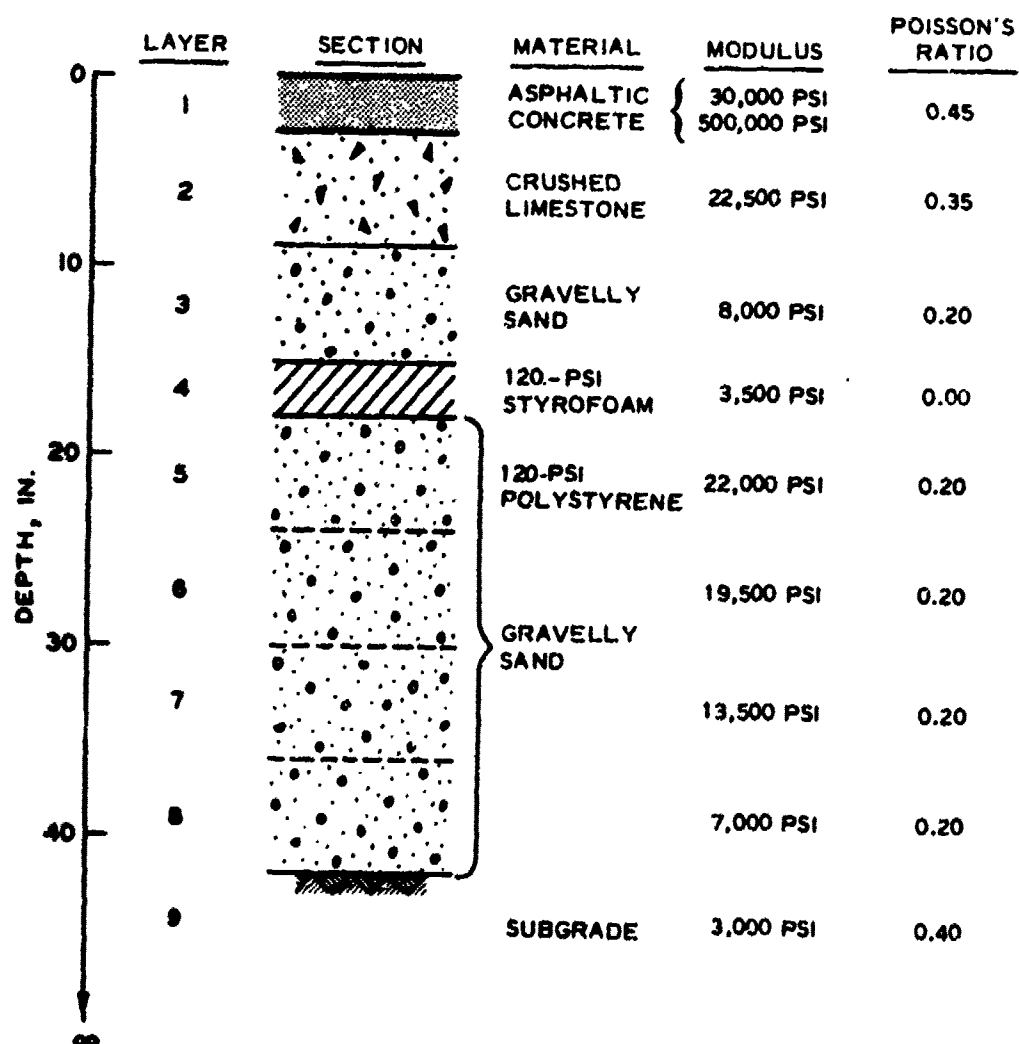
Figure 32. Representation of the material characterization for subitem 5d, flexible pavement test section

89
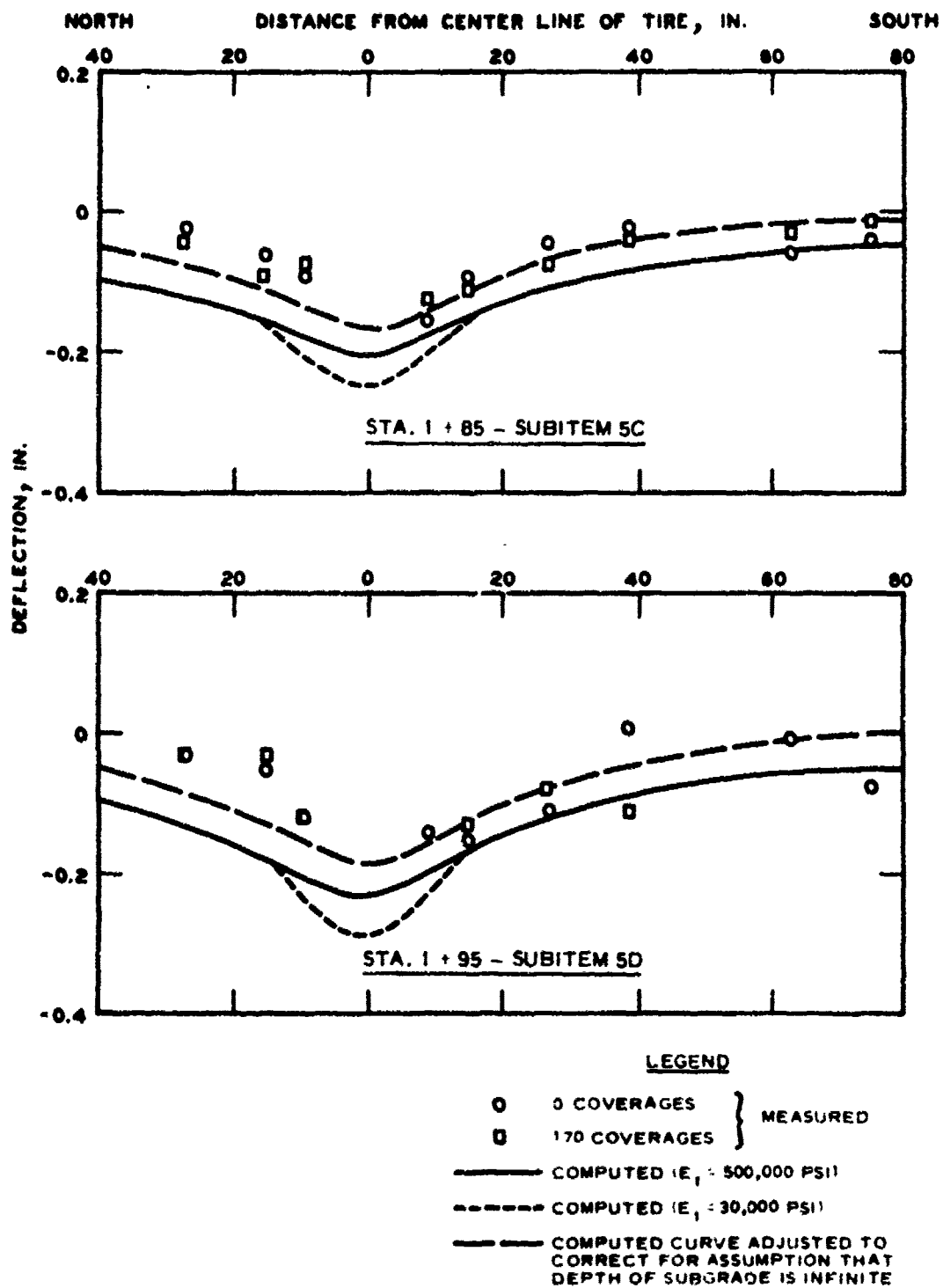
Figure 33. Comparison of measured and computed deflections for subitems 5c and 5d when loaded with a 50-kip single-wheel assembly
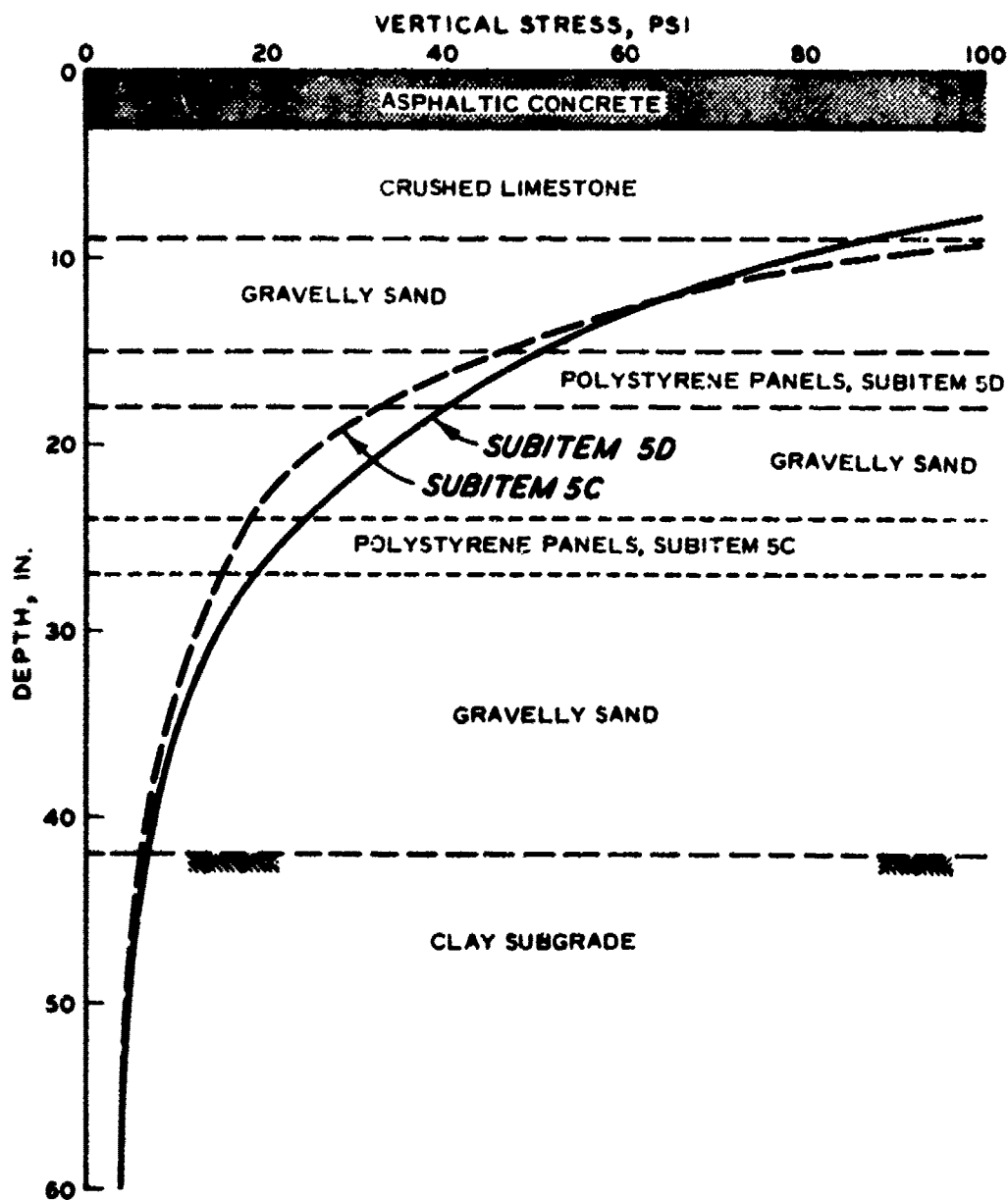
Figure 34. Distribution of vertical stress beneath center
of tire with depth for subitems 5c and 5d, summer conditions
(E_1 = 30,000 psi)
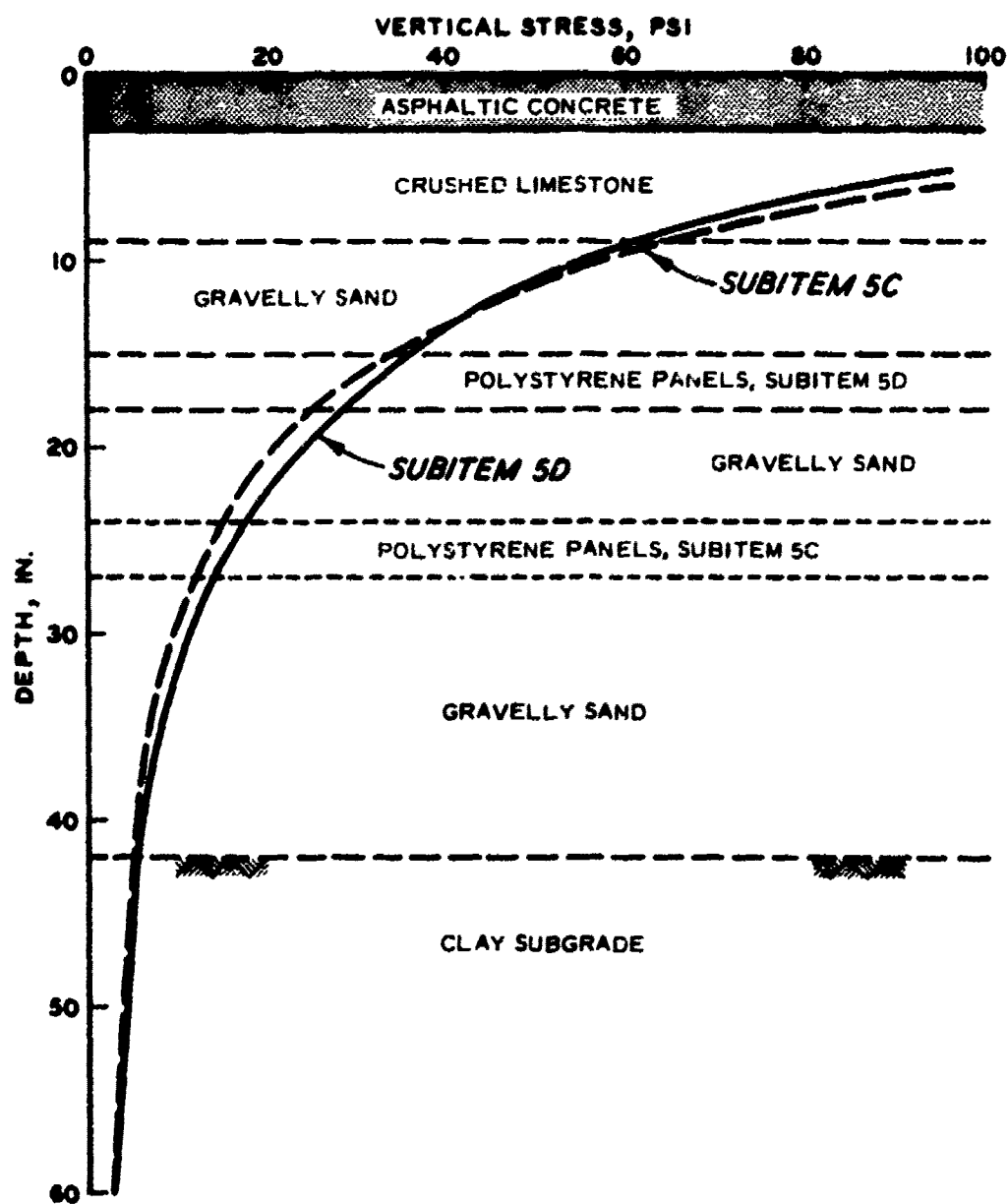
Figure 35. Distribution of vertical stress beneath center of tire with depth for subitems 5c and 5d, winter conditions $(E_1 = 500,000 \text{ psi})$
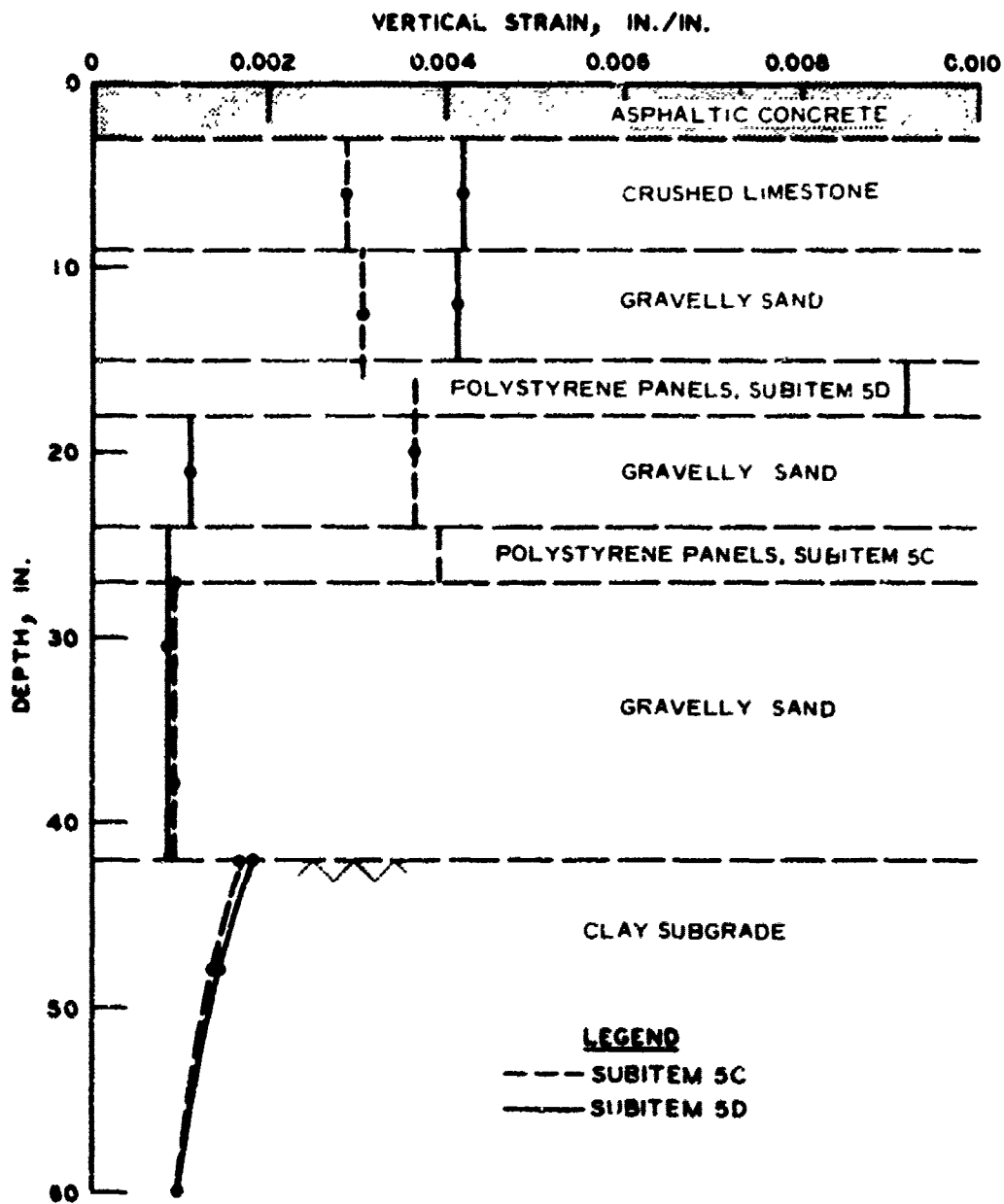
Figure 36. Distribution of vertical strain beneath center of tire with depth for subitems 5c and 5d, summer conditions $(E_1 = 30,000$ psi)
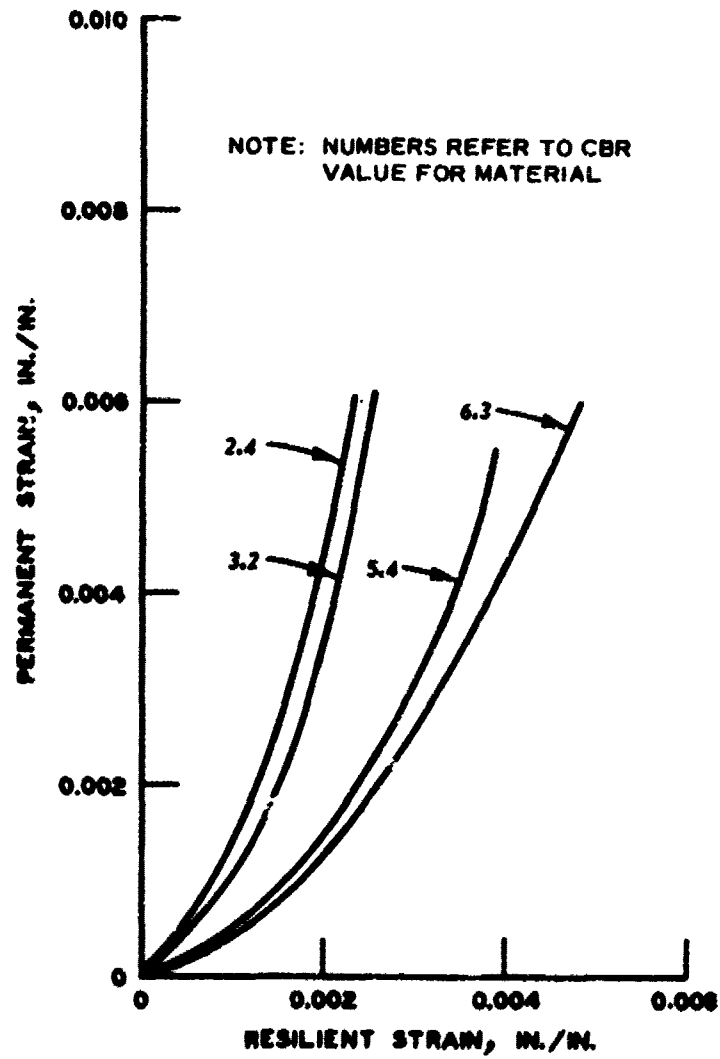
Figure 37. Relationship between perma-
nent strain and resilient strain for
clay subgrade
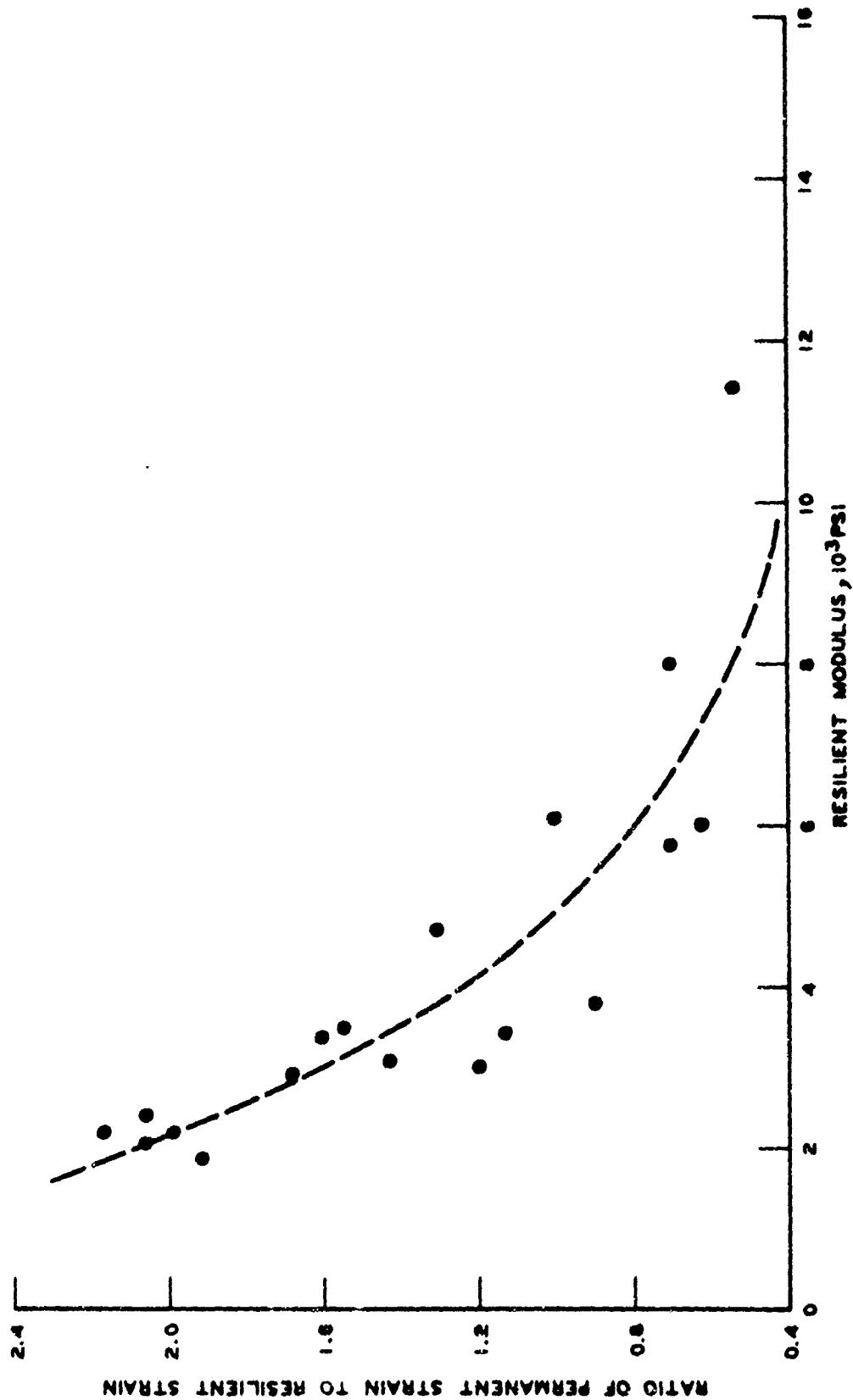
Figure 38. Relationship between the ratio of permanent strain to resilient strain and resilient modulus for 100 stress repetitions, clay subgrade

95
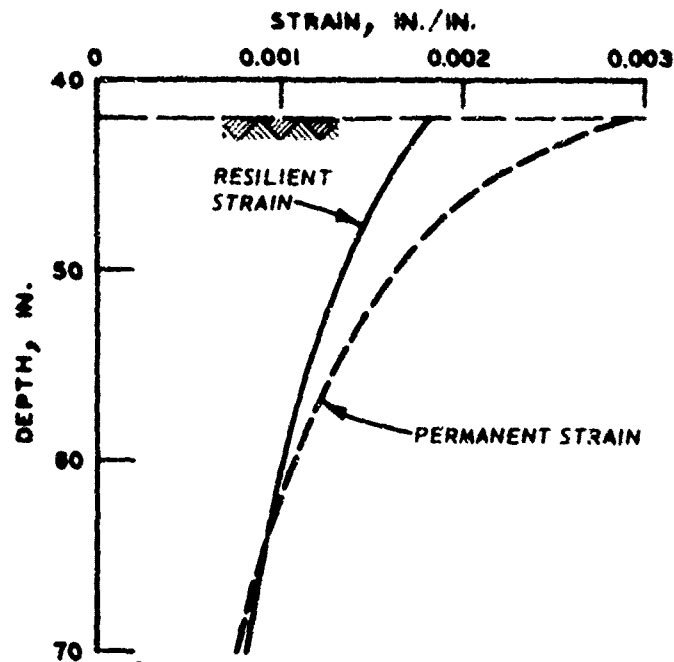
Figure 39. Comparison of resilient and permanent strain in the subgrade of subitem 5d, flexible pavement test section
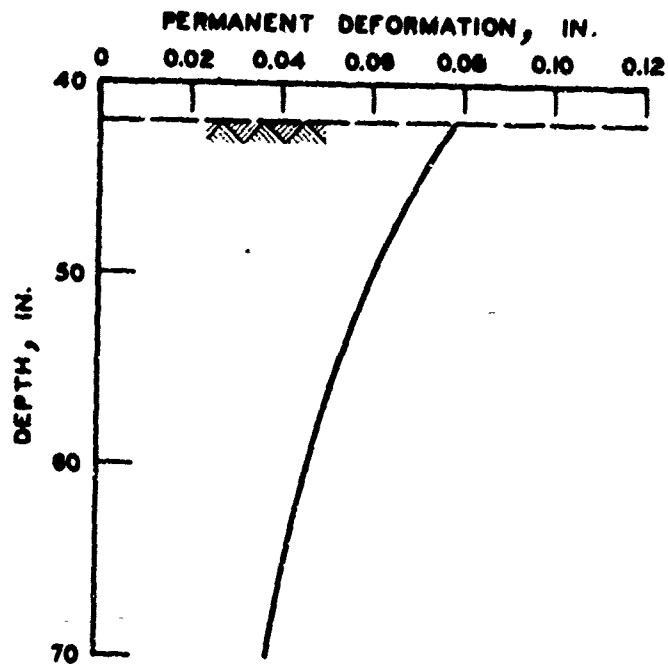
Figure 40. Permanent deformation within the subgrade of subitem 5d, assuming zero permanent strain at 120-in. depth, flexible pavement test section

96
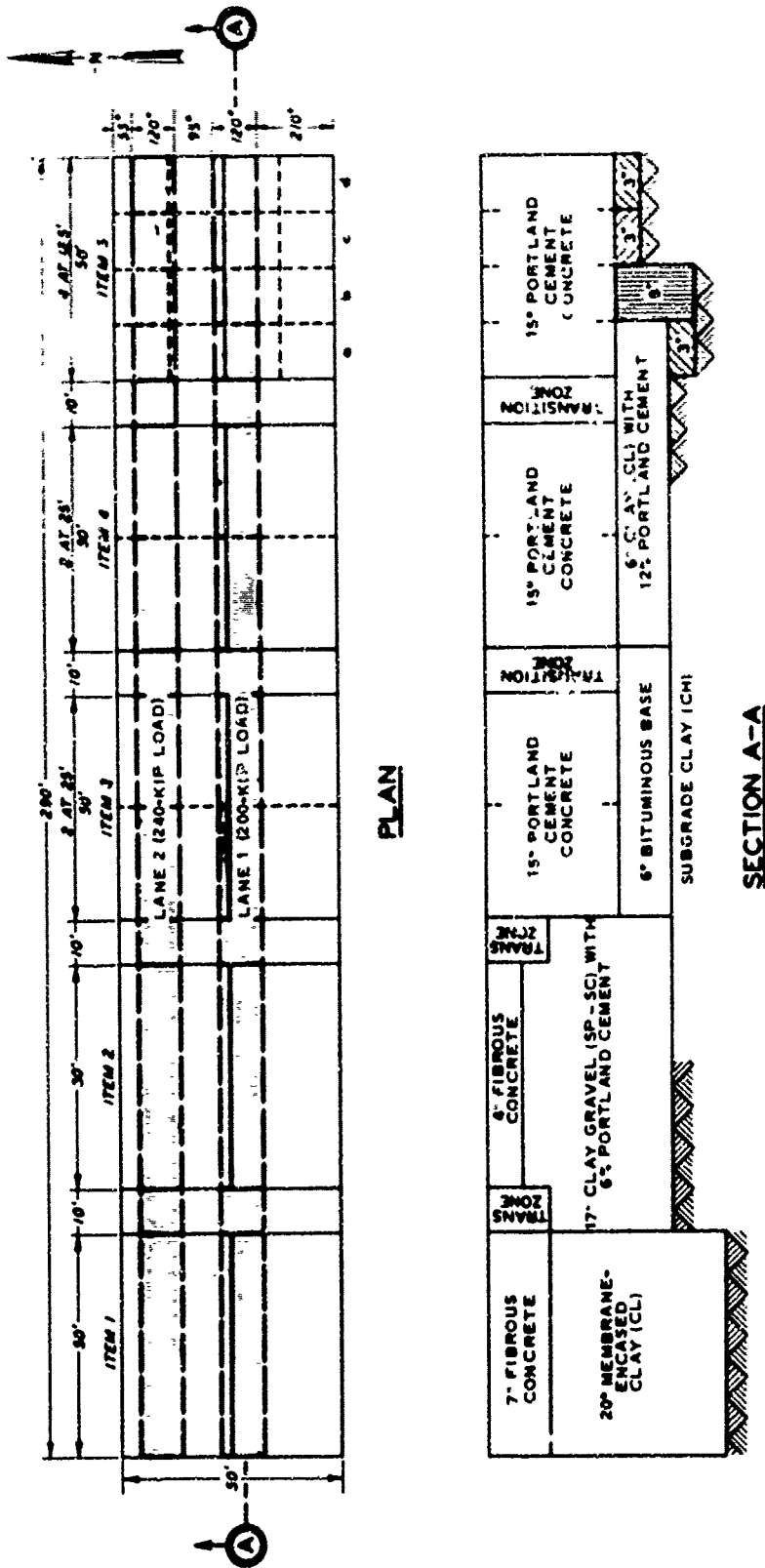
Figure 41. Layout of the rigid pavement test section
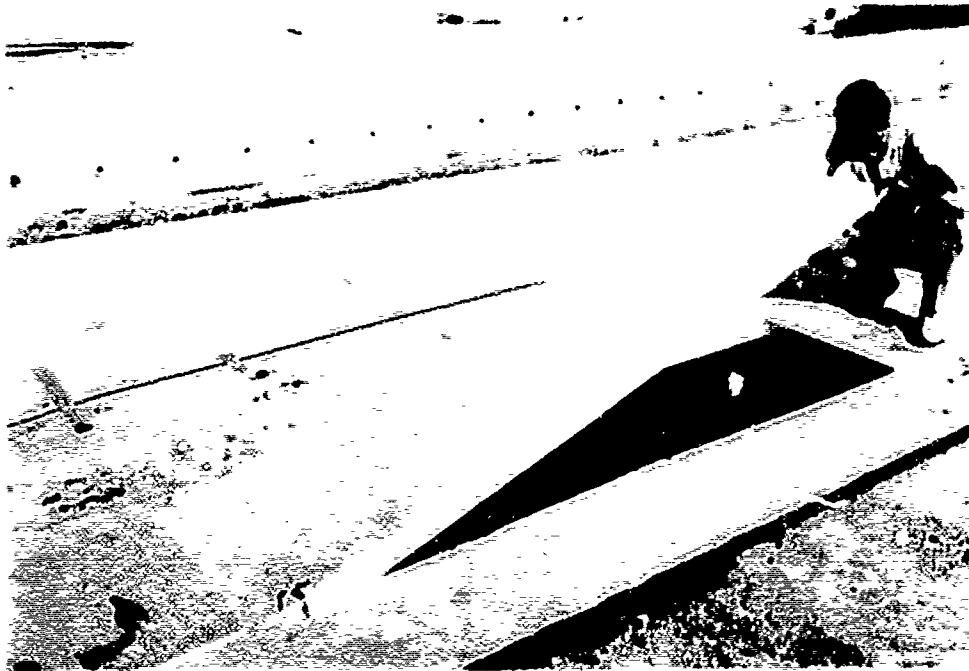
Figure 42. Polystyrene panels in place in subitem 5a, rigid pavement test section
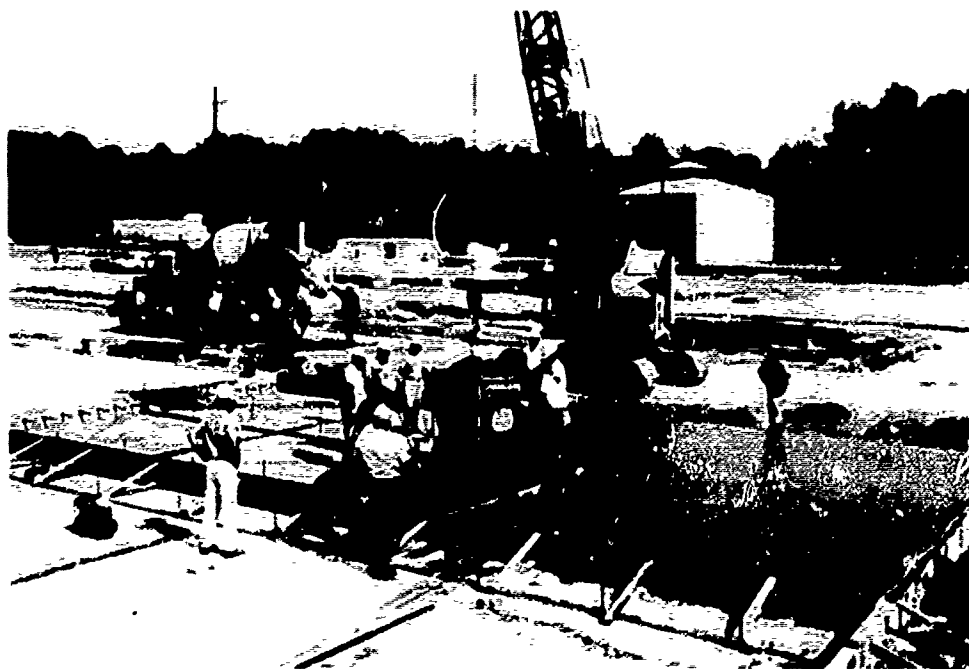
Figure 43. Placement of PCC in north lane of of item 5, rigid pavement test section

0.5"

JOINT SEALANT

0.75"

7.5"

2.25"

15"

3"

NO. 5 DEFORMED TIE BARS,
30 IN. LONG, SPACED
30 IN. C TO C

1.5"
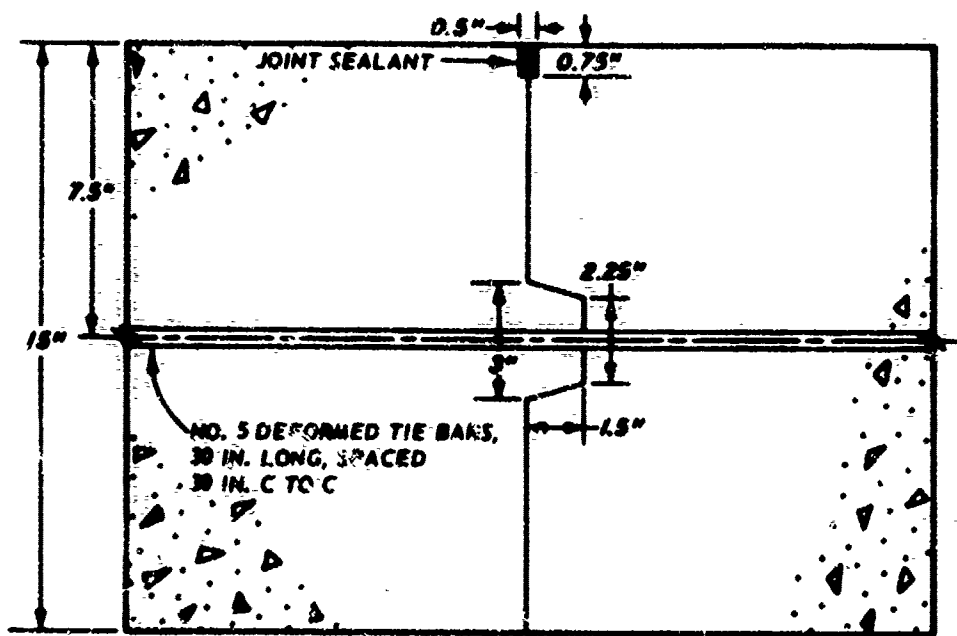
KEYED-AND-TIED JOINT

Figure 44.   Details of longitudinal construction joint

99
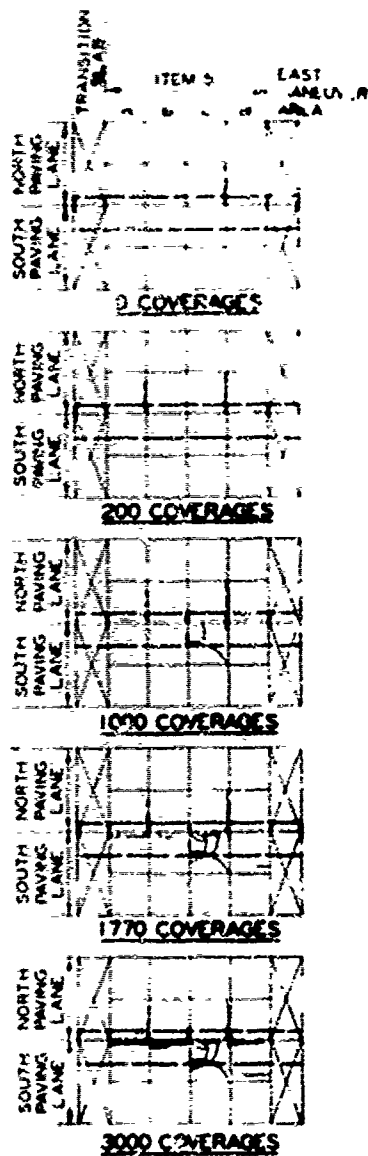
a. LANE 1. 200-KIP LOADING   b. LANE 2. 240-KIP LOADING

LEGEND

—————— BOUNDARY OF TRAFFIC LANE

* CRACKING SHOWN DEVELOPED DURING COLLECTION OF STATIC
INSTRUMENTATION DATA IN LANE 2

TRAFFIC WAS APPLIED BEYOND 540 COVERAGES, BUT NO ADDITIONAL
LOAD-ASSOCIATED CRACKS DEVELOPED
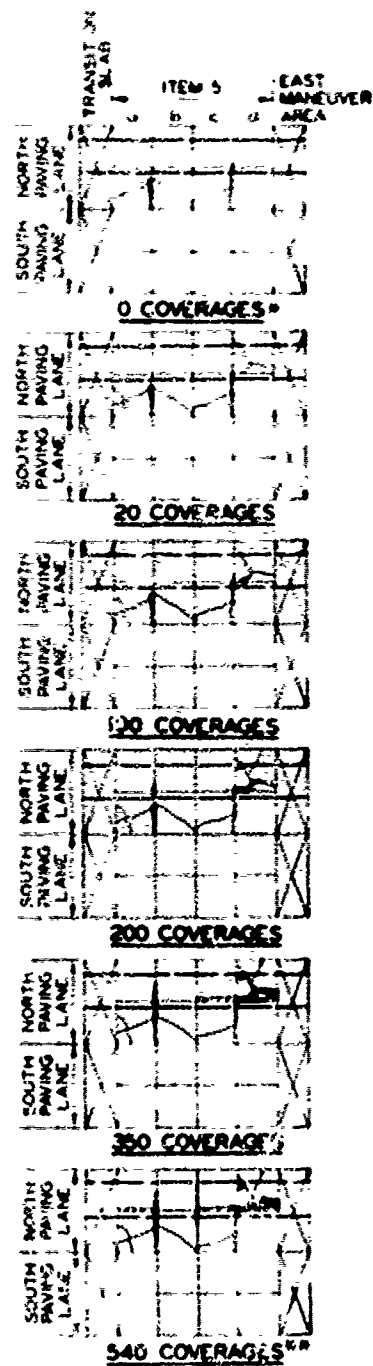
Figure 45. Crack development in item 5, rigid
pavement test section
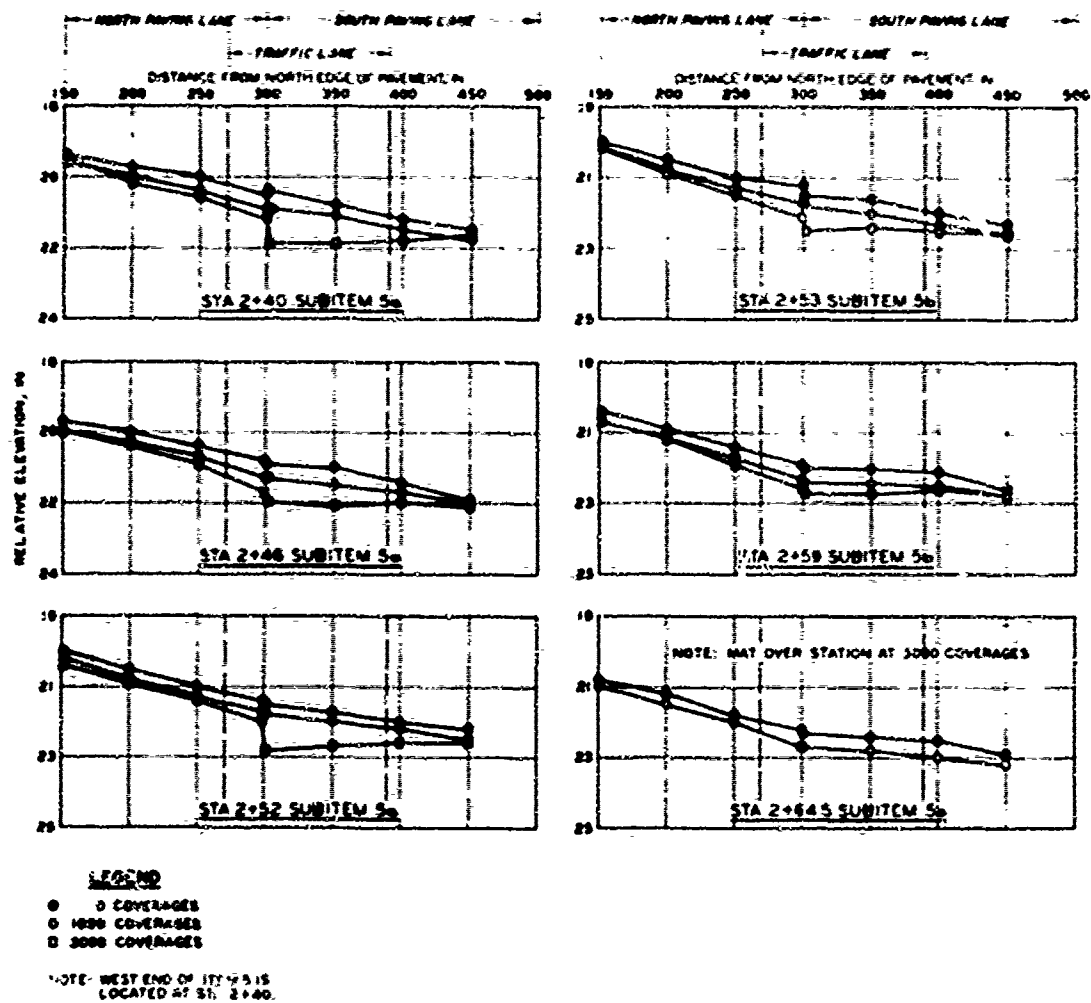
Figure 46. Surface deformation in subitems 5a and 5b,
lane 1, rigid pavement test section
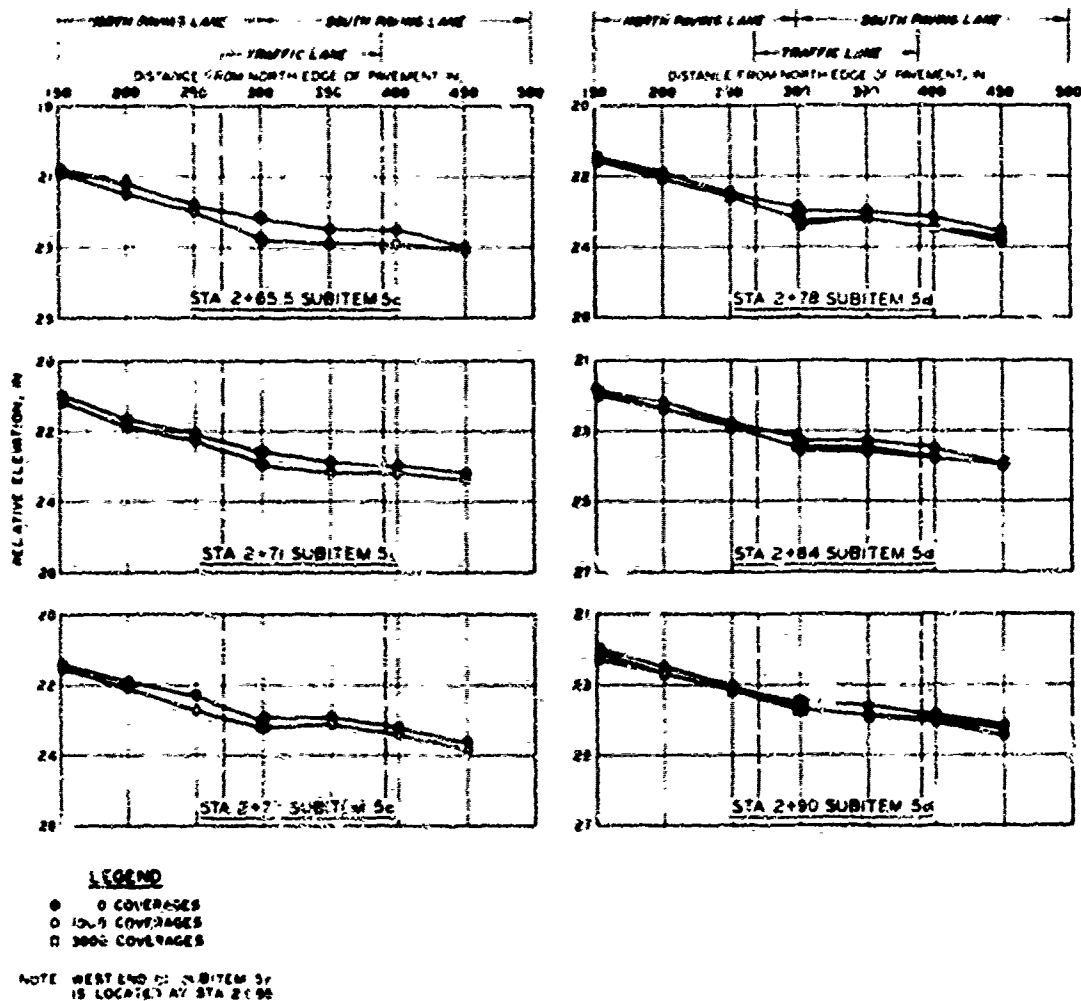
Figure 47. Surface deformation in subitems 5c and 5d, lar 1, rigid pavement test section
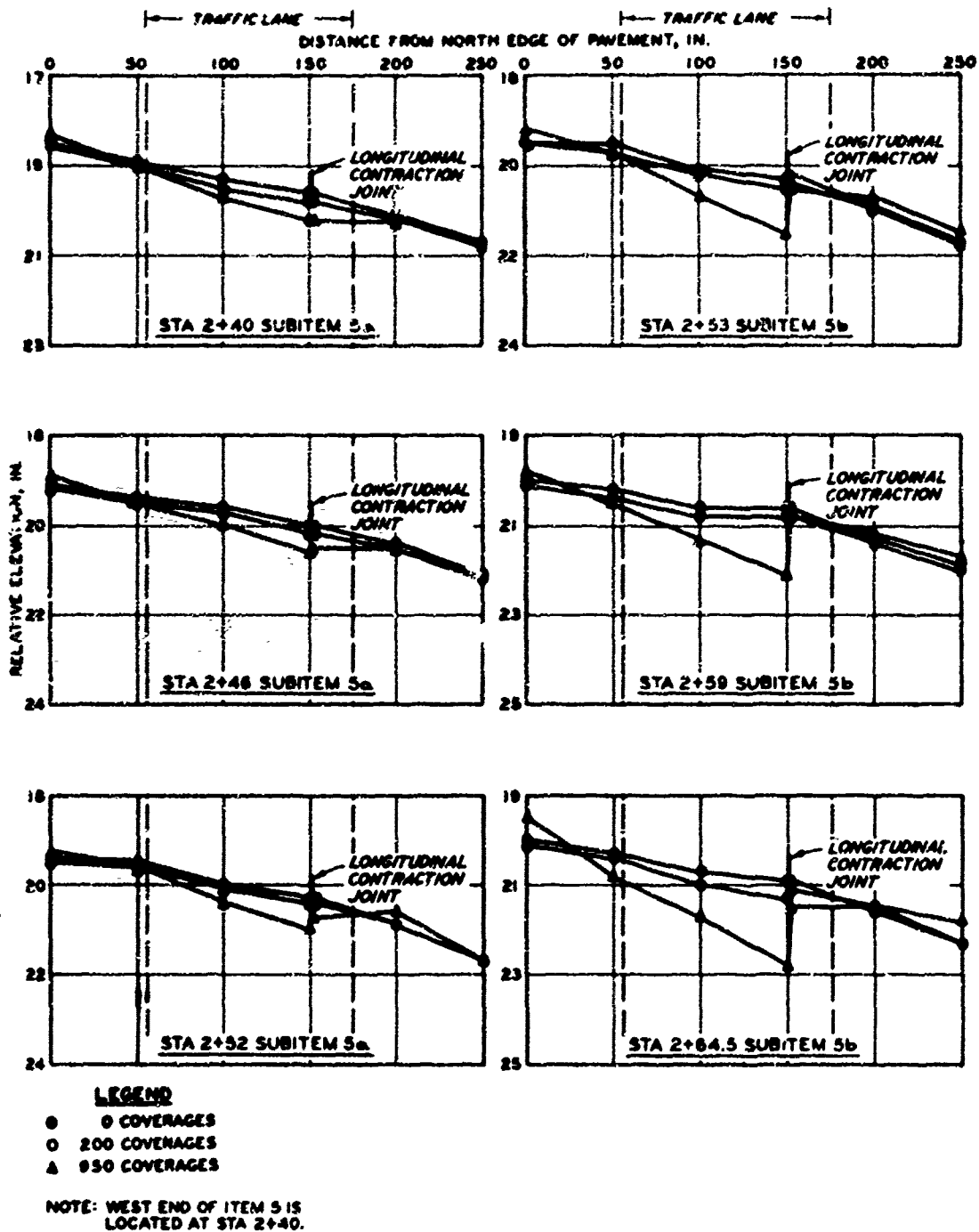
Figure 48. Surface deformation in subitems 5a and 5b, lane 2, rigid pavement test section
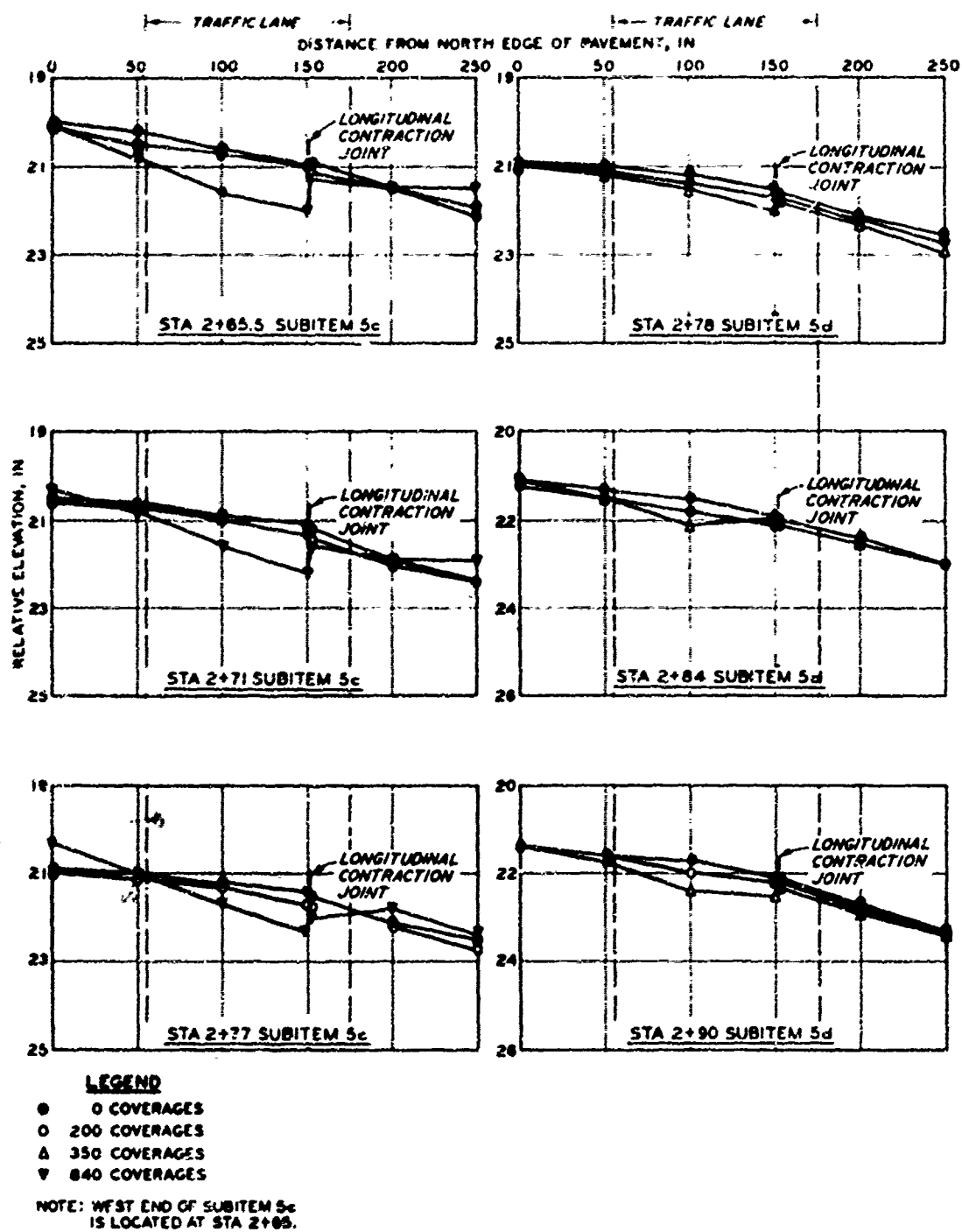
Figure 49. Surface deformation in subitems 5c and 5d, lane 2, rigid pavement test section
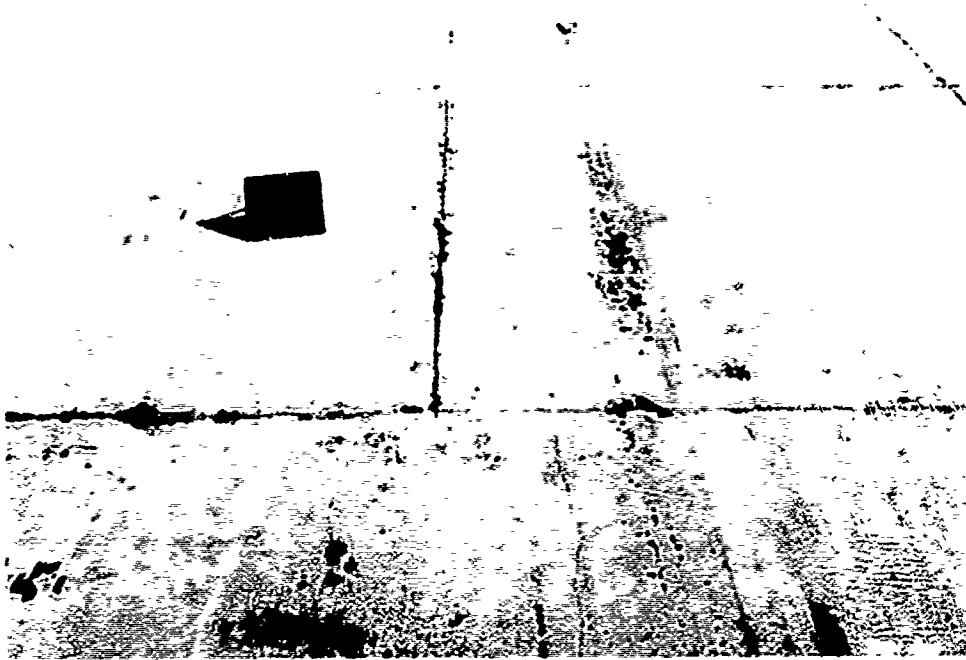
Figure 50. Early cracking in subitem 5a, lane 1, 1770 coverages, rigid pavement test section

Figure 51. Condition of subitem 5a, lane 1, at completion of traffic, 3000 coverages, rigid pavement test section

Figure 52. Condition of subitem 5a, lane , before traffic,
rigid pavement test section
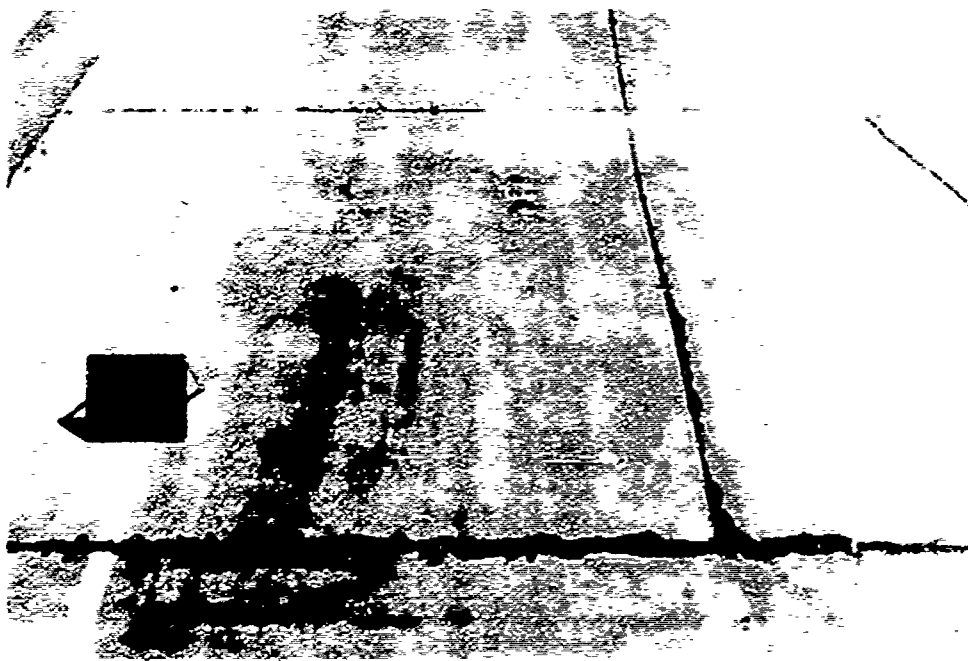
Figure 53. Condition of subitem 5a, lane , after traffic,
rigid pavement test section
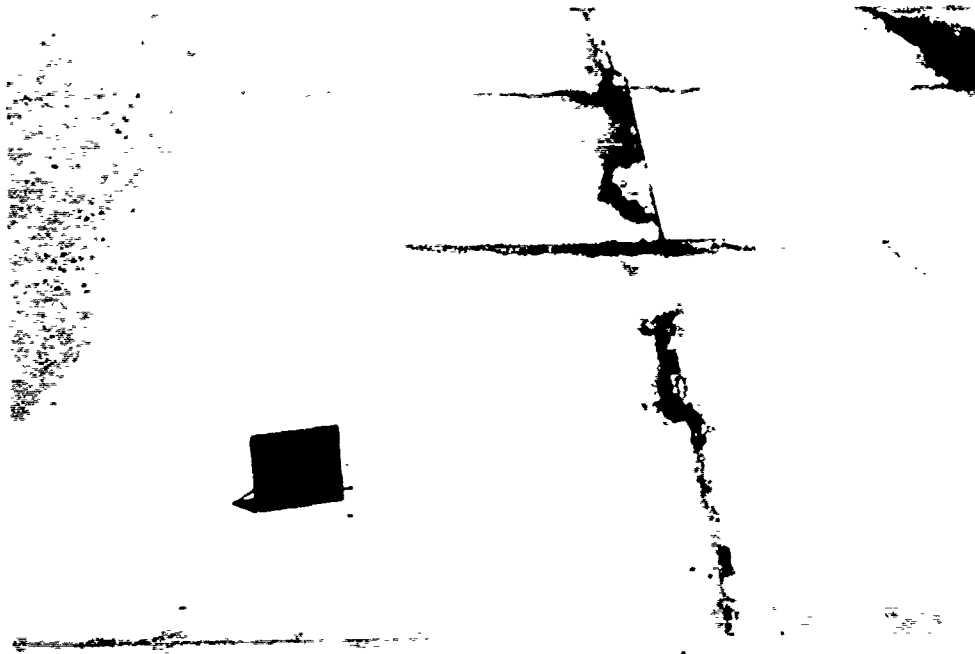
Figure 54. Condition of subitem 5a, lane 2, 950 coverages, rigid pavement tes· section
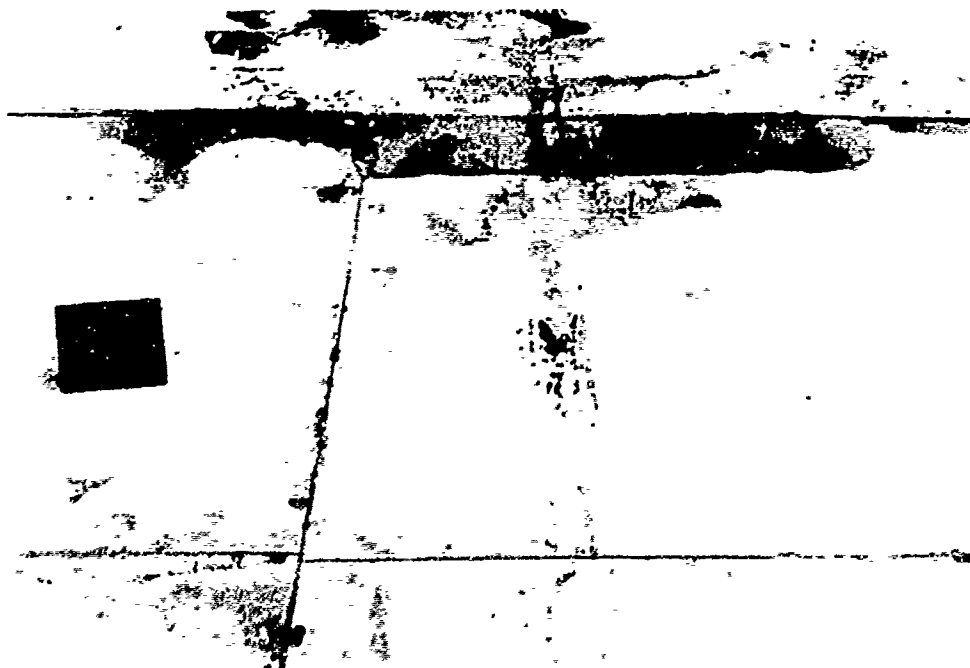
Figure 55. Condition of subitem 5b, lane 1, 1770 coverages, rigid pavement test section
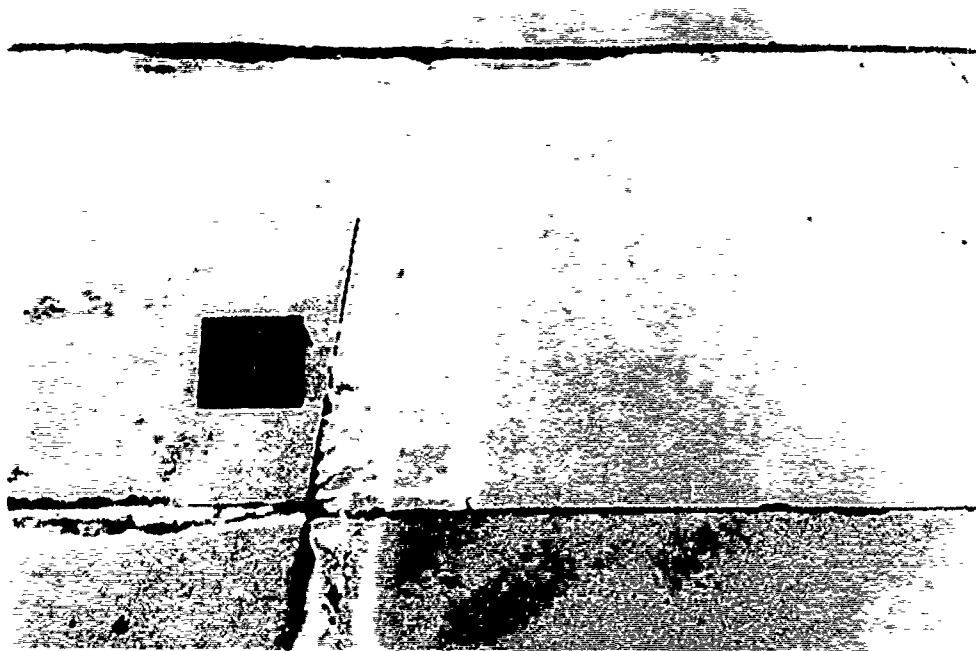
Figure 56. Condition of subitem 5b, lane 1, 3000 coverages, rigid pavement test section

Figure 57. Condition of subitem 5b, lane 2, 950 coverages, rigid pavement test section
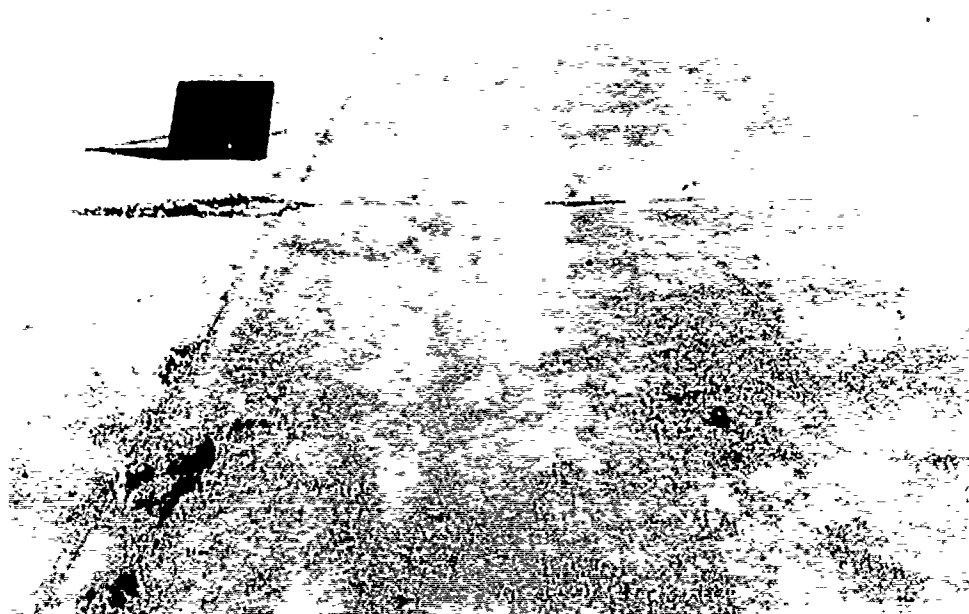
Figure 58. Condition of subitem 5c, lane 1, 1000 coverages, rigid pavement test section

Figure 59. Condition of subitem 5c, lane 1, 1230 coverages, rigid pavement test section
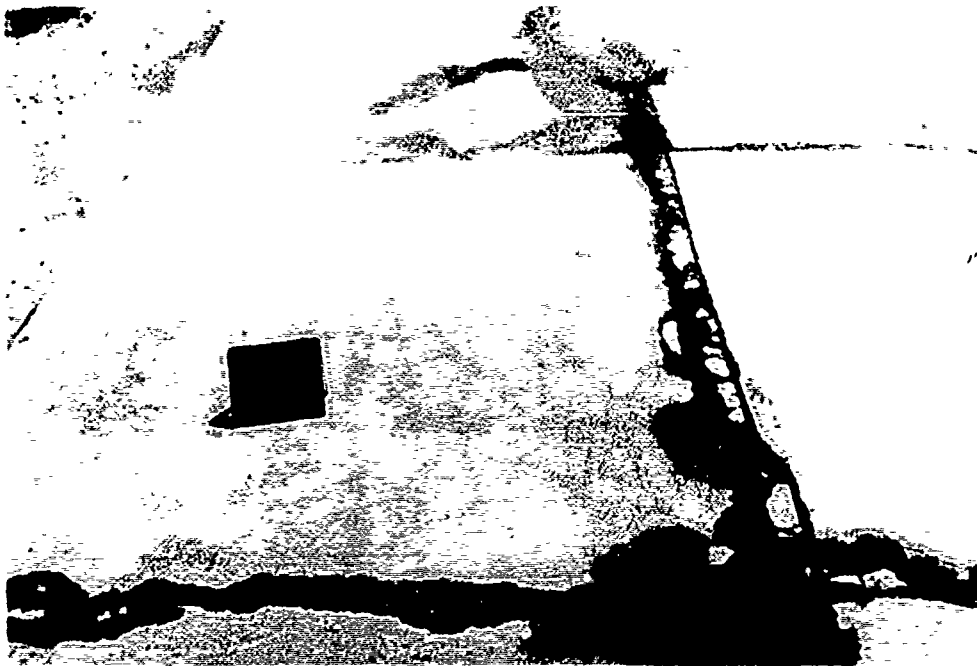
Figure 60. Condition of subitem 5c, lane 2, 840 coverages, rigid pavement test section
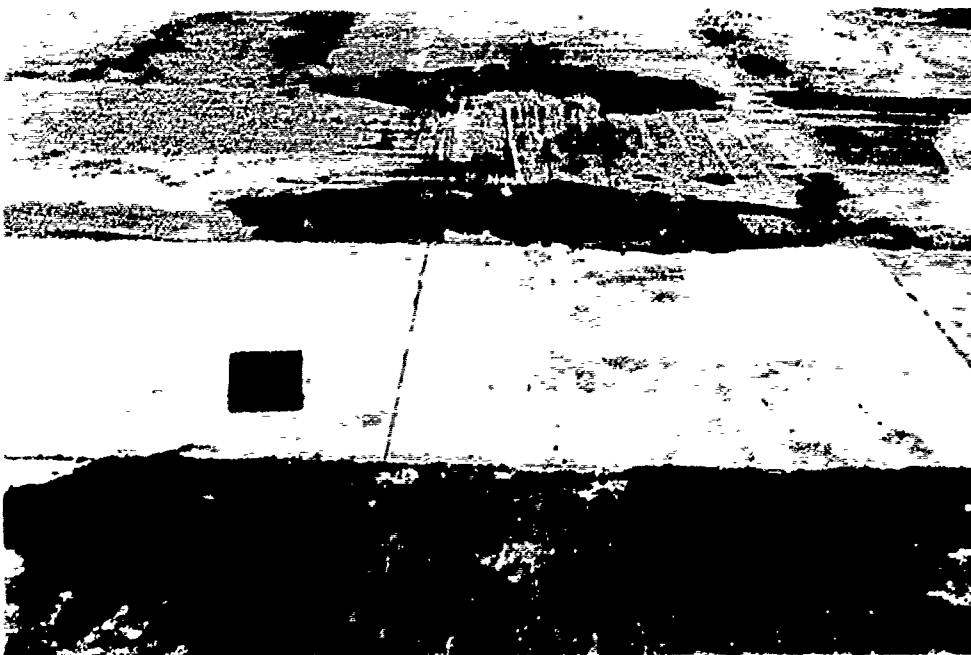
Figure 61. Condition of subitem 5d, lane 1, 1770 coverages, rigid pavement test section

Figure 62. Condition of subitem 5d, lane 1, 3000 coverages, rigid pavement test section

Figure 63. Condition of subitem 5d, lane 2, 200 coverages, rigid pavement test section

Figure 64. Condition of subitem 5d, lane 2, 350 coverages,
rigid pavement test section

112
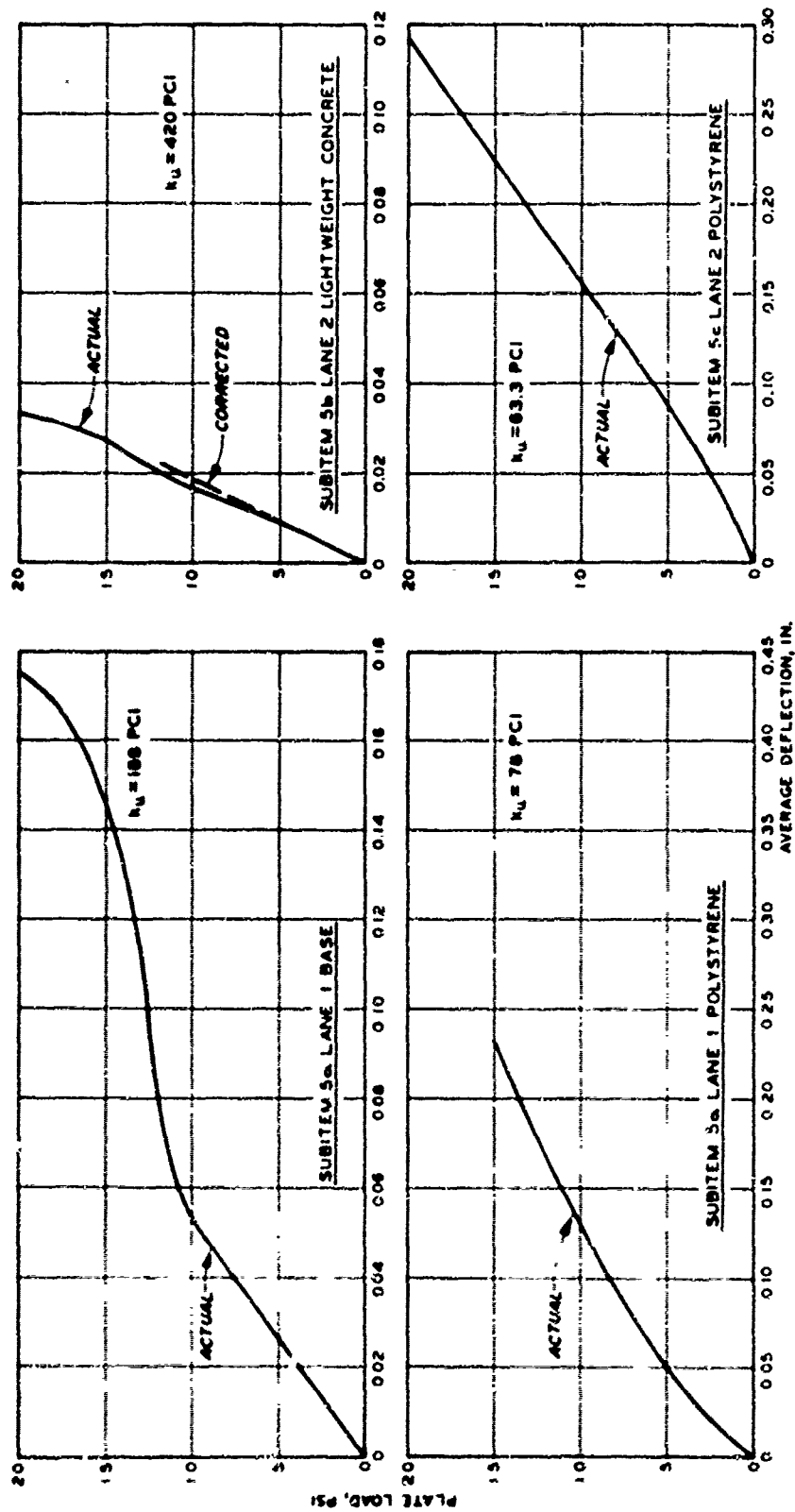
NOTE k_u IS THE MODULUS OF SOIL REACTION, IN POUNDS PER CUBIC INCH, UNCORRECTED FOR SATURATION.

Figure 65. Plate bearing tests, subitems 5a-5c, lanes 1 and 2, rigid pavement test section

113

Figure 66. Plate bearing tests, subitems 5c and
5d, lanes 1 and 2, rigid pavement test section
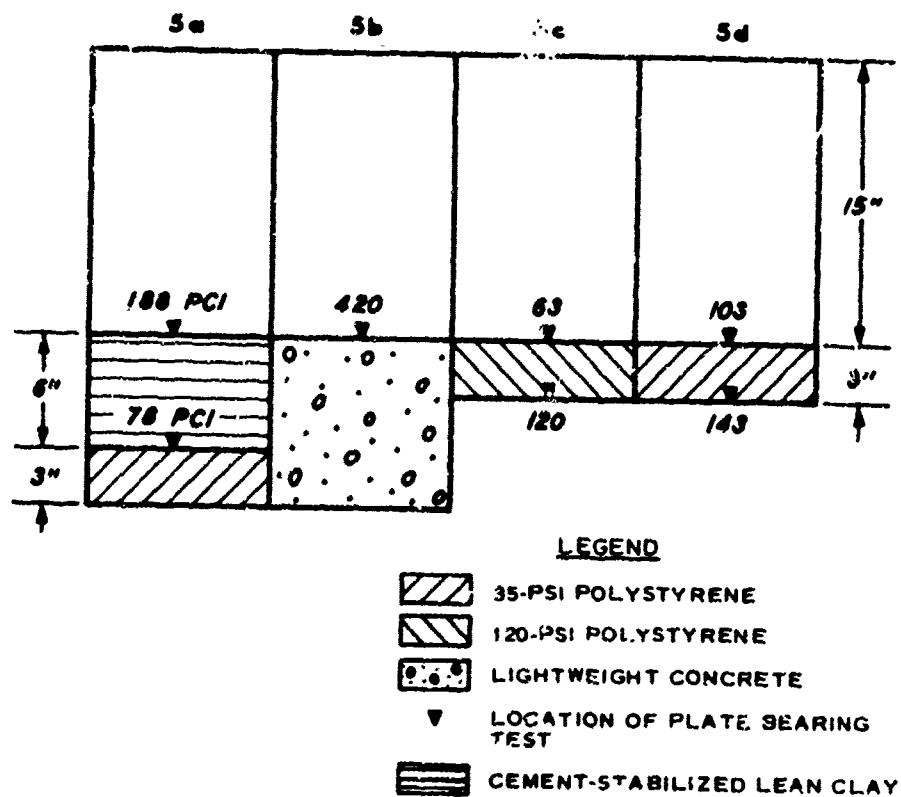
Figure 67. Location of plate bearing tests in item 5, rigid pavement test section

Figure 68. Condition of 120-psi polystyrene panels
along longitudinal construction joint in subitem 5c,
lane 1, rigid pavement test section
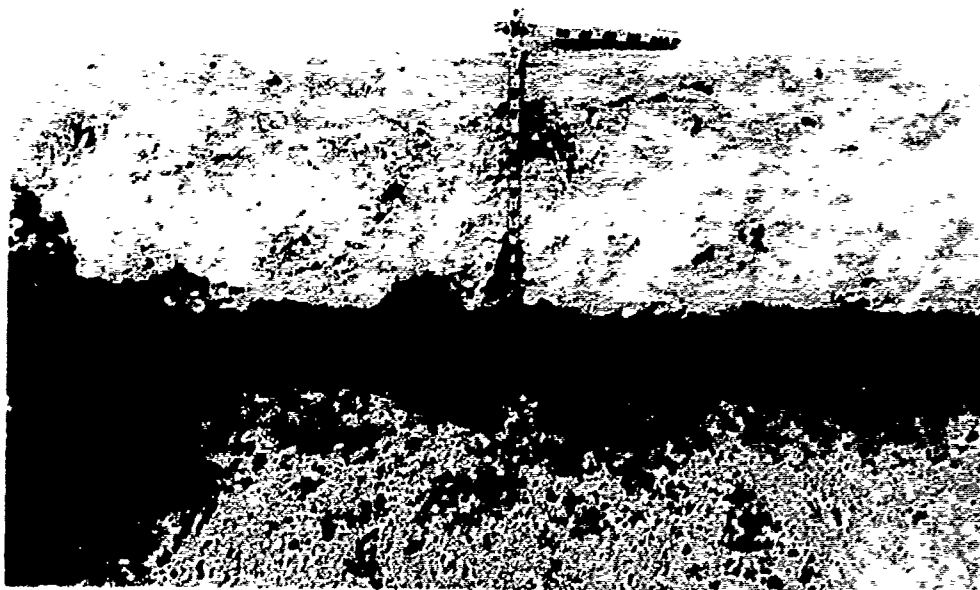
Figure 69. Test pit in subitem 5b, rigid pavement test
section, illustrating differential deformation in light-
weight concrete along the longitudinal contraction joint

Figure 70. Test pit in subitem 5b, rigid pavement test section, illustrating pumping of clay subgrade through crack in lightweight concrete
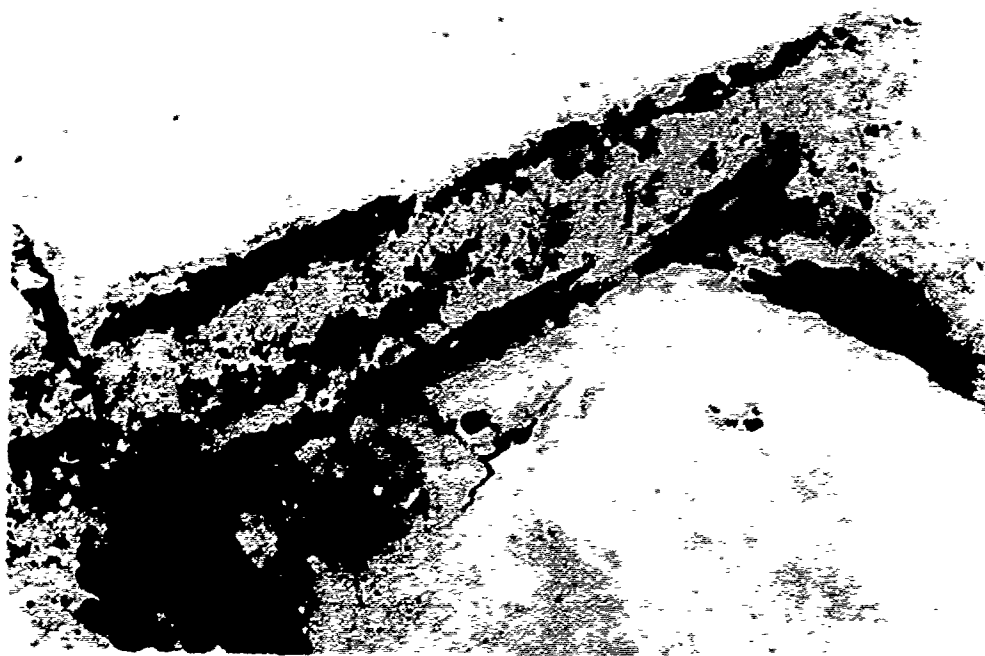
Figure 71. Condition of 120-psi polystyrene panels along longitudinal contraction joint in subitem 5c, lane 2, rigid pavement test section
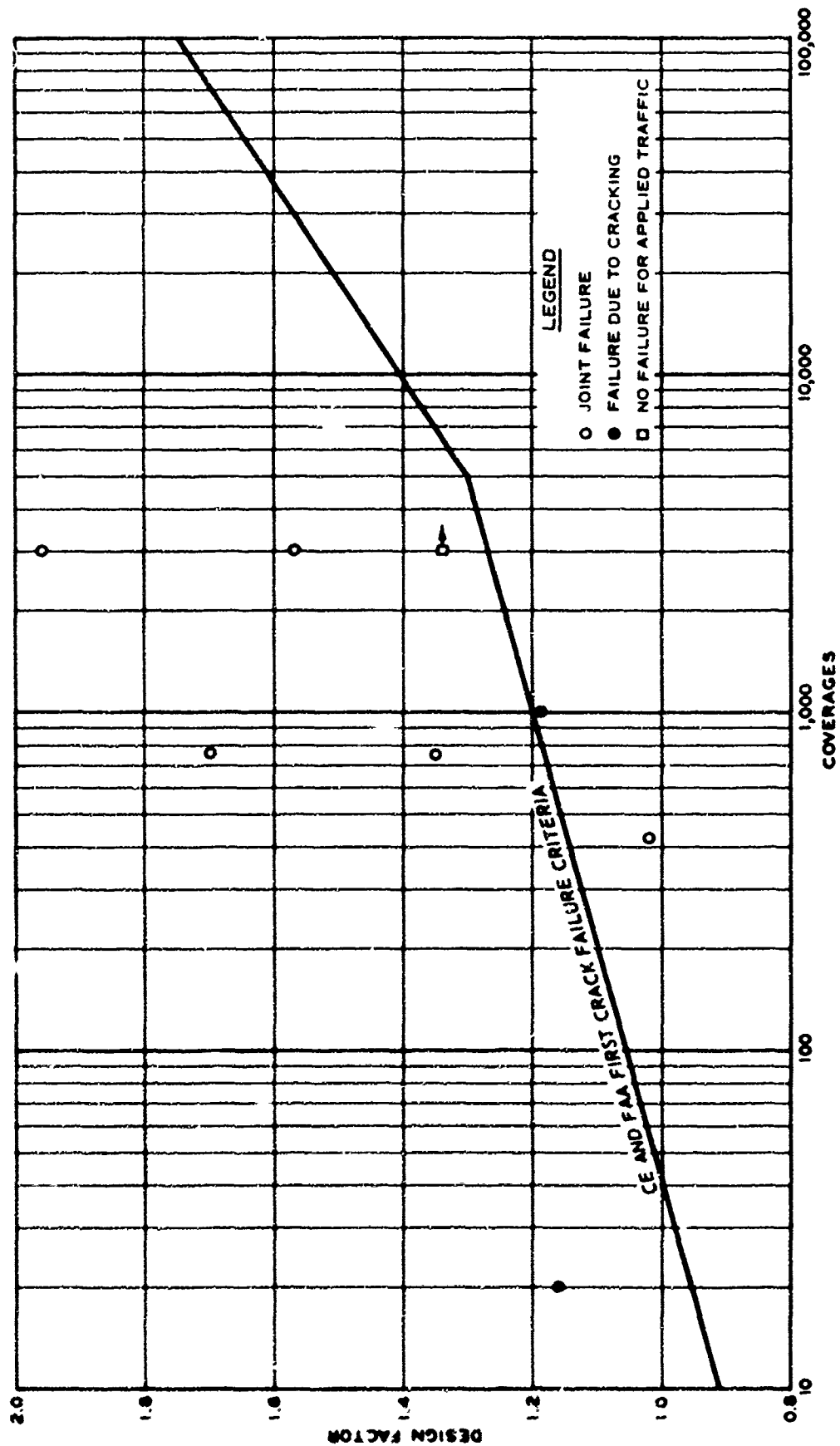
Figure 72. Comparison of rigid pavements containing insulating layers with established performance criteria

a. LONGITUDINAL CONSTRUCTION JOINT   b. LONGITUDINAL CONTRACTION JOINT
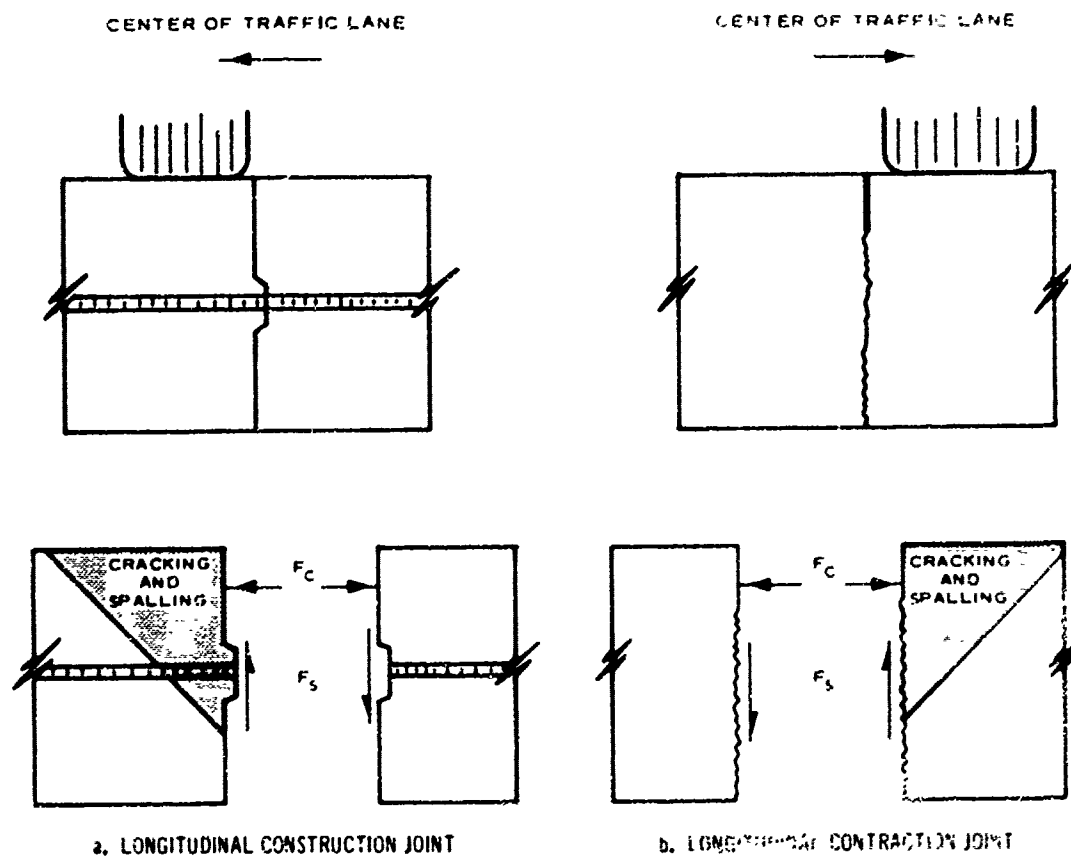
Figure 73.   Forces on face of joint causing spalling and
cracking along side of maximum traffic

119
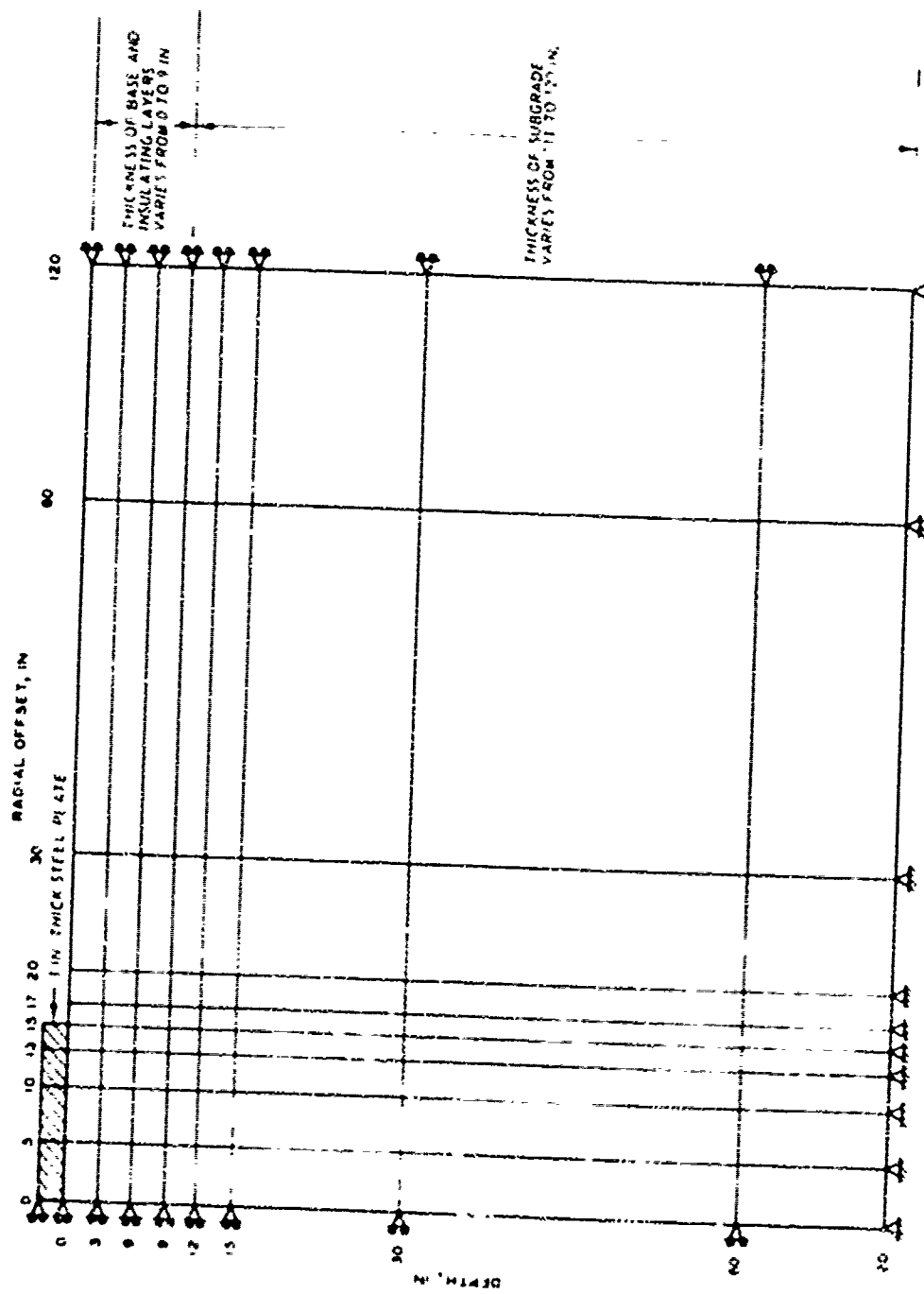
Figure 74. Finite element mesh for simulation of plate bearing tests on subgrade and insulating layers
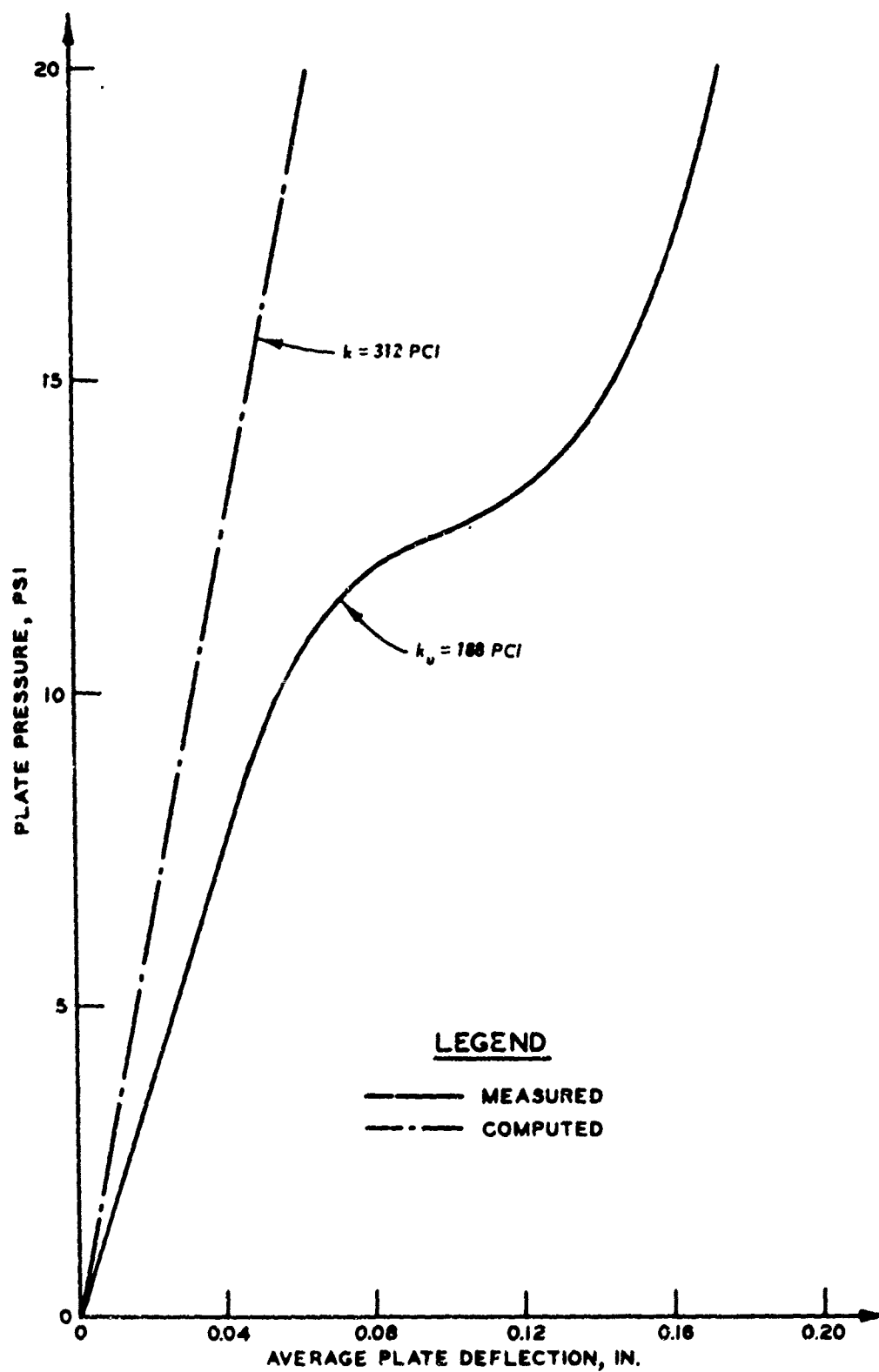
Figure 75. Load-deflection curves from plate bearing tests on
cement-stabilized clay over 35-psi polystyrene in subitem 5a

121
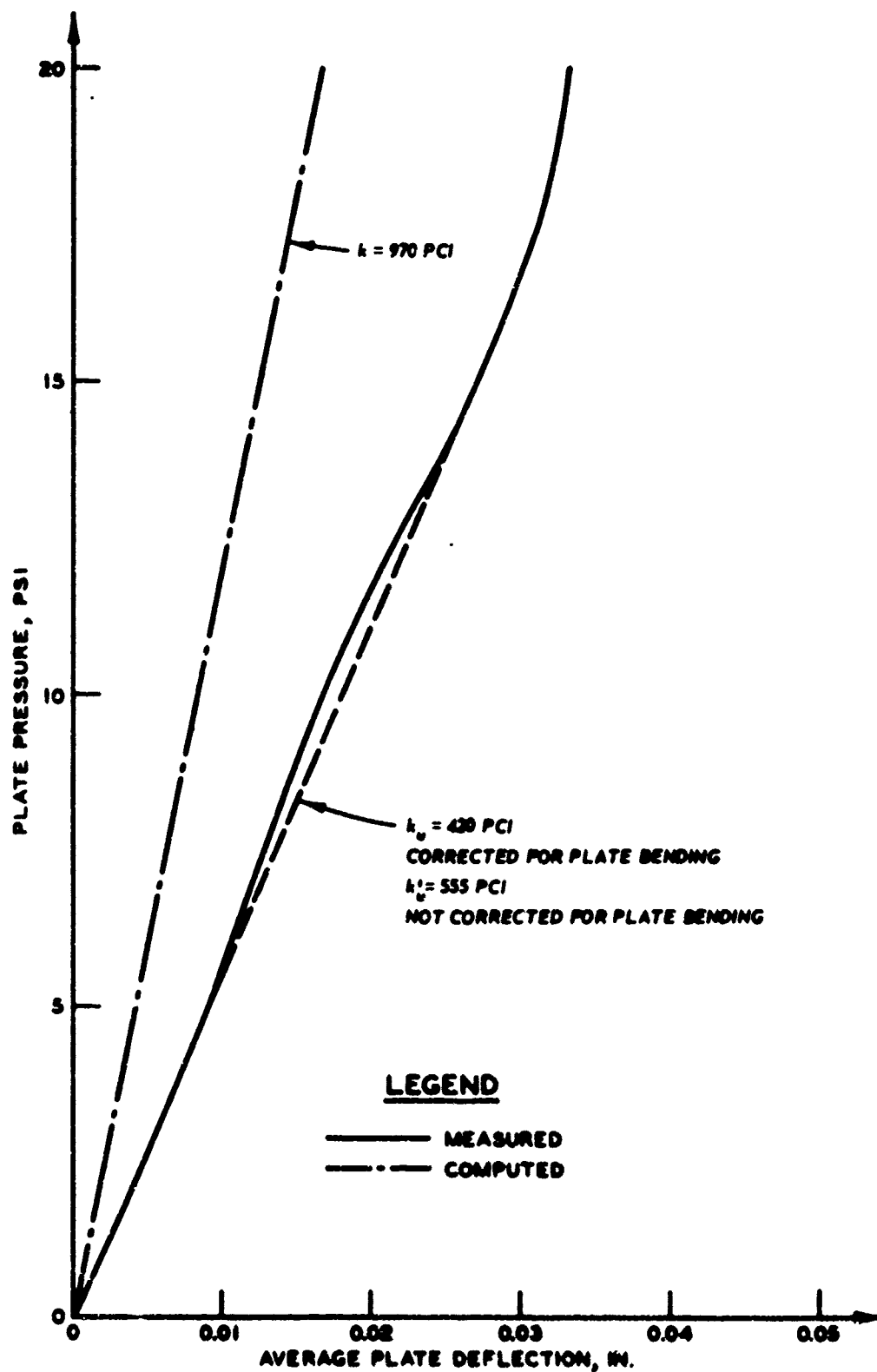
Figure 76. Load-deflection curves from plate bearing
tests on lightweight concrete in subitem 5b
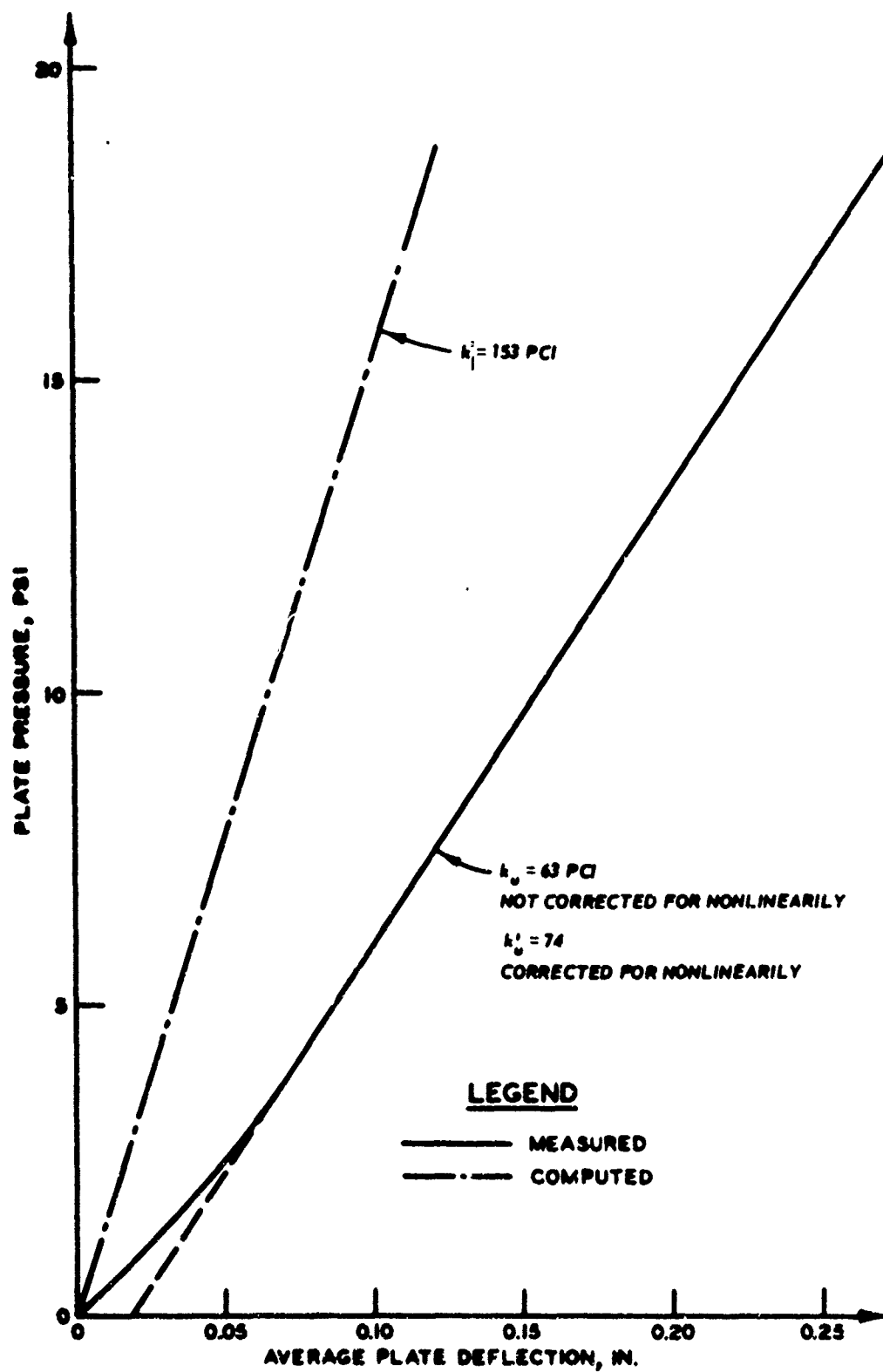
Figure 77. Load-deflection curves from plate bearing tests on 120-psi polystyrene in subitem 5c
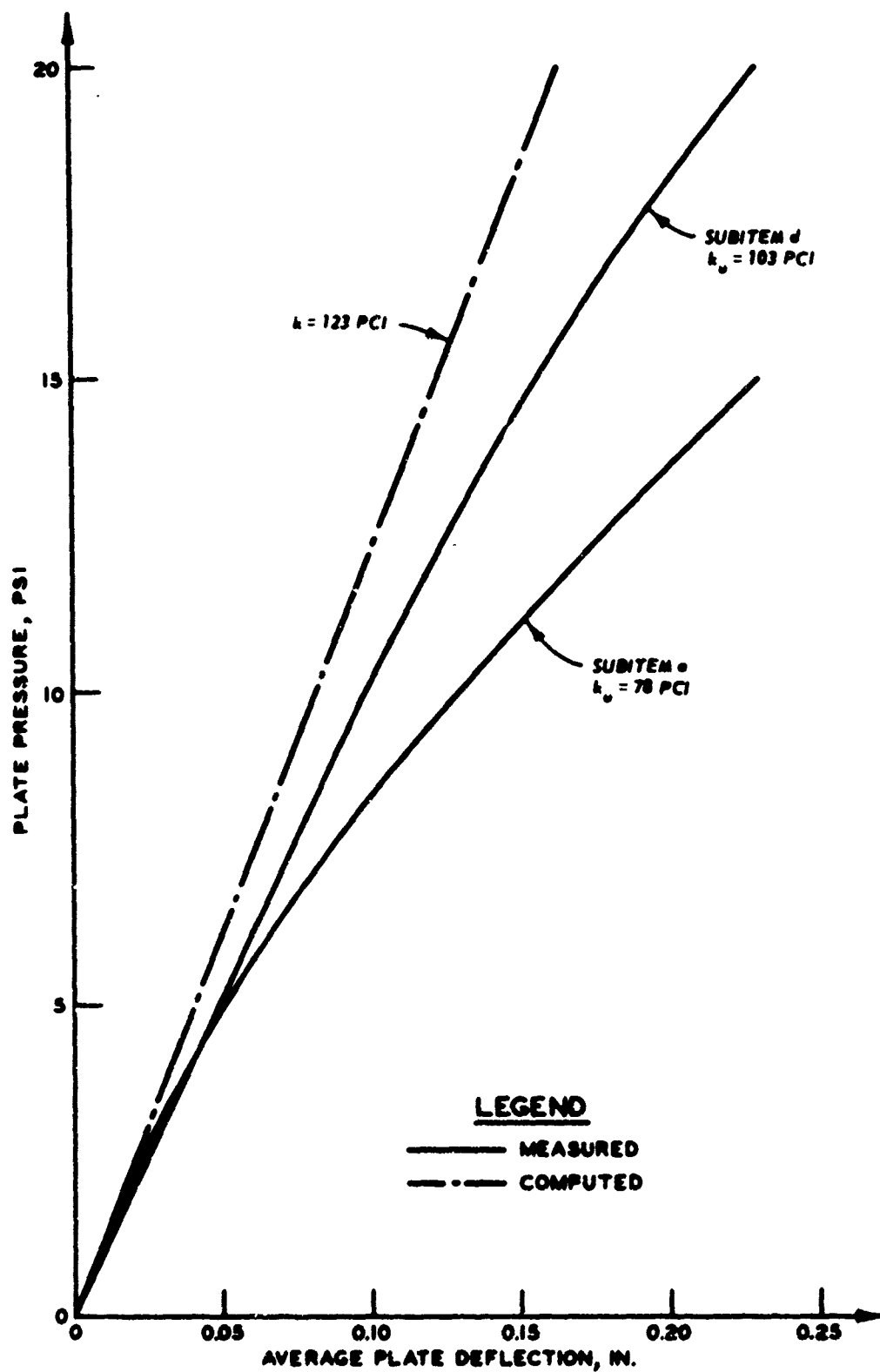
Figure 78. Load-deflection curves from plate bearing
tests on 35-psi polystyrene in subitem 5d

Figure 79. Illustration of discrete element representation of rigid
pavement subitems containing insulating layers

125
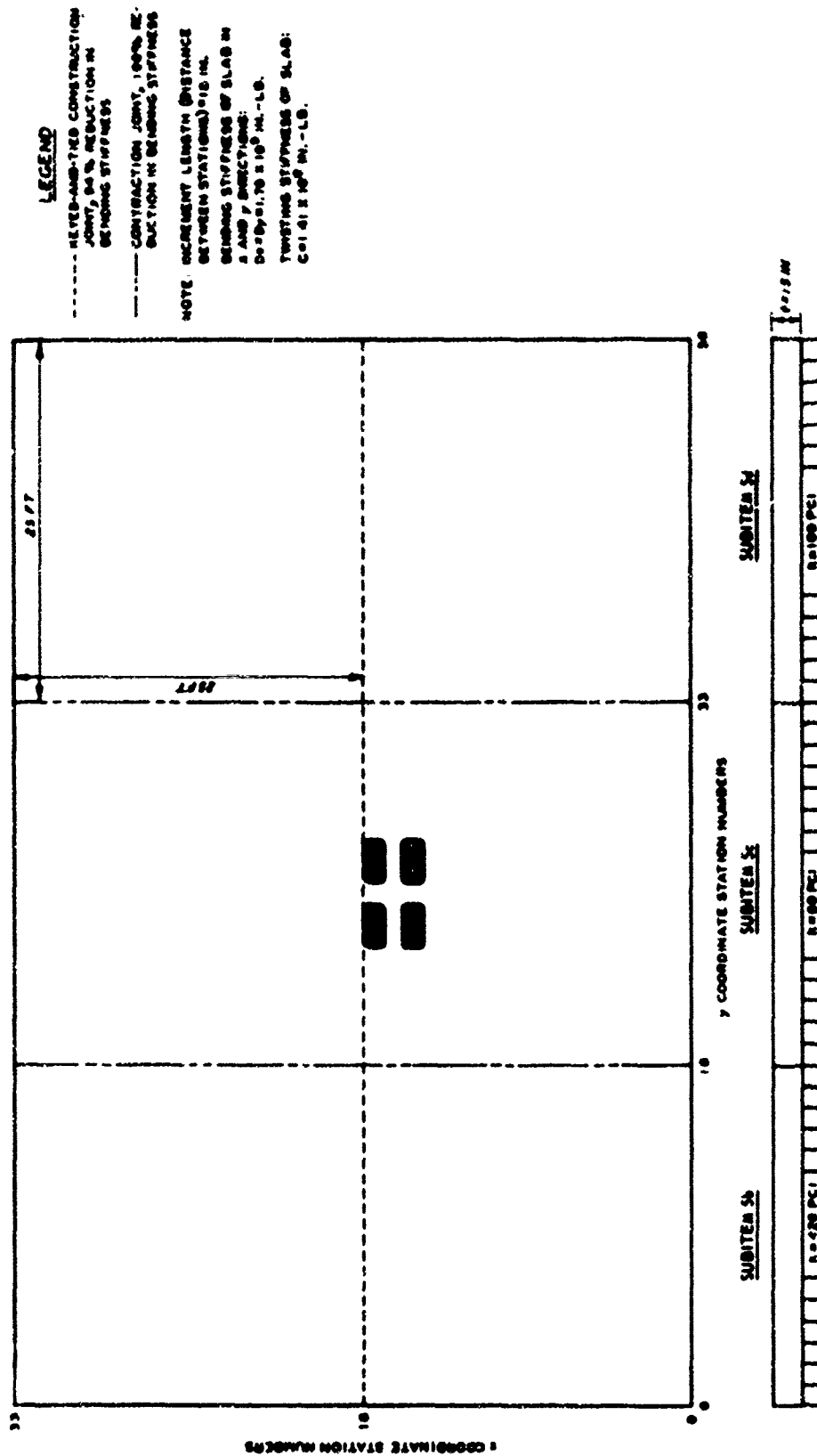
Figure 80. Illustration of discrete element representation of rigid pavement subitems 5b-5d with the slab size assumed to be 25 by 25 ft; loading of subitem 5c, lane 1
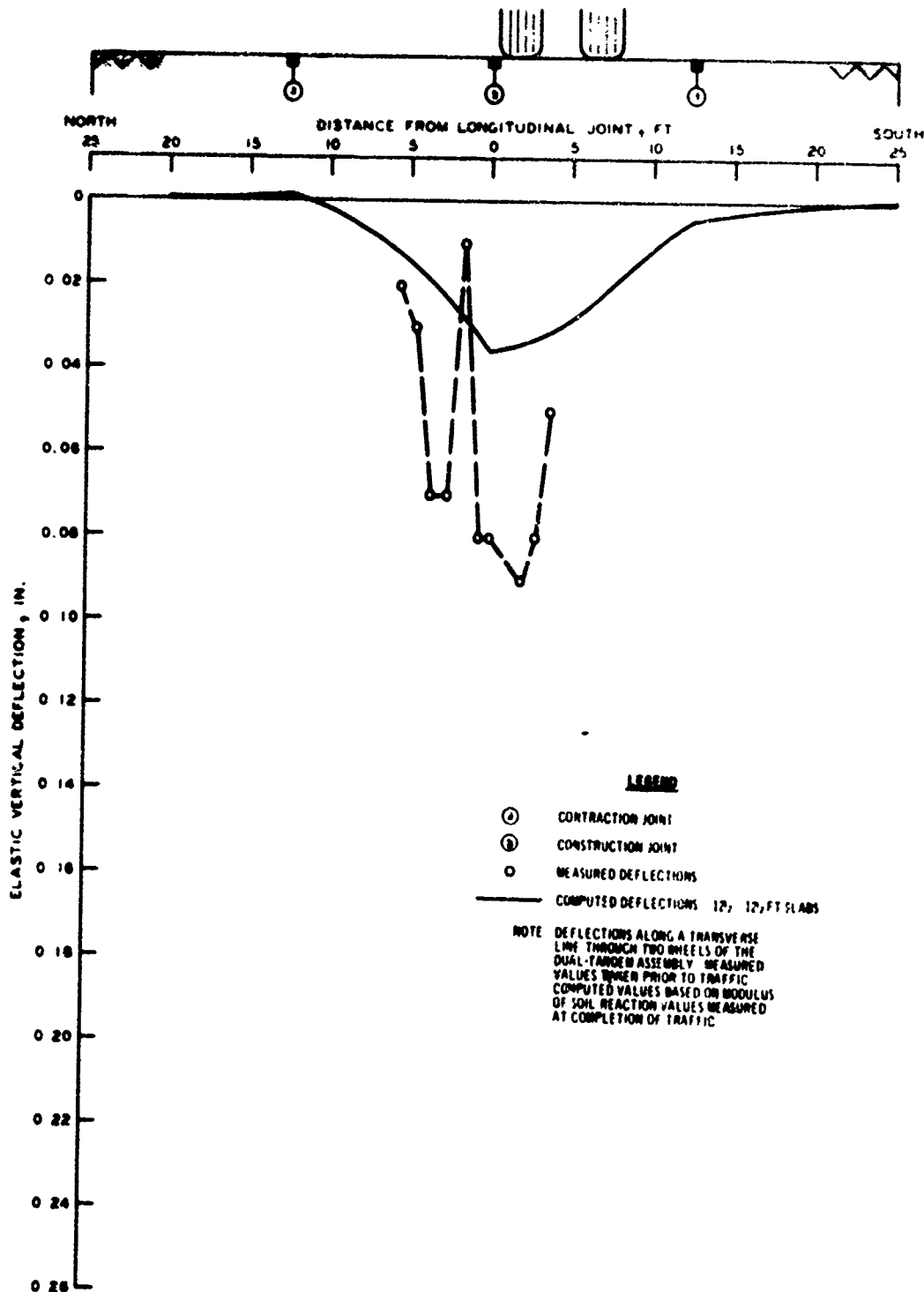
Figure 81.   Deflections for subitem 5a, lane 1, along
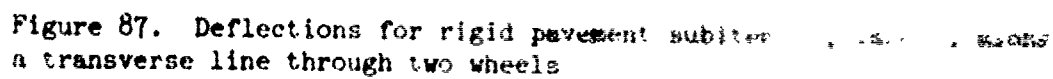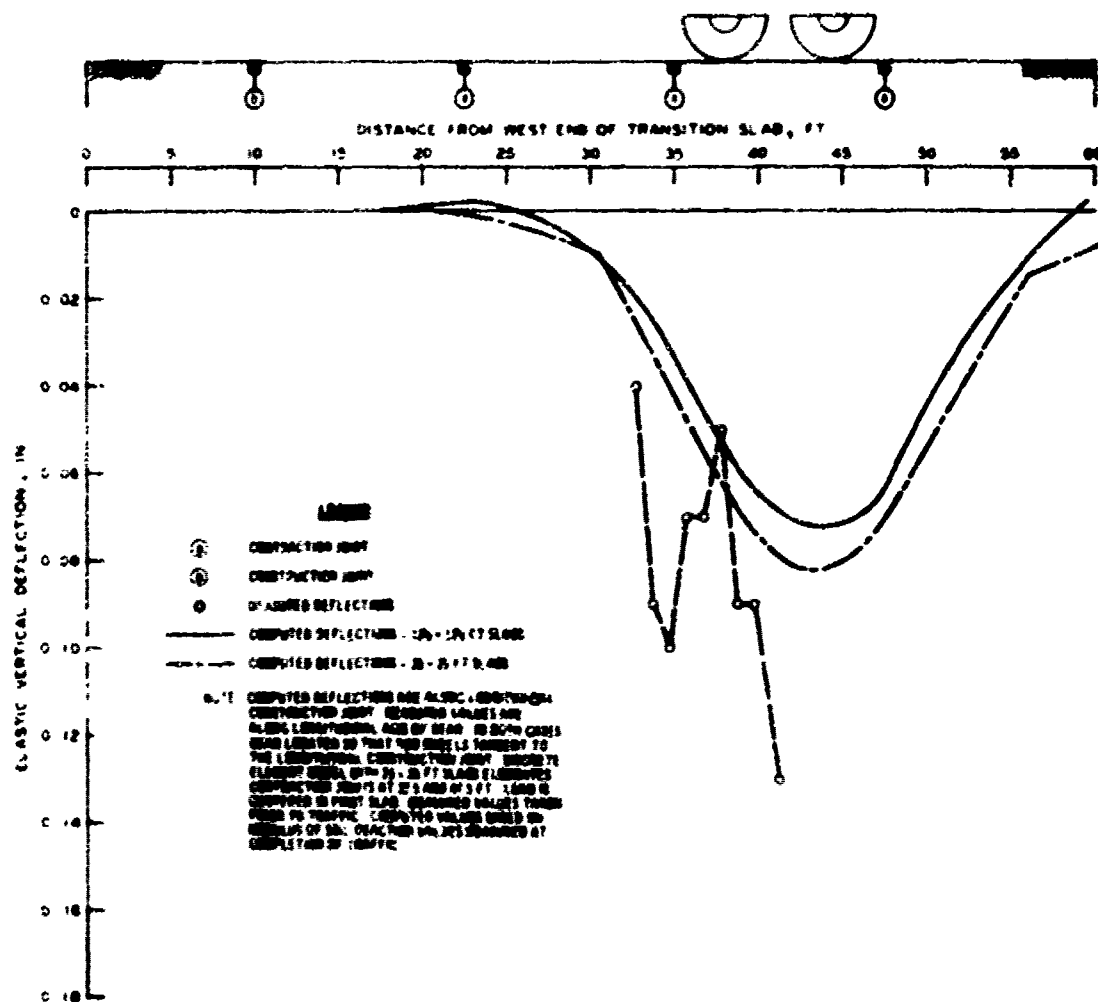a transverse line through two of the wheels
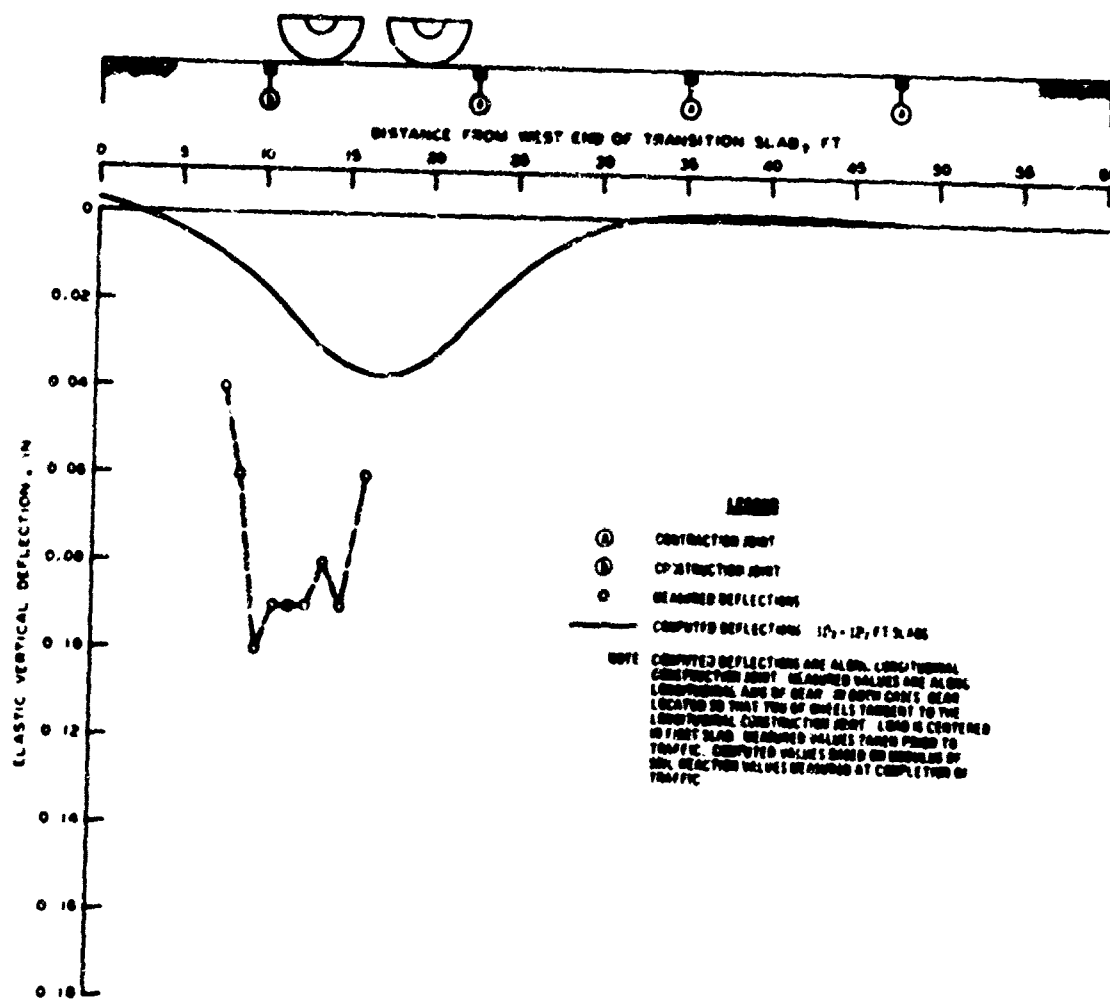
Figure 82. Deflections for rigid pavement subitem 5a, lane 1, along the longitudinal construction joint
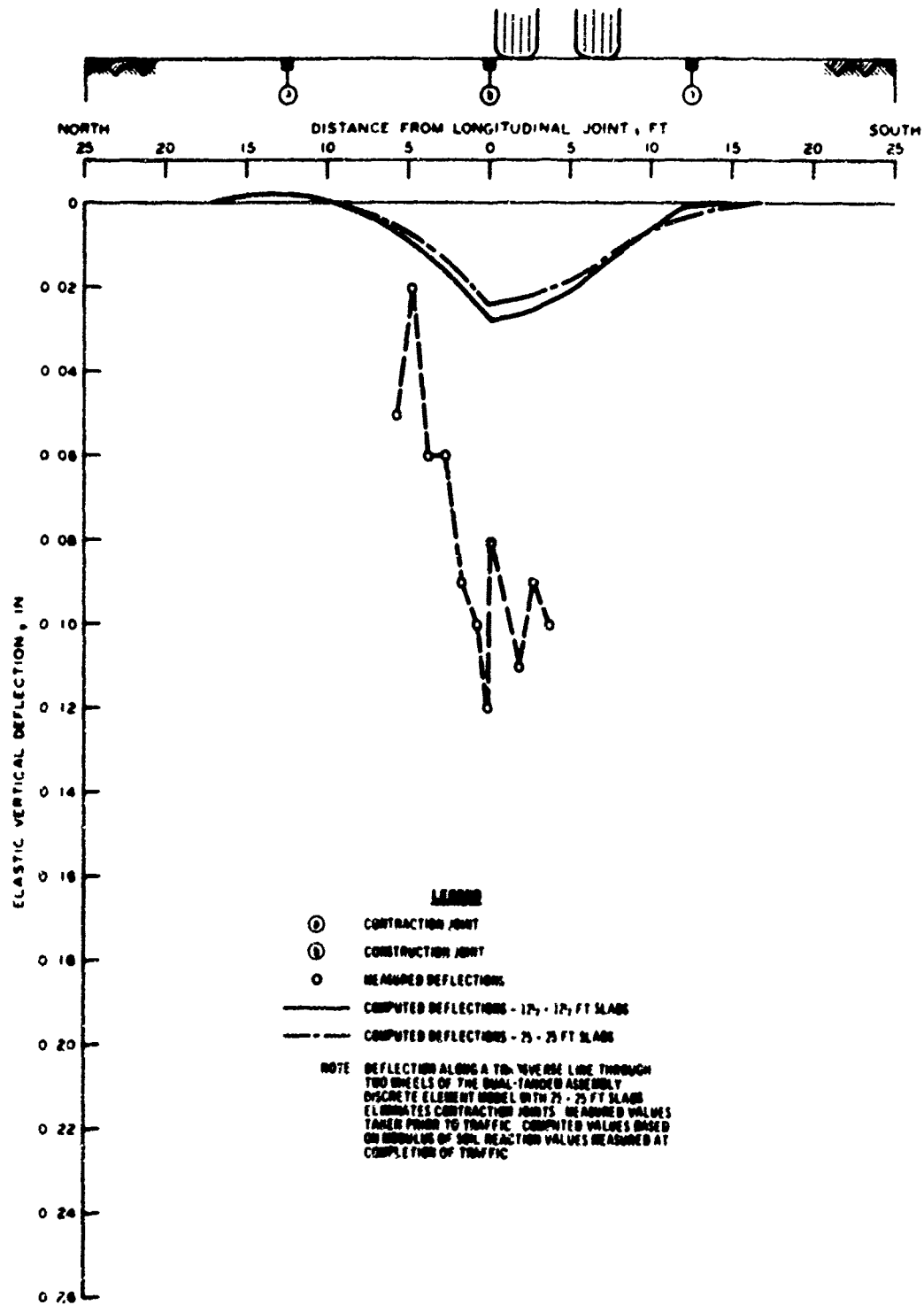
Figure 83. Deflections for rigid pavement subitem 5b, lane 1, along a
transverse line through two of the wheels

129
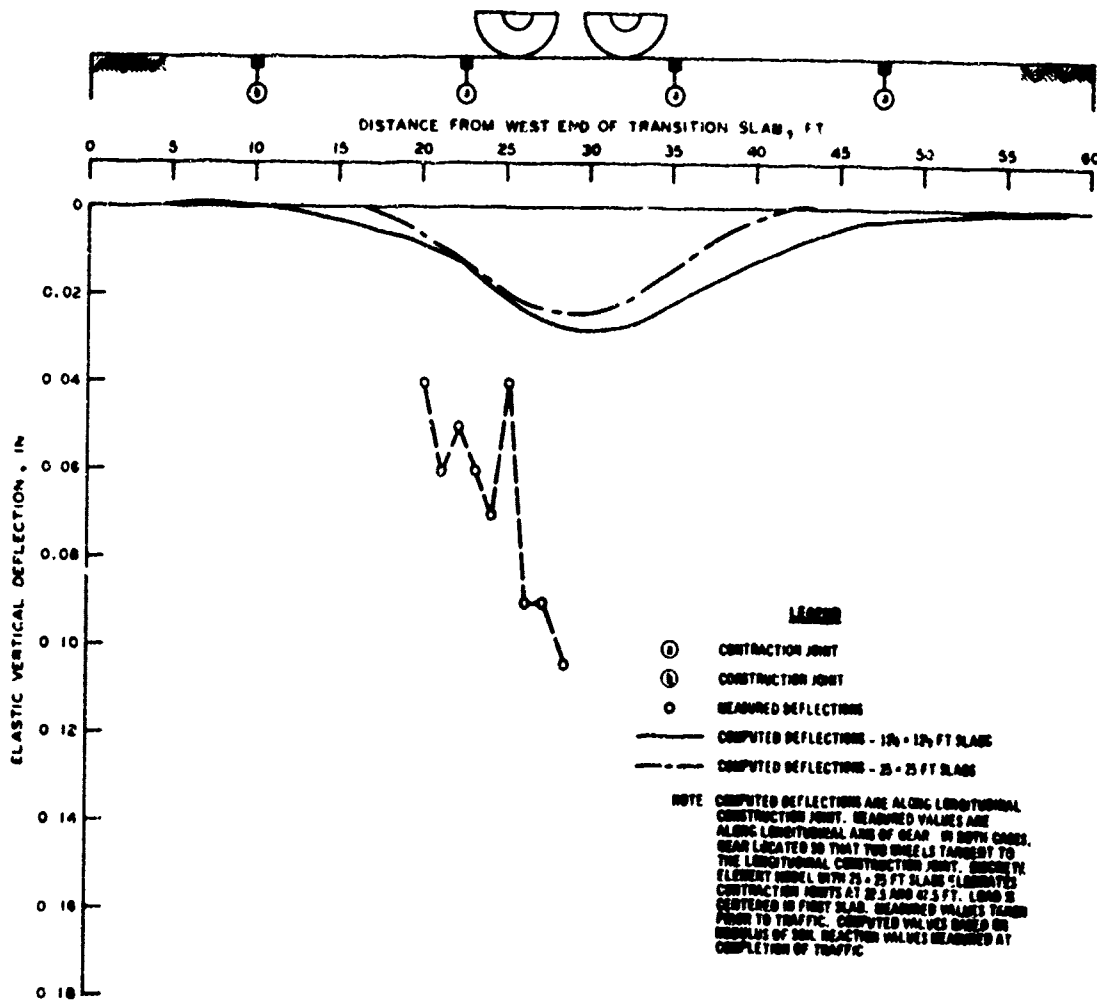
Figure 84.   Deflections for rigid pavement subitem 5b, lane 1, along
the longitudinal construction joint

130
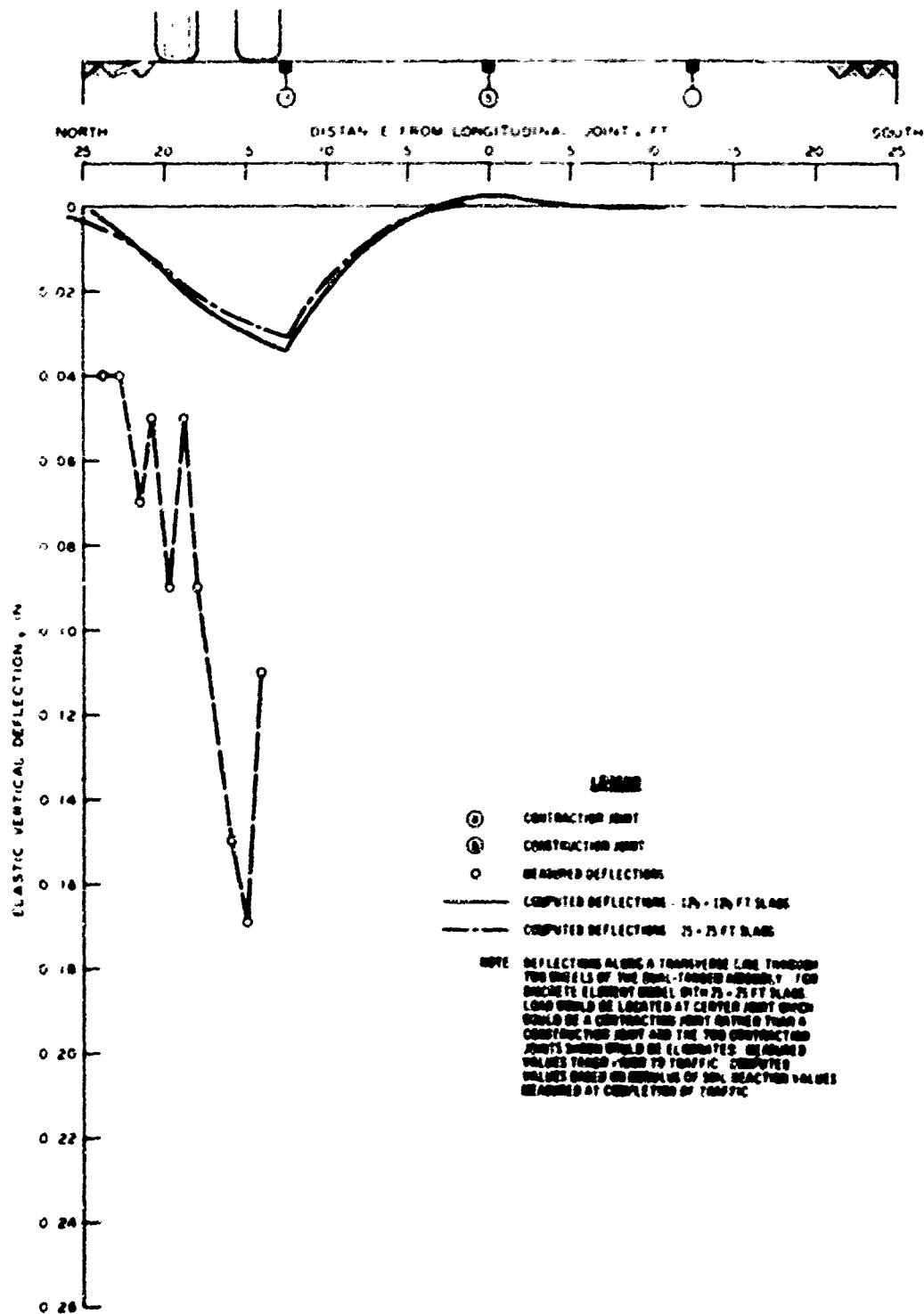
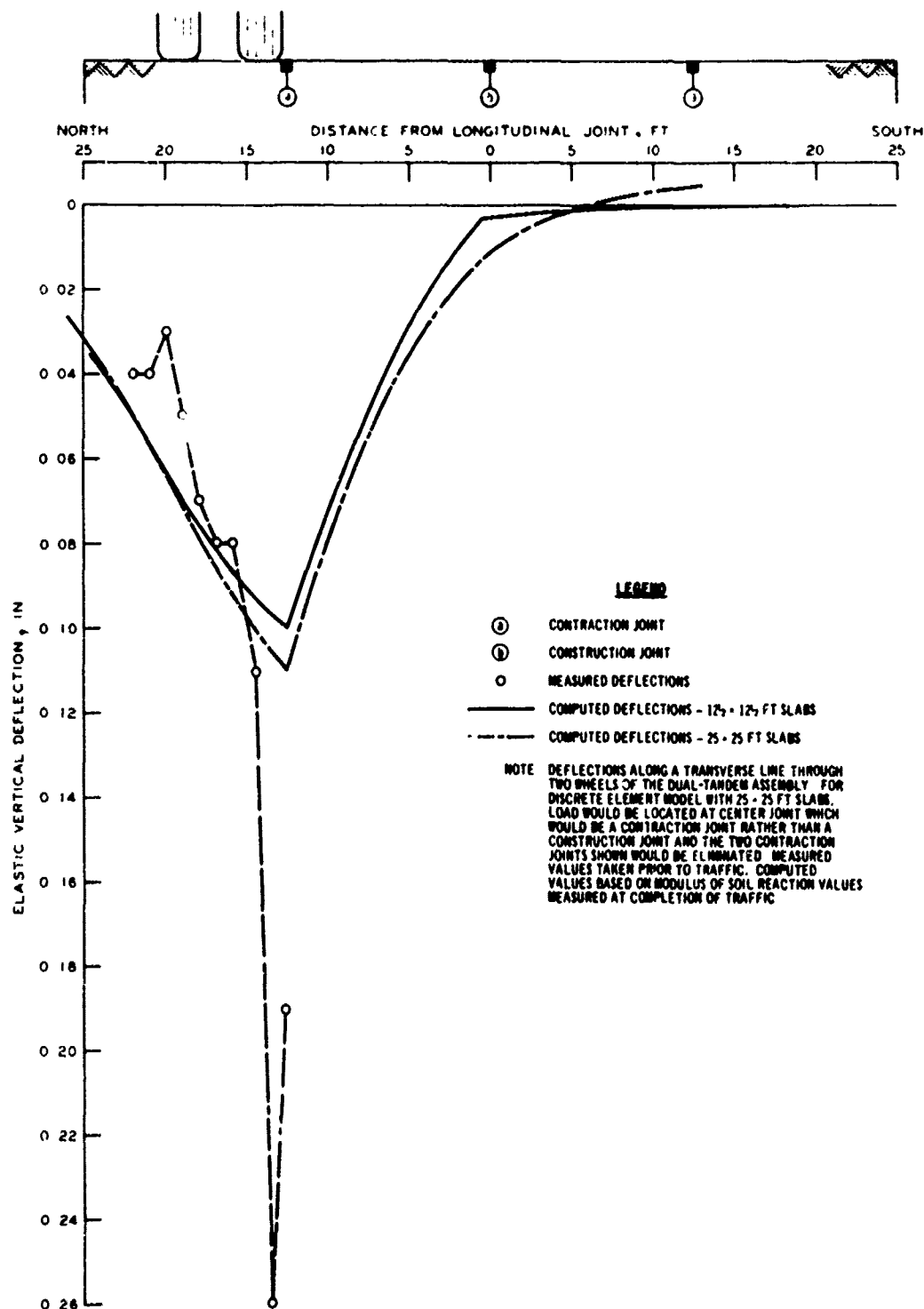Figure 85. Deflections for rigid pavement subitem 5b, lane 2, along
a transverse line through two wheels
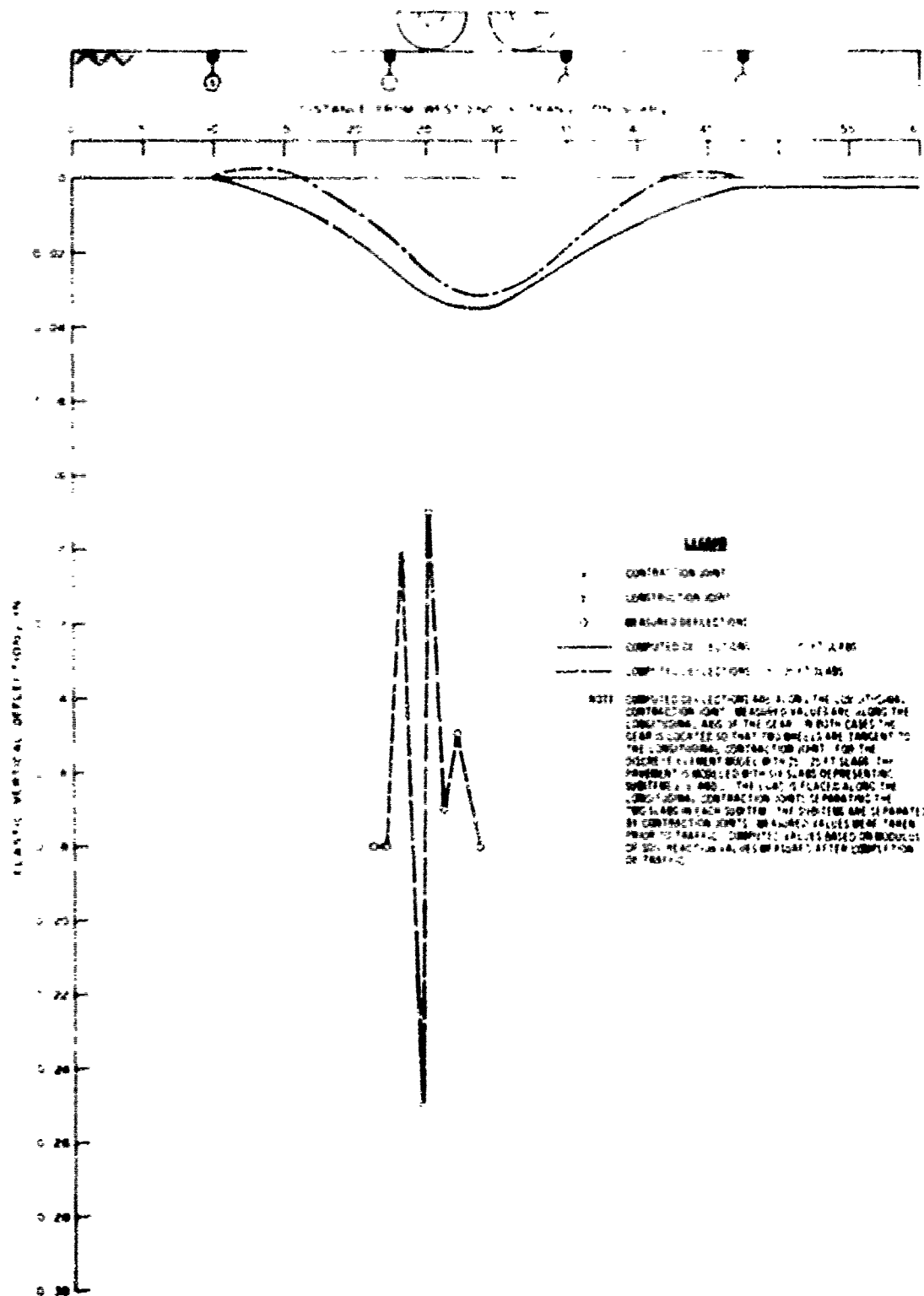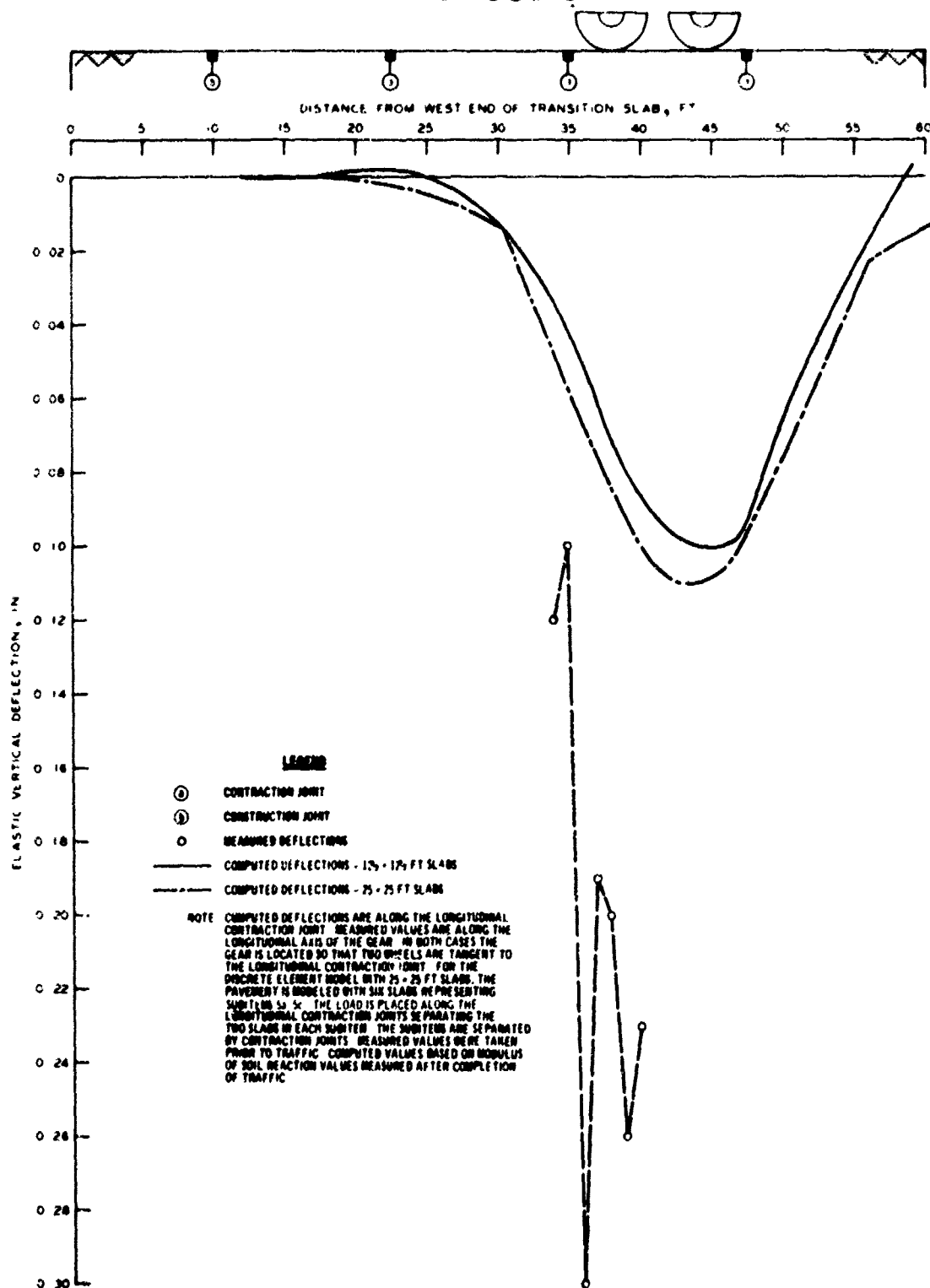
Figure 86. Deflections for rigid pavement subitem 5b, lane 2, along the longitudinal contraction joint

Figure 87. Deflections for rigid pavement subject to loads along a transverse line through two wheels

Figure 88. Deflections for rigid pavement subitem 5r, lane 1, along the longitudinal construction joint

Figure 89. Deflections for rigid pavement subitem 5c, lane 2, along a transverse line through two wheels

135

Figure 90. Deflections for rigid pavement subitem 5c, lane 2, along the longitudinal contraction joint

136
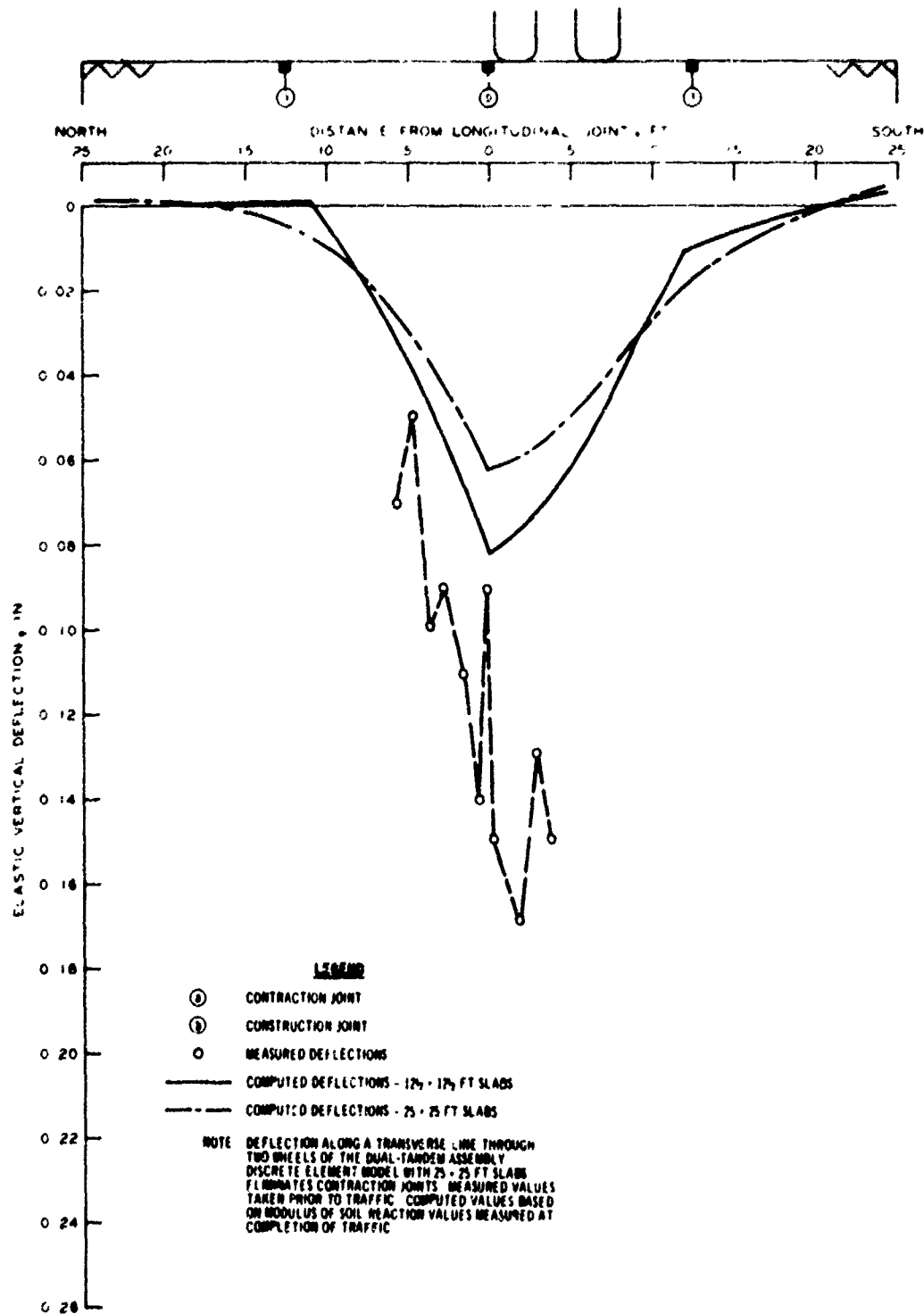
Figure 91. Deflections for rigid pavement subitem 5d, lane 1, along
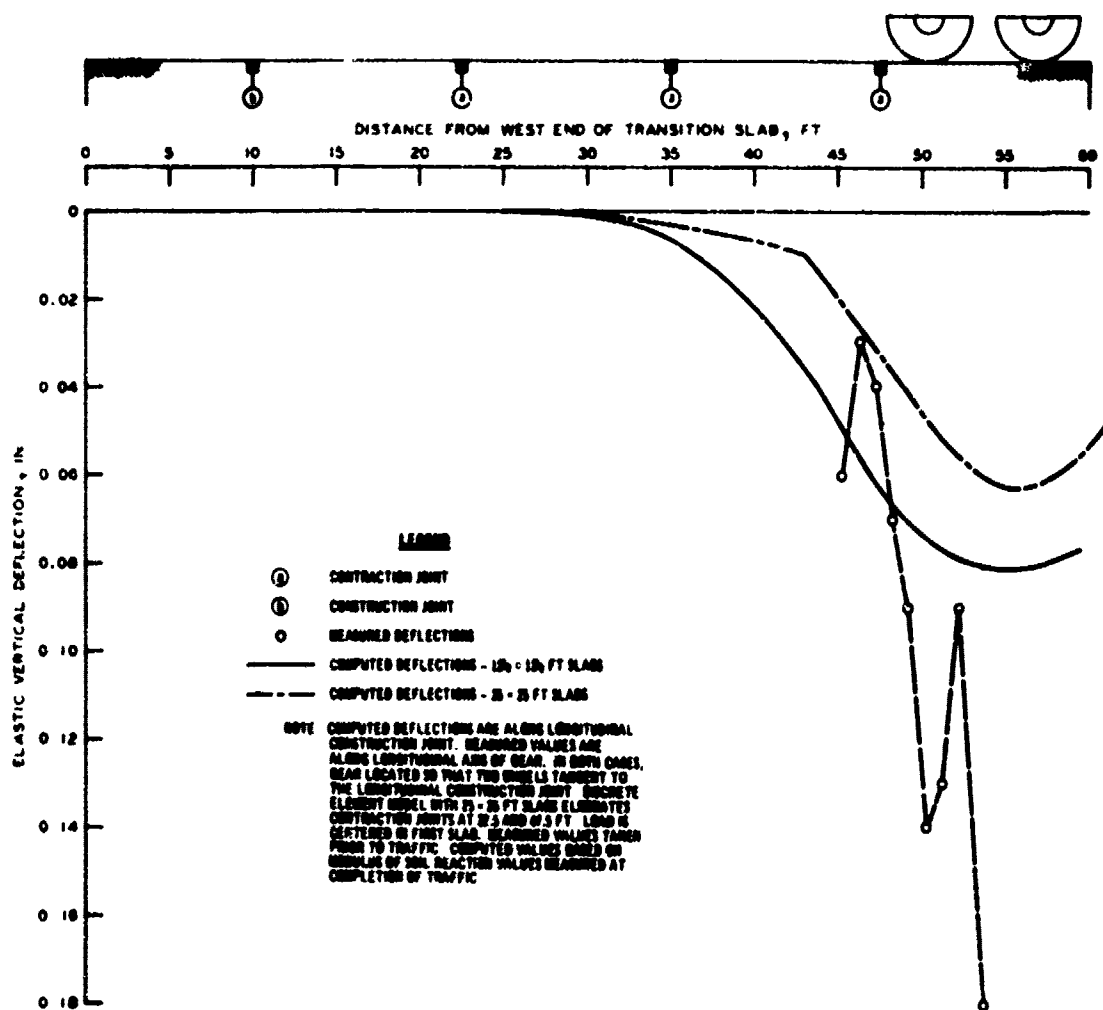a transverse line through two wheels

137

Figure 92. Deflections for rigid pavement subitem 5d, lane 1, along the longitudinal construction joint
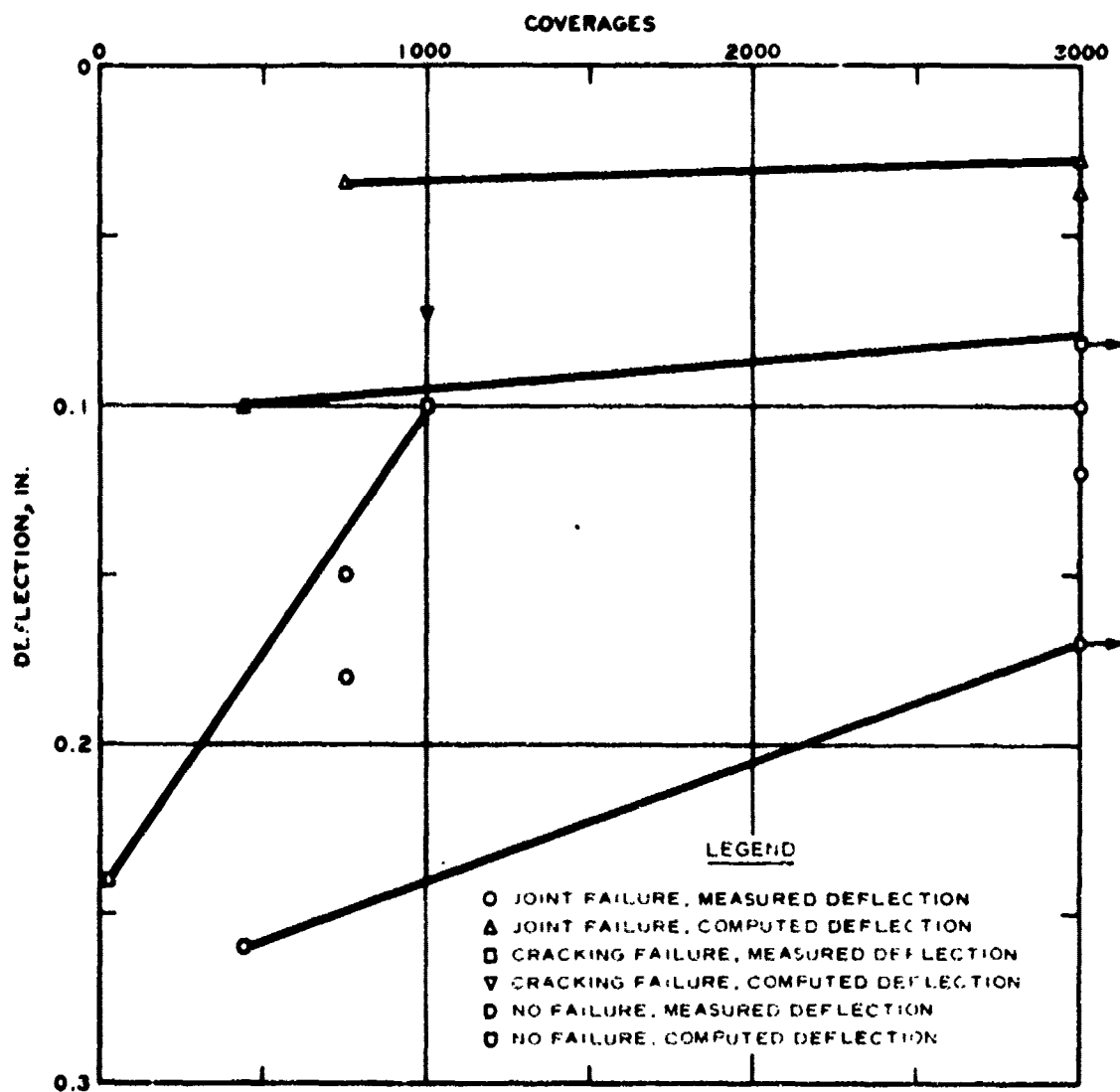
138

Figure 93. Joint deflection versus coverage level for rigid
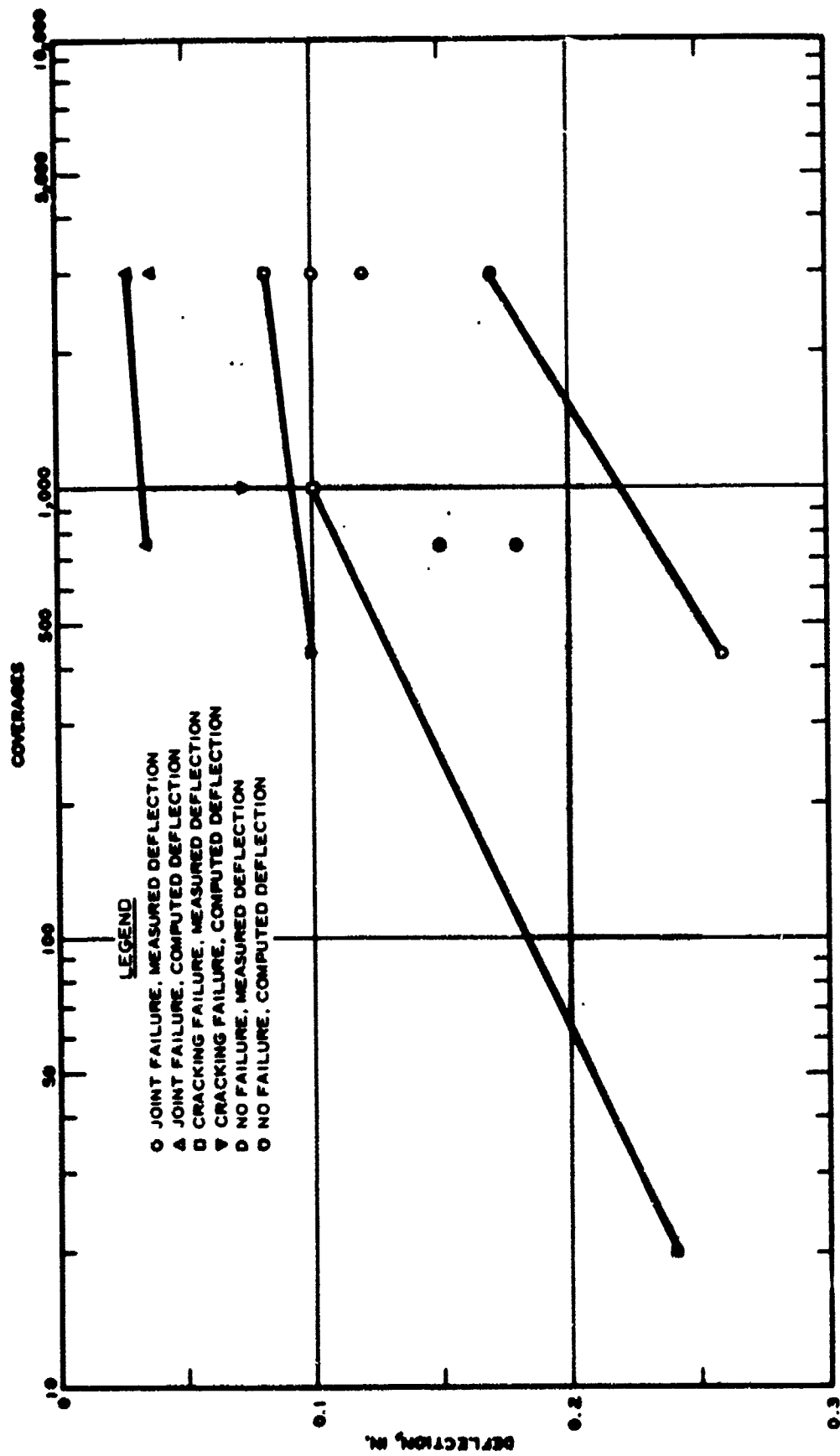pavement subitems containing insulating layers

Figure 94. Joint deflection versus log of coverage level for rigid pavement subitems containing insulating layers

REFERENCES

1. Burns, C. D. et al., "Comparative Performance of Structural Layers in Pavement Systems; Design, Construction, and Behavior Under Traffic of Pavement Test Sections," Report No. FAA-RD-73-198, Vol I, Jun 1974, Federal Aviation Administration, Washington, D. C., and Technical Report S-74-8, Vol I, Jun 1974, U. S. Army Engineer Waterways Experiment Station, CE, Vicksburg, Miss.

2. Hohwiller, F. and Köhling, K., "Styropor-Filled Lightweight Concrete," Badische Anilin- & Soda-Fabrik AG, 1968, Federal Republic of Germany.

3. American Society for Testing and Materials, "Standard Method of Test for Compressive Strength of Cylindrical Concrete Specimens," Designation: C 39-71, 1972 Annual Book of ASTM Standards, Part 10, 1972, Philadelphia, Pa.

4. U. S. Army Engineer Waterways Experiment Station, CE, Handbook of Concrete and Cement, Aug 1949 (with quarterly supplements), Vicksburg, Miss.

5. American Society for Testing and Materials, "Standard Method of Test for Flexural Strength of Concrete (Using Simple Beam with Third-Point Loading)," Designation: C 78-64, 1972 Annual Book of ASTM Standards, Part 10, 1972, Philadelphia, Pa.

6. _____, "Standard Method of Test for Static Modulus of Elasticity and Poisson's Ratio of Concrete in Compression," Designation: C 469-65, 1972 Annual Book of ASTM Standards, Part 10, 1972, Philadelphia, Pa.

7. _____, "Standard Method of Making and Curing Concrete Test Specimens in the Laboratory," Designation: C 192-69, 1972 Annual Book of ASTM Standards, Part 10, 1972, Philadelphia, Pa.

8. _____, "Standard Method of Test for Moisture-Density Relations of Soil Using 5.5-lb Rammer and 12-in. Drop," Designation: D 698-70, 1972 Annual Book of ASTM Standards, Part 11, 1972, Philadelphia, Pa.

9. Michelov, J., "Analysis of Stresses and Displacements in an n-Layered Elastic System Under a Load Uniformily Distributed on a Circular Area," Sep 1963, California Research Corp., Richmond, Calif.

10. Barker, W. R. and Brabston, W. N., "Development of a Structural Design Procedure for Flexible Airport Pavements," Report No. FAA-RD-74-199, Sep 1975, Federal Aviation Administration, Washington, D. C., and Technical Report S-75-17, Sep 1975, U. S. Army Engineer Waterways Experiment Station, CE, Vicksburg, Miss.

11. Morgan, J. R. and Scala, A. J., "Flexible Pavement Behavior and Application of Elastic Theory--A Review," Proceedings, Australian Road Research Board, Vol 4, Part 2, 1968, pp 1201-1243.

12. General Services Administration, "Sealing Compound, Hot Poured Type, for Joints in Concrete," Federal Specifications SS-S-164(4), Aug 1964, Washington, D. C.

13. Department of Defense, "Method 104, Modulus of Soil Reaction," Military Standard 621-A, Test Method for Pavement Subgrade, Subbase, and Base-Course Materials, Dec 1964, Washington, D. C.

14. American Society for Testing and Materials, "Standard Method of Test for Splitting Tensile Strength of Cylindrical Concrete Specimens," Designation: C 496-71, 1972 Annual Book of ASTM Standards, Part 10, 1972, Philadelphia, Pa.

15. Westergaard, H. M., "Stresses in Concrete Pavements Computed by Theoretical Analyses," Public Roads, Vol 7, No. 2, Apr 1926, pp 25-35.

16. _____, "Analytical Tools for Judging Results of Structural Tests of Concrete Pavements," Public Roads, Vol 14, No. 10, Dec 1933, pp 185-188.

17. _____, "Stresses in Concrete Runways of Airports," Proceedings, 19th Annual Meeting of the Highway Research Board, Dec 1939, pp 197-202.

18. _____, "Stress Concentrations in Plates Loaded over Small Areas," Transactions, American Society of Civil Engineers, Vol 108, Paper No. 2197, 1943, pp 831-886.

19. _____, "New Formulas for Stresses in Concrete Pavements of Airfields," Transactions, American Society of Civil Engineers, Vol 113, Paper No. 2340, 1948, pp 425-444.

20. Pickett, G. et al., "Deflections, Moments, and Reactive Pressures for Concrete Pavements," Bulletin No. 65, Oct 1951, Kansas State College, Manhattan, Kans.

21. Pickett, G. and Ray, G. K., "Influence Charts for Concrete Pavements," Transactions, American Society of Civil Engineers, Vol 116, Paper No. 2425, 1951, pp 49-73.

22. Hudson, W. Ronald and Matlock, Hudson, "Discontinuous and Ortho-
    tropic Plates and Pavement Slabs," Report No. 56-6, May 1966,
    Center for Highway Research, The University of Texas, Austin, Tex.

23. Panak, John J. and Matlock, Hudson, "A Discrete-Element Method of
    Multiple-Loading Analysis for Two-Way Bridge Floor Slabs," Report
    No. 56-13, Jan 1970, Center for Highway Research, The University
    of Texas, Austin, Tex.

GPO 914-319